# Mapping intra-and inter-annual dynamics in wetlands with multispectral, thermal and SAR time series

Dissertation

zur

Erlangung des Doktogrades

der

Mathematisch-Naturwissenschaftlichen Fakultät

der

Rheinischen Friedrich-Wilhelms-Universität Bonn

vorgelegt von

Javier Muro Martín

aus

Madrid, Spanien

Bonn, May 2019

Angefertigt mit Genehmigung der Mathematisch-Naturwissenschaftlichen Fakultät
der Rheinischen Friedrich-Wilhelms-Universität Bonn

1. Gutachter: Prof. Dr. Bernd Diekkrüger
2. Gutachter: Prof. Dr. Björn Waske

Tag der Promotion: 17. Oktober 2019

Erscheinungsjahr: 2019

*To my wife*

**Acknowledgments**

Endings often determine whether a story was worth reading or not. In many of them, the protagonist realizes that what he fought for was not truly important, obtaining instead something else of greater value; friendship, self-confidence, purpose... A PhD is similar. It has been almost 4 years of hard work conducting, repeating, and refining analyses; struggling to convey the importance of my research to others; getting past picky reviewers, or even overcoming the loss of a mentor. But on the way I have had the opportunity to interact with people with my same passions and curiosity, colleagues eager to lend their experience, and others willing to learn from my insights. I've met people whose values differed from mine, offering enriching experiences. I've felt the sense of belonging when racing against time along my teammates to submit a document; or when experts of other disciplines really valued my work and found it useful for their own reports and management plans. And I've also met parts of myself; some good, others, not so much. The 4, 5, or 6 years that takes us to complete the PhD are growing experiences of much greater value. The defense marks the ending of such intense period.

To you all that were part of this last 4 years, I thank you.

## Table of Contents:

**List of Figures**

**List of tables**

**Acronyms and abbreviations**

| | |
|---|---|
| AAT | Annual Aggregation Trends |
| ASIG | Albanian State Authority for Geospatial Information |
| AWS | Amazon Web Services |
| BFAST | Breaks For Additive Season and Trend |
| CVA | Change Vector Analysis |
| DEM | Digital Elevation Model |
| EO | Earth Observation |
| ESA | European Space Agency |
| ETM | Enhanced Thematic Mapper |
| FAO | Food and Agriculture Organization |
| GEE | Google Earth Engine |
| GSW | Global Surface Water |
| LST | Land Surface Temperature |
| LULC | Land Use Land Cover Change |
| MAES | Millennium Assessment of Ecosystem Services |
| MODIS | Moderate |
| MSI | Multispectral Instrument |
| MrVBF | Multiresolution Index of Valley Bottom Flatness |
| NDBI | Normalized Difference Bare soil Index |
| NDVI | Normalized Difference Vegetation Index |
| NDWI | Normalized Difference Water Index |
| OLCI | Ocean Land Color Instrument |
| OLI | Operational Land Imager |
| OLS | Ordinary Least Squares |
| PWM | Potential Wetlands Mask |
| RGB | Red Green Blue |

| | |
|---|---|
| SAGCOT | Southern Agricultural Growth Corridor Of Tanzania |
| SAR | Synthetic Aperture Radar |
| SDG | Sustainable Development Goals |
| SNAP | Sentinels Application Platform |
| SRTM | Shuttle Radar Topography Mission |
| STM | Season Trend Model |
| TSA | Time Series Analysis |
| TSC | Terrain Surface Convexity Index |
| TWI | Topographic Wetness Index |
| USGS | United States Geological Survey |

**Abstract**

The important value and wide array of ecosystem services provided by wetlands are widely recognized by scientific and government institutions alike: they are highly productive, supporting directly many human communities; they provide pollution control, clean water and soil formation; they store larger amounts of Carbon than forests; they are a key habitat for 40% of the world's species, and they provide protection against natural disasters, among many other services. However, they are still being degraded globally at fast rates by human activities. Agriculture and dam building are two of the main drivers of wetland degradation.

Due to wetlands' seasonality, their difficult access and ecotone character, determining their actual extension and trends over time is a complex task. Earth Observation systems are the most appropriate available tool to monitor their spatio-temporal patterns (seasonal changes and long term trends) at global scales, and to study the effects that human activities have in their physical and biological properties.

I use time series of radar (Sentinel-1), multispectral (Sentinel-2) and thermal (MODIS) imagery to map the spatio-temporal patterns in 5 study areas with wetlands of different characteristics: 1) Fuente de Piedra, an endorheic small wetland in Spain; 2) Camargue, a complex of coastal marshes in the south of France; 3) Kerkini Lake, an artificial wetland in Greece; 4) Albania, a country that harbors one of the few remaining systems of undammed large rivers in Europe; 5) and the Kilombero Floodplain, a complex of swamps and seasonally inundated grasslands in Tanzania.

First, I introduce in chapter 1 the problematic of wetlands' definitions and their degradation trends. I continue with a brief introduction on remote sensing, time series analysis, and their applications on wetlands' research and management. In chapters 2 and 3 I implement an algorithm for change detection of time series of Sentinel-1 images, and compare its performance with Landsat datasets and conventional change detection methods. In chapter 2 I perform the analysis in a desktop computer, but in chapter 3 I make use of the cloud computing platform Google Earth Engine. I demonstrate the advantages of cloud computation for operational monitoring of seasonal patterns and other short-term changes.

In chapters 4 and 5 I address two of the main causes of wetland degradation: dam building and agricultural expansion.

Albania hosts one of the few remaining systems of large undammed rivers of Europe. While the authorities are planning to invest in hydropower, they are facing opposition from

conservation, local and scientific organizations. In chapter 4 I use dense time series of Sentinel-1 and Sentinel-2 images to compute multitemporal metrics and map all the wetlands of Albania. I evaluate the synergic advantages of fusing multispectral and radar imagery in combination with knowledge-based rules for classification of wetlands.

In chapter 5 I present how the Kilombero Floodplain has been degraded during the last years due to uncontrolled farmland expansion. Due to weak management systems, the increasing pressure on the wetland has caused a loss in ecosystem services and social conflicts between the many stakeholders of the area. I use a time series of thermal imagery (MODIS) spanning from 2000 until 2017 and land use change maps to map the effect of the land use changes that the wetland has gone through during the last 18 years. I compare three models for time series analysis and reveal how farming practices have increased the land surface temperature of the farmed area, as well as in adjacent still natural wetlands. Lastly, I show how the land surface temperature can be used as an indicator to detect trends and changes in the water and energy fluxes of the Earth's surface.

## Zusammenfassung

Der hohe Wert und der Reichtum an Ökosystemdienstleistungen, die von Feuchtgebieten bereitgestellt werden, wecken die Aufmerksamkeit sowohl von Forschung als auch von staatlichen Institutionen. Feuchtgebiete sind bedeutende Ökosysteme, die zahlreichen Menschen als Lebensgrundlage dienen und regulierend auf den Boden- und Wasserhaushalt wirken. In Feuchtgebieten können größere Kohlenstoffmengen gespeichert werden als in Wäldern. Außerdem leben rund 40 % aller auf der Welt existierenden Tier- und Pflanzenarten in Feuchtgebieten. Feuchtgebiete sind vielfältige Lebensräume und bieten u.a. Schutz vor Naturgefahren. Allerdings werden sie weltweit und in zunehmender Intensität durch menschliche Aktivitäten zerstört. Zu den Hauptverursachern für den Verlust von Feuchtgebieten zählen u.a. die Landwirtschaft und der Bau von Staudämmen.

Die Analyse der aktuellen räumlichen Verbreitung und der zeitlichen Entwicklung von Feuchtgebieten stellt eine äußerst komplexe Aufgabe dar, welche durch die Saisonalität, die schwierige Zugänglichkeit und die besonderen Eigenschaften als Ökoton bedingt ist. Erdbeobachtungssysteme sind somit das am besten geeignete Werkzeug, um zeitliche und räumliche Muster von Feuchtgebieten auf globaler Ebene zu beobachten (saisonale Veränderungen und Langzeit-Trends) und um den Einfluss der menschlichen Aktivitäten auf ihre physischen und biologischen Eigenschaften zu untersuchen.

Zur Kartierung von raum-zeitlichen Mustern wurden Zeitreihen von Radar- (Sentinel-1), Multispektral- (Sentinel-2) und Thermal-Satellitendaten (MODIS) in fünf Untersuchungsgebieten mit für Feuchtgebiete unterschiedlichen typischen Charakteristika untersucht: 1) Fuente de Piedra, ein kleines, endorheisches Feuchtgebiet in Spanien, 2) Camargue, ein komplexes Küstenmarschlandgebiet in Südfrankreich, 3) Kerkini, ein künstliches Feuchtgebiet in Griechenland, 4) Albanien, das eines der wenigen verbliebenen nicht regulierten Flusssysteme Europas beherbergt und 5) Kilombero, eine Überflutungsebene in Tansania mit einer Reihe von Sumpfgebieten und saisonal überschwemmten Graslandschaften.

In Kapitel 1 werden die Problematik in Bezug auf die Definition von Feuchtgebieten erläutert und allgemeine Degradations-Trends beschrieben. Anschließend folgt eine Einführung in die Fernerkundung von Feuchtgebieten, die Zeitreihenanalyse und deren Anwendung auf Feuchtgebiete. Die Kapitel 2 und 3 beinhalten einen Algorithmus, um Veränderungen mithilfe von SAR-Zeitreihen festzustellen. Die Ergebnisse werden mit denen von multispektralen Datensätzen und konventionellen Methoden der Veränderungsdetektion verglichen. Die Analysen in Kapitel 2 basieren auf der Durchführung mit einem Desktop-Computer., In Kapitel 3 basiert die Analyse auf der Cloud-Computing-Plattform Google Earth Engine (GEE). Hier werden die Vorteile des Cloud-Computings für das operationelle Monitoring saisonaler Muster und die Erkennung kurzfristig auftretender Veränderungen verdeutlicht.

In den Kapiteln 4 und 5 werden die zwei Hauptursachen für den Verlust von Feuchtgebieten behandelt: der Staudammbau und die Ausdehnung landwirtschaftlicher Flächen.

In Albanien befindet sich das letzte nicht regulierte Flusssystem Europas. Während die Behörden Investitionen in Wasserkraftanlagen planen, macht sich eine Opposition von Naturschützern und lokalen sowie internationalen wissenschaftlichen Organisationen gegen diese Pläne stark. In Kapitel 4 werden dichte Zeitreihen multispektraler (Sentinel-2) und SAR-Daten (Sentinel-1) verwendet, um multitemporale Metriken, d.h. Maße der deskriptiven Statistik, zu berechnen und die Feuchtgebiete Albaniens landesweit zu kartieren. Die synergetischen Vorteile, die sich durch die Fusionierung von multispektralen und SAR-Daten für die Klassifikation ergeben, werden dabei herausgestellt. Das Endprodukt ist ein konsistentes Inventar der Feuchtgebiete Albaniens mit einer bislang einzigartigen räumlichen und thematischen Auflösung, das den Entscheidungsträgern sowie lokalen Behörden und Entscheidungsträgern dienen soll.

Kapitel 5 veranschaulicht, dass die Kilombero-Überschwemmungsebene in Tansania ein großes und bedeutendes Feuchtgebiet ist, das in den vergangenen Jahren infolge der weitgehend unkontrollierten Ausbreitung landwirtschaftlicher Flächen in seiner Ausdehnung und seiner Ökologie stark beeinträchtigt wurde. Ein schwaches Managementsystem sowie der steigende Bevölkerungs- und Nutzungsdruck, der auf den Feuchtgebietskomplex ausgeübt wird, haben zu Ökosystemdienstleistungsverlusten und zu Konflikten unter verschiedenen Interessensvertretern geführt. Um die Auswirkungen der Landnutzungsänderungen des Feuchtgebietes während der vergangenen 18 Jahre zu analysieren, wurden eine Zeitreihe (2000 bis 2017) thermaler Daten (MODIS) und Landnutzungsänderungskarten verwendet. Die drei für die Zeitreihenanalyse angewandten Modelle zeigen, wie landwirtschaftliche Praktiken die Landoberflächentemperatur in den landwirtschaftlich genutzten Gebieten sowie in den angrenzenden natürlichen Feuchtgebieten erhöht haben. Abschließend wird dargestellt, dass die Landoberflächentemperatur als Indikator für Tendenzen und Änderungen der Wasser- und Energieflüsse auf der Erdoberfläche infolge von Landnutzungsänderungen genutzt werden kann.


## Resumen

La importancia de los humedales y los servicios ecosistémicos que proveen está ampliamente reconocida por gobiernos y organizaciones científicas: los humedales hacen posible la existencia de miles de comunidades de personas dada su alta productividad; regulan los ciclos de nutrientes y la contaminación, produciendo agua limpia y contribuyendo a la formación de suelo; son sumideros de carbono 3 veces más potentes que los bosques terrestres; también son un hábitat clave para un 40% de las especies de la tierra, y proveen protección contra determinados desastres naturales, entre otros muchos servicios. Sin embargo, sus tasas de desaparición y degradación debido a actividades humanas siguen siendo altas. La agricultura y la construcción de presas son dos de las principales causas de degradación de humedales.

Debido a la estacionalidad de los humedales, su difícil acceso y sus características de ecotono, determinar su actual extensión y sus tendencias a lo largo del tiempo es una tarea compleja. Los sistemas de observación terrestres son la herramienta disponible más apropiada para monitorear sus patrones espacio-temporales (estacionalidad y tendencias a largo plazo) a escalas globales, y para estudiar los efectos que las actividades humanas causan en sus propiedades físicas y biológicas.

En esta tesis uso series temporales de imágenes radar (Sentinel-1), multiespectrales (Sentinel-2) y termales (MODIS) para mapear los patrones espacio-temporales de 5 áreas de estudio con humedales de diferentes características: 1) Fuente de Piedra, una pequeña laguna endorreica en el sur de España; 2) Camargue, un complejo sistema de marismas costeras en el sur de Francia; 3) Kerkini, un lago artificial en Grecia; 4) Albania, un país que alberga uno de los pocos sistemas de grandes ríos sin represar de Europa; 5) y Kilombero, un complejo sistema de pantanos, lagunas y llanuras inundables en Tanzania.

El en capítulo 1 describo los retos que derivan de las diferentes definiciones que existen de los humedales. También presento las tendencias globales de degradación que la mayoría de los humedales continúan experimentando en los últimos años. Continúo con una breve introducción de los sistemas de teledetección remota, análisis de series temporales, y sus aplicaciones a la investigación y gestión de los humedales. En los capítulos 2 y 3 implemento un algoritmo de detección de cambios para series temporales de imágenes radar, y comparo su efectividad con respecto a imágenes multiespectrales y métodos convencionales de detección de cambios. En el capítulo 2, los análisis se hacen en un ordenador local, pero en el capítulo 3 uso la plataforma Google Earth Engine, en la que los análisis se hacen en la nube. Con ello, muestro las ventajas de usar sistemas de computación en la nube para monitorear la estacionalidad de los humedales y otros cambios en la cobertura del suelo a corto plazo.

En los capítulos 4 y 5 trato con dos de las causas más comunes de degradación de humedales: la construcción de presas y la expansión de la agricultura.

Albania cuenta con uno de los pocos sistemas de ríos grandes sin represar que quedan en Europa. El país busca aumentar su capacidad para producir energía hidroeléctrica, pero organizaciones conservacionistas, científicas y locales se han posicionado en contra de algunos de estos proyectos. En el capítulo 4, uso series temporales de imágenes multiespectrales (Sentinel-2) y radar (Sentinel-1) en Google Earth Engine para generar métricas multitemporales y mapear todos los humedales del país. Primero, evalúo las ventajas sinérgicas de fusionar imágenes radar y multiespectrales en una clasificación supervisada. Finalmente, usando reglas lógicas genero un mapa de suficiente resolución espacial y temática para que pueda ser usado por sectores interesados y gestores.

Las llanuras inundables de Kilombero, en Tanzania, son un extenso complejo de humedales que han sido degradados durante los últimos años debido a la expansión incontrolada de la agricultura. Los escasos sistemas de gestión existentes no fueron capaces de controlar la

presión ejercida sobre los humedales, lo que causó una degradación de sus servicios ecosistémicos y numerosos conflictos sociales entre los múltiples sectores presentes en el área. Usando series temporales de imágenes termales (MODIS) desde 2000 hasta 2017 y mapas de cambios de usos del suelo, determino los efectos que estos cambios han tenido en el humedal durante los últimos 18 años. Comparo 3 modelos diferentes de análisis de series temporales y muestro cómo la expansión de la agricultura ha incrementado la temperatura superficial terrestre, no solo de la zona cultivada, sino también de zonas adyacentes aún naturales. Por último, demuestro como la temperatura superficial terrestre puede ser usada como un indicador para detectar tendencias y cambios en los flujos de agua y energía en la superficie.

# Chapter 1

# Introduction

*"Words have power. Words can light fires in the minds of men. Words can wring tears from the hardest hearts."*

*— Patrick Rothfuss, The Name of the Wind.*

## 1.1. The ontology of wetlands

Wetlands are ecosystems at the interface between land and water systems. This transitional character is known as "ecotone" (Mitsch and Gosselink, 2000). Wetlands are also present in a very wide variety of biomes: from the coastline mangroves of the tropics to the boreal peatbogs that the retreating glaciers leave, through the ephemeral oases in deserts. This causes one of the main challenges that wetland practitioners encounter: a definition, which has, inevitably, spatial connotations. It is not enough to define an area as a wetland without specifically delineating its boundaries. Besides, wetlands cannot be classified apart from other ecosystems using a common land cover type the way forests are identified by their trees, or grasslands by grass (Gallant, 2015). Although wetlands are expected to have water, that is not always the case due to the high variability in the water dynamics of many of them. This makes them a "moving target" from a remote sensing perspective (Gallant et al 2015). Their different water fluctuations can also determine their species composition by controlling, for instance, the dispersion of the seeds (Pétillon et al., 2010; Tyler et al., 2018; Valk, 2005). On the other hand, although in some wetlands the water is always present (e.g. some mangroves), it remains under a thick layer of vegetation. The water is then, not visible from space unless using long wavelength radar sensors.

Multiple definitions of wetlands have been developed. For Tiner (Tiner, 2015) wetlands are lands that are at least periodically wet during the growing season or the wet phase of the hydrological cycle in most years. This definition is very broad and incorporates very different types of ecosystems such as permanent water bodies, estuaries, peatlands, marshlands and mangroves, each with very different requirements, water regimes, species compositions and services provided. Other definitions require the presence of distinctive riparian vegetation to distinguish them from uplands and open ocean (Tiner, 2015). This, for example, excludes some ephemeral rivers -land forms of fluvial origin common in very arid regions (Scoones, 1992). They contain water only during brief flashfloods periods that can occur every several years and they have very little to no vegetation. Figure 1.1 shows a Sentinel-2 image of the river banks of the Vjosa River, in Albania. The Vjosa River forms part of one of the last unregulated river systems of Europe. The recurrence of flooding in their floodplains can be of several years.

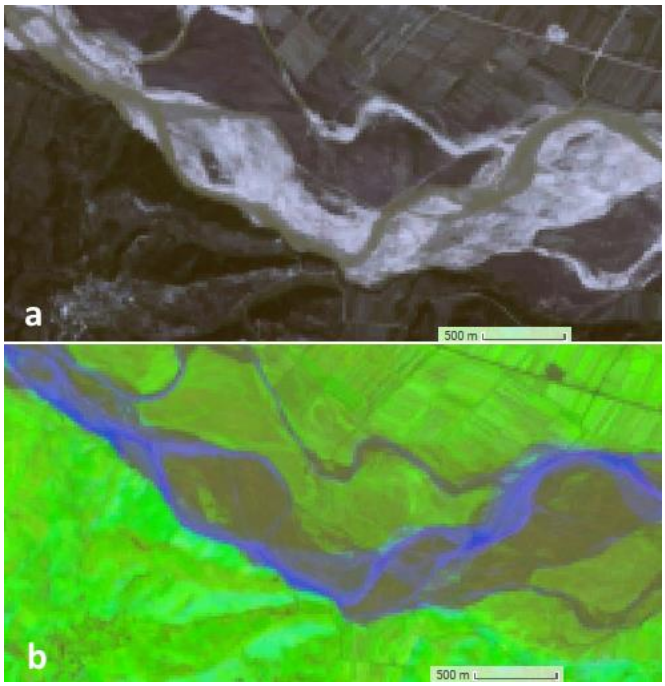


Figure 1.1: Natural color Sentinel-2 image (a) and multitemporal color composite (b) of the floodplains and riverbanks of the Vjosa River, in Albania. The RGB color composition of b is: bare soil index, vegetation index and water index. The red colors of b indicate lack of water during the period of image acquisition (2016-2018)

There is also a fundamental distinction between natural and artificial wetlands. For instance, a dam that has been constructed over a peatland might not provide the same ecosystem services in terms of carbon storage nor biodiversity than the original peatland, despite both are wetlands. On the other hand, artificial wetlands such as flooded agriculture should still be considered wetlands since they serve as habitat for wetland fauna, especially when their natural habitats are temporarily dry (Czech and Parsons, 2002). Besides, for an integrated management that considers the water-food-and energy nexus it is important to include agricultural areas, whether they are in use or not.

Definitions vary also between continents. In North America for instance, water bodies deeper than 2.5 m are not considered wetlands unless they host persistent self-supporting vegetation. On the other hand, the Ramsar convention considers as wetlands lakes that are up to 6 meters deep. These inconsistencies in definitions make global analyses challenging. Currently, there are 3 main classifications systems adapted to wetlands. In Europe, the Ramsar classification system is applied along with CORINE or MAES classification schemes (Fitoka et al., 2017). In African and Asian countries, the FAO classification system is more commonly used. The USA and part of Central and South America have adopted a

hierarchical classification based on Cowardin et al. (Cowardin et al., 1979). In this system, wetlands are divided into 5 major classes: marine, tidal, lacustrine, palustrine and riverine. They are further divided according to their vegetation cover and hydrologic regime. Some efforts to harmonize different classifications have been carried out using crosswalk tables between pairs of nomenclatures (Fitoka et al., 2017). Other efforts have been directed to build consistent data models that describe the Earth's surface characteristics in a conceptual and transferrable way. Examples of such methods are the FAO Land Cover Meta-Language (Di Gregorio, 2016), and the EAGLE European model (Arnold et al., 2013). They are both frameworks of rules that reconcile nomenclatures at different scales and geographic locations.

The classification of wetlands is sometimes a complex issue for which we need as much information as possible about their characteristics in terms of species and chemical compositions, but also about their inter- and intra-annual dynamics.

### 1.2. Wetland trends

The direct and indirect benefits that wetlands provide are well recognized by the scientific community and governmental institutions of most countries (Mitsch and Gosselink, 2000; Tiner, 2015, Ramsar, 2018;). For instance, wetland ecosystem services produce over 44.000 US$ $ha^{-1}$ $year^{-1}$ (Maes et al., 2016) while they cover between 3% and 8% of the land surface. When we compare it to the 3.278 US$ $ha^{-1}$ $year^{-1}$ produced by forests (Maes et al., 2016) wetlands importance becomes clearer (Amler et al., 2015). The recognition of wetland's value has materialized into policies and engineering works all over the world to try to compensate for their loss: from wetland restoration and rewetting campaigns to the creation of constructed wetlands and the proliferation of paludiculture –the sustainable use of peatlands for wet agriculture and forestry- (Joosten and Clarke, 2002). However, we keep losing wetland extent. Current global rates of wetland loss suggest that since the beginning of the $20^{th}$ century we have lost 64%-71% of our wetlands (Davidson, 2014), and 6% was lost only between 1993 and 2007 (Prigent et al., 2012). According to the Global Wetland Outlook report from Ramsar, wetland destruction rates have increased since 2000 (Ramsar, 2018).

World population is increasing at rates of ~1% annually (UN, 2015), and the consumption of certain goods per capita such as meat has also grown in all 5 continents (Ritchie and Roser, 2017). More people and higher consumption rates imply a need of increasing agricultural production. Due to war conflicts, land degradation and local declines of precipitation, populations are and will be pushed to occupy more productive areas (Scoones, 1992). As a

consequence, the world has experienced an expansion of subsistence and cash crops at the expense of forests, but also at the expense of wetlands (Figure 1.2) (Leemhuis et al., 2017; Ramsar, 2018). Most wetlands act as a sink of soil nutrients, making them very fertile. These land conversions have been more pronounced in Asia and Africa because of the fast increase in their populations and economic growth (FAO, 2003), but also because many European and North American wetlands are already cultivated, or were dried out in the past to fight vector-borne diseases. It is estimated that by 1985, over half of the European and North American wetlands were converted into intensive agriculture (Tiner, 2015).


Figure 1.2 Natural wetlands and grasslands converted to agriculture over the Kilombero Floodplan, Tanzania. The image on the right shows the burn scars from slash and burn practices carried out to boost grass growth. Credits: right Javier Muro, left Ian Games.

The case of peatland degradation is particularly notorious. Whereas they cover only 3% of the land surface, they store more carbon than forests, which cover 30% of the planet's surface (FAO, 2018). When turned into arable land and harvested, peatlands release greenhouse gases. It is estimated that in Europe alone, 125.000 $km^2$ of farmland extend over former peatlands (Joosten and Clarke, 2002). That is approximately 1/3 of the extension of Germany.

Mangroves are another type of wetland very efficient in carbon sequestration that is also disappearing due to timber extraction and aquiculture, especially shrimp farming. By 2001, 35% of the world mangroves had disappeared, and the current loss rate is around 1% per year (Valiela et al., 2001). As in peatlands, C stored below soil will be released if disturbed.

The fast economic and demographic growth of low and middle income countries often takes place without the infrastructure or knowledge needed to do it sustainably. The substitution

of subsistence agriculture by cash crops has rapidly pushed the boundaries of the agricultural frontier to formerly natural or semi natural areas. The case of the Kilombero Ramsar site, in Tanzania is a good example. In a basin of 40.240 $km^2$ and a Ramsar site of 8000 $km^2$, 2000 $km^2$ of wetlands and natural grasslands were transformed to cropland only between 2004 and 2014 (Leemhuis et al., 2017). Besides, another 1800 $km^2$ were reported to be transformed from grasslands to bare soil. An increase in the number of herders that practice slash and burn techniques could be partly behind this last conversion (Leemhuis et al., 2017).

Wetland degradation is not exclusive of tropical wetlands. Some emergent economies in western societies are looking to increase their electric energy production by increasing the number of hydropower plants (Vejnovic and Gallop, 2018). Although hydropower is often seen as a source of renewable energy and carbon sequestration, dams are often built at the expense of large extensions of natural wetlands. Dams also implement a physical barrier for aquatic species, barring catadromous (born in the sea, mature up the rivers) and anadromous (born in fresh waters, and mature in the sea) species from reaching their key reproductive habitats, and deprive coastal estuaries of sediments. Countries of the former Yugoslavia such as Albania, whose economy has been growing steadily for the last decade, are seeking to invest in small and large hydropower plants (EcoAlbania, 2017; Vejnovic and Gallop, 2018). Their rough orography makes them suitable for that. However, developers have found opposition from locals, scientists and Non-Governmental Organizations (NGOs). Some of the reasons argued against are: damage to their rich riverine and coastal ecosystems downstream, displacement of the population that live off those rivers and wetlands, finite lifespans of the dams because of sediment deposition, and the opacity with which sometimes these projects have been implemented (EcoAlbania, 2017; Vejnovic and Gallop, 2018). Hydropower supporters argue that it will boost national and local economies while complying with carbon emission commitments. Development institutions such as the World Bank finances hydropower projects with that purpose. Such macro-projects must be based on solid spatial and quantitative data. Else, the loss of ecosystem services that dam building often involves (including carbon sequestration) could out-weight the advantages it promises (Maavara et al., 2017). Unfortunately, the spatial information used is often limited to assess hydropower potentials according to discharge data, neglecting the loss of ecosystem services and not really assessing the life span of the dam (Condé et al., 2019; ECOWAS, 2017).

Accurate mapping products derived from Earth Observation Systems can help to determine the viability of such macro-projects by delivering information about:

- the habitats that will be lost to the dam up and down stream,
- the amount of population and agricultural surface that will be affected,
- the lifespan of the dam before sediment deposition reduces the storage volume,
- evapotranspiration rates throughout all the year.

### 1.3. Remote sensing of wetlands

National and local agencies need accurate spatial information to fulfill national and international reporting commitments such as the Ramsar convention, the Convention on Biological Diversity, the Sustainable Development Goals (SDGs), or the European Habitats or Water Framework Directives. Despite the wide availability of satellite data and the well acknowledged value of wetlands, many countries still lack a comprehensive inventory of wetlands at national level. One reason is the difficulty in accessing them, which makes fieldwork expensive. Another one is the difficult task of their definition that I explained in subchapter 1.1. But the greatest challenge that wetland practitioners have to deal with when mapping and monitoring wetlands is their spatio-temporal dynamics. As previously mentioned, from a remote sensing perspective wetlands are a "moving target" (Gallant, 2015). Many present variable inter- and intra-annual dynamics, and sometimes even daily dynamics (e.g. intertidal mudflats) that cannot be captured using a single image. In some occasions, these dynamics are a criterion to distinguish their typology (e.g. again, intertidal mudflats).

The last years have seen an increase in studies and projects that use mutitemporal imagery for wetland mapping (e.g. SWOS, GlobWetlands Africa, DeMo, GlobE). There are several events that have enabled the use of multitemporal imagery of optical, radar and thermal sensors. The first ones are the opening of the Landsats archive in 2008 and the launch of the Sentinel constellation in 2014. The release of huge amounts of spatial information has allowed scientists from all over the world to conduct landscape studies on a variety of ecosystems. The latest brake through has been the emergence of cloud computing platforms such as Google Earth Engine (GEE), the Amazon Web Services, or the Thematic Exploitation Platforms from the European Space Agency (ESA). All these events have given companies, researchers, NGOs or individuals free or affordable access to resources with which they could produce outputs used by policy makers, other researches or stakeholders.

This increase in mapping capabilities is showing perspectives that can change the way people see their surroundings, and broadens the audiences engaged by scientists through what is known now as viral cartography (Robinson, 2018).

During the next 5 sub-chapters I give a very broad overview of key remote sensing concepts. I start with an introduction to multispectral and thermal sensors followed by radar sensors, the different types of resolutions (spatial, spectral, radiometric and temporal), time series analysis, and finalized with a brief introduction to cloud computing platforms before presenting the thesis structure.

### 1.3.1. Multispectral and thermal sensors

All the multispectral remote sensing science is based on the principle that a specific cover type reflects the sun's energy with different intensities at different wavelengths of the electromagnetic spectrum. The variation of intensity reflected with the wavelength for that same cover type is called the spectral signature. The spectral signature allows classification algorithms to distinguish different cover types, the same way our own eyes can distinguish different colors and shades. Multispectral sensors divide the electromagnetic spectrum into portions often called "bands" that measure the intensity reflected by the Earth's surface at specific wavelengths. Figure 1.3 shows the different parts of the electromagnetic spectrum that are measured by three of the most common multispectral sensors still in orbit: Landsat-7 ETM, Landsat-8 OLI, and Sentinel-2 MSI. Figure 1.1 also shows three representative examples of spectral signatures for water (blue), vegetation (green) and bare soil (brown).

Table 1 shows a list of satellites (sometimes referred as platform) and the sensors they carry to help the reader distinguish between them.

Table 1.1 List of some of the most well-known satellites and the sensors they carry

| **Platform** | **Sensor** |
|---|---|
| Landsat-7 | Enhance Thematic Mapper (ETM) |
| Landsat-8 | Operational Land Imager (OLI) |
| Sentinel-2 | Multispectral Scanner Instrument (MSI) |
| Sentinel-1 | Synthetic Aperture Radar (SAR) |
| Sentinel-3 | Ocean and Land Color Instrument (OLCI) |
| Terra & Aqua | Moderate Resolution Imaging Spectroradiometer (MODIS) |

Bands 2, 3 and 4 of Sentinel-2 cover the same portion of the spectrum than our eyes (blue, green and red). Bands 5-8 cover the Near Infra-Red (NIR) portion, where healthy vegetation

reflects the radiation with higher intensities. Bands 11 and 12 are the Short Wave Infrared (SWIR), sometimes used in mineralogy studies or to identify roof types. The Thermal Infrared (TIRS) bands are capable of measuring the thermal properties of the terrain. They are not present in Sentinel-2, but we can find them in Landsat-7 (band 6) and Landsat-8 (bands 10 and 11). They are also present in other sensors such as Sentinel-3 Ocean and Land Color Instrument (OLCI) and the Moderate Resolution Imaging Spectroradiometer (MODIS) instrument on board of the Terra and Aqua satellites. Information from these bands is not commonly used for classification, but rather for estimating soil moisture content, drought, risk of fire, or the urban heat island phenomena. Bands 1, 9 and 10 of Sentinel-2 are used for detecting and masking clouds and haze, as well as bands 1 and 9 of Landsat-8.

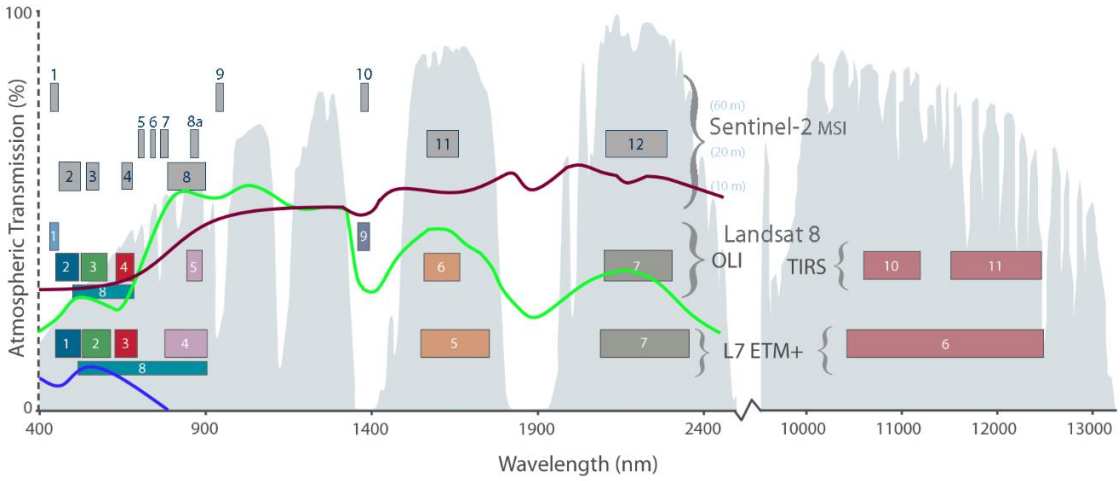


Figure 1.3: Spectral bands of Sentinel-2 and Landsat 7 & 8. Spectral signatures of vegetation, soil, and water are depicted in green, brown and blue respectively. Modified from (USGS, 2017).

### 1.3.2. Radar sensors

Radar sensors such as the Synthetic Aperture Radar (SAR) of Sentinel-1 work in a different way. Whereas multispectral sensors (passive) measure the sun's radiation reflected by the Earth's surface, SAR sensors (active) emit a signal of longer wavelength and measure the signal returned, also known as the backscatter. The intensity of the backscatter is dependent on the dielectric constant (function of the water content) and the geometry of the object. For example, water surfaces tend to have very low backscatter because they reflect away the SAR signal and nothing returns to the sensor. This is called specular behavior. Buildings tend to have high backscatter because the SAR signals bounces several times against horizontal

and vertical structures, and many return to the sensor. This is called double bounce behavior. But most surfaces do not exhibit specular nor double bounce behavior. Rather, the waves are often reflected in many different directions, some of which return back to the sensor and can be measured. This is called diffuse behavior.

While it is often said that radar sensors are weather independent, that is inaccurate. SAR sensors can penetrate through clouds and most atmospheric sources of noise, but rain and strong winds over water surfaces will distort the signal. It is more accurate thus to say that they are independent on cloud and illumination conditions. Their penetration range allows them to get information from underneath the canopy or from below the first layers of soil. This has allowed for example, to find inundated forest in the Amazonia (Hess et al., 2015), or to spot paleo-rivers under the Sahara (Skonieczny et al., 2015). Although the information provided by this magnitude-only form is limited, SAR sensors have many useful applications on their own. Instruments such as the RADARSAT-2 from the Canadian Space Agency emit a signal with 4 polarizations that can be decomposed into specular scattering, volume scattering and double bounce scattering. This allows to identify flooded vegetation because of its high double bounce scattering (White et al., 2015).

Change detection is a common application of multitemporal SAR data. Backscatter intensity data is sometimes used to measure significant changes in the land surface. However, it is difficult to control the rates of false positives and negatives, even if using histogram-based thresholding techniques such as the Otsu threshold method (Otsu, 1979) (Conradsen et al., 2016; Muro et al., 2016; Nielsen et al., 2017). Change detection results are often better when using coherence-based methods. The coherence is a property of radar interferometric pairs of images that is often used in change detection for disaster monitoring; if the positional and physical conditions of a land cover type have not changed between two acquisitions, their signal returned is coherent. This means that waves oscillate at unison, i.e. their phases are correlated. But if there was a significant change between acquisitions, both waves would not be coherent and a change would be flagged (Figure 1.4).

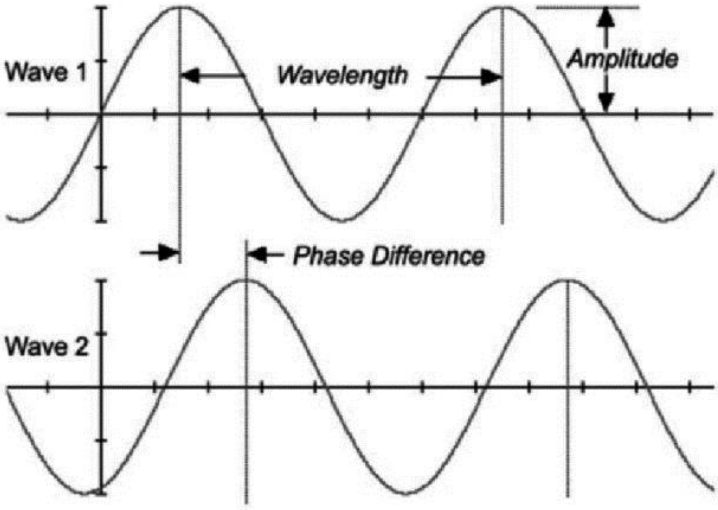


Figure 1.4: SAR basic concepts. SAR intensity signal is function of the amplitude, wavelength and phase. Two signals with same amplitude and wavelength might have a different phase. (Massom and Lubin, 2006).

Interpreting the change in coherence is itself a very challenging task because it is not directly transferable to increases or decreases of some biophysical parameter, like in a vegetation index. Besides, a change in coherence does not necessarily mean a change in the land cover. Many land covers types present an inherent low coherence, meaning that the coherence between two images close in time (e.g. 3 days) will be high, but it will progressively decrease in time due to phenomena other than land cover changes: phenological changes (leaf-off, leaf-on), or circumstantial events such as wind or rain that can temporarily increase the soil moisture. Although this seems to render coherence impractical for classification, some habitats can actually be distinguished by their coherence. Cities have very high coherence because their features remain static for long periods of time. Forests tend to have a lower coherence than cities, and crops the lowest coherence of the three because of all the different stages of the crop. For example, Brisco et al. (Brisco et al., 2017) extracted phase changes that are related to changes in water level in wetlands, and used it along with backscatter intensities to improve classification of marshes and swamps. Also, the ESA project SinCohmap (https://sincohmap.org/) aims at developing mapping methodologies that use coherences. Thus, the coherence represents additional temporal information that helps to classify different land cover types.

### 1.3.3. Resolutions; the importance of temporal resolution in wetland mapping

Spectral resolution refers to the pixel size. For example, one pixel of a Landsat image is 30 m x 30 m. Temporal resolution is associated with the frequency of pass of the platform where the sensor is; i.e. how many times the sensor flies over the same place. Sentinel-2 A and B have together a temporal resolution of 6 days at the equator. Spectral resolution indicates the number of bands a sensor has. Landsat and Sentinel-2 are called multispectral sensor because they have 6-12 bands. Hyperspectral sensors count on up to thousands of bands to produce very detailed information on the spectral behavior of land surfaces.

The remote sensing needs for monitoring environmental variables have often been focused on the spectral resolution to distinguish vegetation types with slightly different spectral signatures. In this regard, SAR and optical data are sometimes used together to generate additional information on the surface properties, increasing the spectral resolution of the information we work with. This is called data fusion. Efforts have also been directed towards improving the spatial resolution for capturing smaller features. Pan-sharpening is a technique that combines a higher resolution panchromatic band with a lower resolution multispectral image to produce a higher resolution color image. This technique is used by Google Maps, for instance.

Less attention is often paid to the temporal resolution, except for improving the chances of getting a single cloud free image. For rather static land covers such as forests one can get often good enough classification results using a single image. In agricultural areas, images from winter and summer seasons are used to distinguish single or double cropping practices. The seasonality of agricultural areas and forests is often rather constant. On the other hand, wetlands tend to have very variable inter- and intra-annual dynamics that depend on less constant patterns such as precipitation. One image from the dry season and another one from the wet season is not enough to capture all their dynamics. Besides, if the interpreter uses climatic criteria (temperature or precipitation) to define the driest and wettest periods of the wetland, the selection of the images might be biased and will not correspond with the true driest and wettest stages of the wetland. For instance, in Mediterranean ecosystems of the northern hemisphere the highest temperatures (*dies caniculares* or dog days) take place from late July to late August. However, many artificial and natural wetlands retain water during this period acting as a refuge for fauna or water storage. The lowest water table levels can take place from September until even December (see chapter 3 for an example). Another example are intertidal flats. Although they have constant dynamics, these do not correspond

with seasonal patterns. Therefore, besides good spatial resolution and multiple spectral bands, we need a high cadence of images capable of capturing the different stages that wetlands go through. Several studies have demonstrated how the use of multitemporal imagery improves classification accuracies in a variety of landscapes (Blaes et al., 2005; Brisco and Brown, 1995; Waske and Braun, 2009).

### 1.4. Time series analysis

Time Series Analyses (TSA) are commonly employed in economy, social or meteorological applications. Many important variables present seasonal patterns, such as flourishing of vegetation during the growth season and leave shedding during fall. A variable can also present temporal trends; i.e. increase or decrease on the long term. It can also present break points; points in time when an event triggers a change in direction or intensity in the trend (e.g. an already decreasing trend starts decreasing even faster). TSA study a variable distributed through time, its seasonality, its interannual trends and its break points. Remote sensing imagery is a good source of data for performing TSA due to their consistency, distribution and repeatability (Verbesselt et al., 2010). The United States Geological Survey (USGS) has recently re-pre-processed all their Landsat archive into a new collection of images optimized for TSA (USGS, 2017), and new sensors launched are designed to be compatible with data taken by older sensors. The ESA Sentinel-2 covers at least the same regions of the spectra than the Landsat constellation (Figure 1.1) except for the thermal bands. Sentinel-3 has been designed to continue the data collection of ENVISAT-MERIS, and Sentinel-1 grants continuity to the ENVISAR-ASAR archive (Künzer et al., 2015).

Remote sensing sensors can capture long term processes such as the seasonal patterns of the vegetation's phenology (shifts on the start or end of growing seasons) or greening trends caused by vegetation regrowth. They can also detect abrupt changes caused by single events such as forest fires. Trends in biophysical parameters affect the water and energy balances of the Earth's systems and the exchange of carbon, and sometimes, Earth Observation (EO) is the only reliable source of information we have to study the effects of climate change in our ecosystems (Wulder et al., 2012).

The opening of the Landsat archive in 2008 spurred the analysis of long term trends (Banskota et al., 2014; Wulder et al., 2012). It granted researchers access to long records of imagery at finer spatial resolution (30 m) with which to perform reliable TSA. For instance, it has allowed researchers to identify greening trends at planetary scale (Liu et al., 2015; Zhu et al., 2016), or to correlate deforestation with social variables such as movement of people

from rural areas to cities (DeFries et al., 2010). TSA are thus, essential to have an accurate understanding of the long term effects and trends that ecosystems experience naturally and anthropogenically.

Whether it is for classifications of land cover types or for TSA, it is necessary to account for the effect of the seasonality. Time series of data consists of three components; a seasonal pattern (e.g. greening in spring and browning in autumn), a long term directional trend (e.g. revegetation or degradation) and a remainder product of short term stochastic fluctuations (e.g. fires or clouds (Künzer et al., 2015)). Long term studies often look only at the directional trend, dismissing the short-term fluctuations. A convenient way of doing this is to summarize the stack of images into meaningful metrics such as the maximum, mean or minimum values and interpolate a linear or exponential trend (de Jong et al., 2011; Fensholt et al., 2015; Tian et al., 2016). These values are representative of the extreme or mean conditions of the ecosystem; i.e. fully vegetated or inundated, or bare and dry. There are other more complex methods that separate these time series components and can also identify break points within the time series. As mentioned earlier, break points are moments of sudden change within the time series triggered by some event. For instance, a forest fire will cause a break point in an Normalized Difference Vegetation Index (NDVI) time series and will trigger a greening trend afterwards due to forest regrowth. A popular tool to separate the time series components is the Breaks For Additive Season and Trend (BFAST) (Verbesselt et al., 2010). Figure 1.5 shows a time series of NDVI data of a forest over a period of 16 years. The result of the TSA shows a break point after the fourth year that was caused by a harvest, and is followed by a greening trend (*Ti*).

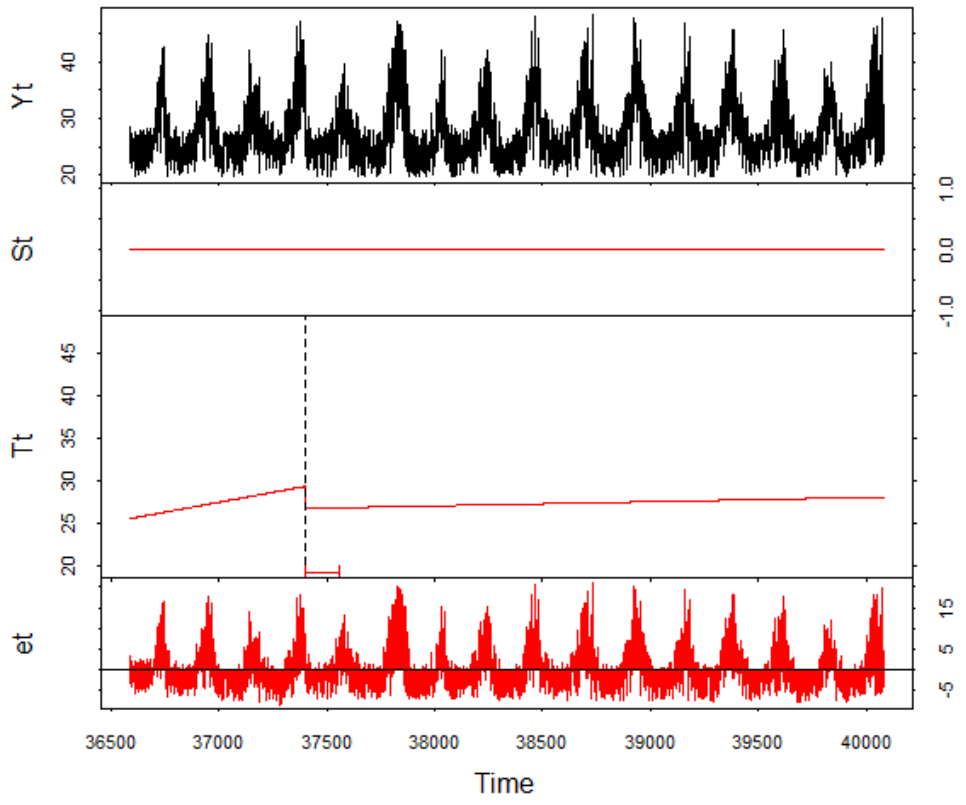


Figure 1.5 Decomposition of NDVI time series (*Yt*). *St* is the overall trend. *Tt* shows a breakpoint with greening trends before and after. The remainder is represented by *et*.

LandTrendr (Landsat-based detection of Trends in Disturbance and Recovery (Kennedy et al., 2010)) is another TSA algorithm. It performs a temporal segmentation of the data and extracts straight line segments to model the important features of the trajectory and eliminate the noise (Figure 1.6). LandTrend algorithm has been implemented in GEE and is used as frequently as BFAST (455 citations for LandTrendr against 469 of BFAST as of March 2019).

In a context where humans are slowly changing the climate, the study of long term trends is especially important. Observed trends are meaningless without understanding their underlying causes. For example, the reported overall greening trends on the Earth's surface (de Jong et al., 2011; Liu et al., 2015) are not exclusively indicative of reforestation patterns. Some of these greening trends are due to the use of fertilizers in agriculture and melting of snow cover at high latitudes (Zhu et al., 2016).

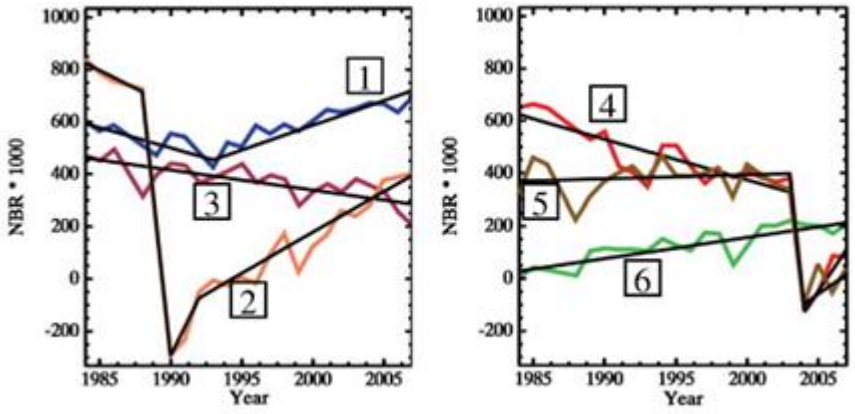


Figure 1.6 Extracted from (Kennedy et al., 2010). Black straight lines are segments that represent temporal trajectories. Colored lines are the spectral signals of SWIR, NIR and R from Landsat 5 and 3. Trajectories 1 and 3 show insect-related mortality. Trajectory 4 shows the insects' effect followed by fire. Trajectory 2 is a clear-cut harvest, 5 is stability followed by fire, and 6 is recovery from prior fire.

### 1.5. Cloud computing platforms

Even at free cost, global scale analyses at finer spatial resolution or TSA of satellite imagery required the download, preprocessing and processing of several terabytes of information. This created an important cap in computation power and expertise (e.g. information technology skills). This cap has triggered the last breaking point in remote sensing science: easy to access and easy to use cloud computing platforms (Gorelick et al., 2017). These platforms such as GEE, Amazon Web Services or the Copernicus Thematic Exploitation Platforms are rapidly evolving the way we deal with data, and changing our perspective and insights. This has been called the Big Data paradigm shift, where instead of bringing the data to the algorithms, the algorithms are being taken to the data. For instance, Hansen et al. (Hansen et al., 2010) estimated global forest losses and gains using 30 years of Landsat imagery. Later on, the procedure was optimized and updated using GEE, creating a living map of forest cover dynamics (Global Forest Watch https://www.globalforestwatch.org/). Cloud computing platforms have open the possibility to establish operational monitoring systems not only for forests, but also for wetlands and other ecosystems (e.g. Global Mangrove Watch).

Künzer et al. (Künzer et al., 2015) compiled a list of the greatest challenges for remote sensing based TSA. Cloud computing platforms help to address most of these (Table 1.2), sparing the analyst from downloading and preprocessing tasks.

Table 1.2: Challenges for remote sensing based time series analysis and how cloud computing platforms have solved some of them. Modified from (Künzer et al., 2015).

| **Challenge related to** | **Possible manifestation** | **Solved by cloud computing platforms** |
|---|---|---|
| Data policy | Acquisition plan | No |
| | Restricted access to data | Yes |
| | Composite products | Yes |
| Sensor | Orbital drift | Partly; erroneous data can be filtered out |
| | Erroneous sensor calibration | Partly; erroneous data can be filtered out |
| | Sensor degradation | Partly; erroneous data can be filtered out |
| | Geolocation errors | Partly; erroneous data can be filtered out |
| | BRDF effects | Partly |
| Location | Cloud cover | Yes, via composites |
| | Water vapor and aerosols | Yes, via composites |
| | Polar night | |
| | Extreme terrain | |
| | Sunglint effects | Yes, with filter operations |
| | Anisotropy effects | |
| | Sudden, disconnected subsidence | Very rare |
| Processing | Download and Storage | Yes |
| | Computing power | Yes |
| | IT skills | Yes |
| | Mathematical statistical skills | Yes |
| | Monthly or annual reprocessing | Yes |
| | Long term preservation | Yes, now data is stored in additional places |

Most of the challenges solved are related to processing, but these are not the only ones. The ever present problem of cloud cover can be partly solved by creating composites i.e. taking the best pixel of each image and synthesize a cloudless image. Erroneous data can be filtered out more easily using the metadata, and most platforms are free or have affordable prices when compared to the price of individual images some years back (about 600 US$ per Landsat image). After the suggestion of the US government in April 2018 of start charging for popular EO data, researchers started to calculate how much their research would cost if they had to pay per image, a cost that would be paid through the cloud computing platform. With most of us using several thousands of images, prices in US$ could easily hit 9 digit numbers. Gärtner (Gärtner, 2018) even gives a GEE code to estimate how much your research would cost.

### 1.6. Research questions

Our society has never had before such large amounts of information about our planet and its dynamics, nor we have deteriorated its resources at such high rates. Despite the well acknowledged value of wetlands, they continue to disappear due to weak management systems and uninformed policy making. Decision makers need accurate, well-timed and ready-to-use data to understand the impact that human actions cause on Earth's systems, to develop informed policies, and to justify decisions for sustainable development. The aim of this thesis is to implement and assess how new remote sensors and technologies can be used to understand wetland dynamics, and how to use them to support wetland management.

My research uses 5 study areas covering a rather broad range of environments:

- Three intensively managed wetlands in Europe (a coastal wetland and an endorheic wetland in chapter 2, and an artificial wetland in chapter 3),
- A set of pristine and less regulated river systems in Albania with potential for hydropower (chapter 4),
- A large system of swamps, rice fields, and floodplains in Tanzania that have been recently degraded.

Using these 5 sites I address the following research questions:

1) How can we use the novel EO products and technologies to improve our understanding of wetland dynamics?
2) How can we condense large amounts of spatiotemporal information into products meaningful and usable by wetland practitioners?
3) Which methods are better to track the effect of human activities on wetlands?
4) How can we apply them to solve societal issues created by a lack of spatial information?

## 1.7. Thesis structure

To address the 4 research questions, I set the following 3 objectives:

### 1.7.1. Objective 1: Evaluation of Sentinel-1 to monitor short-term dynamics in wetlands

Sentinel-1 is the first SAR sensor of open access with the sufficient resolution and cadence to be used for systematic monitoring of wetlands' complex dynamics. In chapter 2 and 3 I implement a novel algorithm for change detection of time series of SAR imagery in three wetlands of different characteristics. I test it against conventional methods that use multispectral imagery and determine its advantages and flaws. In chapter 4, I use multitemporal metrics of Sentinel-1 to generate a classification of wetlands at national scale.

### 1.7.2. Objective 2: Develop and test cloud computing methodologies for wetland mapping and monitoring

Wetland practitioners often hit two caps that hinder the applications of remote sensing in management; limitations in technical capacities and in computational capacities. Powerful computers and programming skills are often needed to process large amounts of images required to cover the complete dynamics of wetlands. In chapters 3 and 4 I use the Google Earth Engine platform to process year time series of Sentinel-1 and Sentinel-2 to produce maps representative of the seasonal dynamics of wetlands.

### 1.7.3. Objective 3: Use time series of EO imagery to understand wetlands dynamics, the effects of human actions on them and support decision making

For this objective I focus on the application of dense time series of EO data to support sustainable management of wetlands. I address this in chapter 4, but more thoroughly in chapter 5. Chapter 5 focuses on the use of longer time series to track the effects of human actions on the biophysical properties of a wetland. I use the results of the mapping products to show how lack of spatial information and weak land management systems can jeopardize wetlands' status and ecosystem services.

### 1.7.4. List of publications

**Chapter 2: Short-term change detection in wetlands using Sentinel-1 time series.**

Muro, J., Canty, M., Conradsen, K., Hüttich, C., Nielsen, A., Skriver, H., Remy, F., Strauch, A., Thonfeld, F., Menz, G., 2016. Short-term change detection in wetlands using Sentinel-1 time series. Remote Sensing 8, 795. https://doi.org/10.3390/rs8100795

**Chapter 3: Mapping wetland dynamics with SAR-based change detection in the cloud.**

Muro, J., Strauch, A., Fitoka, E., Tompoulidou, M., Thonfeld, F., 2019. Mapping wetland dynamics with SAR-based change detection in the cloud. IEEE Geoscience and Remote Sensing Letters 1–4. https://doi.org/10.1109/LGRS.2019.2903596

**Chapter 4: Multitemporal optical and radar metrics for wetland mapping at national level in Albania.**

Muro, J., Varea, A., Strauch, A., Guelmami, A., Fitoka, E., Thonfeld, F., Diekkrüger, B. Waske, B. Submitted on July 2019. Multitemporal optical and radar metrics for wetland mapping at national level: A National Service case for Albania. Heliyon. Currently under review.

**Chapter 5: Land surface temperature trends as indicator of land use changes in wetlands.**

Muro, J., Strauch, A., Heinemann, S., Steinbach, S., Thonfeld, F., Waske, B., Diekkrüger, B., 2018. Land surface temperature trends as indicator of land use changes in wetlands. International Journal of Applied Earth Observation and Geoinformation 70, 62–71. https://doi.org/10.1016/j.jag.2018.02.002

# Chapter 2

## Short-Term Change Detection in Wetlands Using Sentinel-1 Time Series

Remote Sens. 8 (10), 795;

September 2016

Special issue "Monitoring of Land changes"

doi:10.3390/rs8100795

Javier Muro, Morton Canty, Knut Conradsen, Christian Hüttich, Allan Aasbjerg Nielsen, Henning Skriver, Florian Remy, Adrian Strauch, Frank Thonfeld and Gunter Menz

*"Shifting our focus and give the "when" the same weight as the "what" won't cure all our ills, but it is a good beginning."*

*—Daniel. H Pink. WHEN, the scientific secrets of perfect timing.*

**Abstract**

Automated monitoring systems that can capture wetlands' high spatial and temporal variability are essential for their management. SAR-based change detection approaches offer a great opportunity to enhance our understanding of complex and dynamic ecosystems. We test a recently-developed time series change detection approach (S1-omnibus) using Sentinel-1 imagery of two wetlands with different ecological characteristics; a seasonal endorheic wetland in southern Spain, and a coastal wetland in the south of France. We test the S1-omnibus method against a commonly-used pairwise comparison of the same consecutive images to demonstrate its advantages of controlling the rate of errors of omission and commission. Additionally, we compare it with a pairwise change detection method using a subset of consecutive Landsat images for the same period of time. The results show how S1-omnibus is capable of detecting in space and time changes produced by water surface dynamics and agricultural practices, whether these changes are sudden or gradual. When compared to the Landsat-based change detection method, both show an overall good agreement, although certain landscape changes are detected only by either the Landsat-based or the S1-omnibus method. The S1-omnibus method shows a great potential for an automated monitoring of short time changes and accurate delineation of areas of high variability and of slow and gradual changes.

## 2.1. Introduction

Wetlands are often described as ecotones, transitional habitats situated between dry land (upland) and water bodies (Mitsch and Gosselink, 2000). They are very diverse ecosystems, ranging from permanent water bodies to lands that remain completely dry over several months, or areas where water is below a dense vegetation cover, such as peat bogs or mangroves (Tiner, 2015). Besides their spatial variability, some wetlands present a high temporal variability (e.g., temporal water bodies and waterways or intertidal flats). Wetlands also deliver a wide and well-recognized array of ecosystem services: flooding, drought and erosion amelioration, habitat for many keystone species, food and water supply and $CO_2$ sequestration, among many others (Henderson and Lewis, 2008). Thus, automated monitoring systems of wetlands that can capture their high temporal and spatial variability

are essential for wetland management and for the quantification of the ecosystem services they provide (Brisco et al., 2013).

Landscape spatial patterns, and especially those of wetlands, are rarely static due to intra-annual changes in their ecosystem properties, whether they are caused by natural or by anthropogenic factors (Coppin et al., 2004). Mapping of ecosystems and of long-term Land Use and Land Cover Change (LULCC) patterns may be biased by such intra-annual changes in different surface properties (e.g., phenology, hydrology, agriculture, etc.). These surface dynamics sometimes produce transitional states and fine-scale mixtures of classes that may hinder classification and long-term change detection. Some approaches have used fuzzy classifiers and multitemporal optical data to produce fractional cover maps of different wetland classes, capturing these transitional states [6] (Reschke and Hüttich, 2014). Additionally, (Dronova et al., 2015) proposed the term "Dynamic Cover Types" (DCT) to refer to areas of frequent periodic or seasonal change. Examples of DCT in the context of wetlands would be seasonally-inundated floodplains and inland valleys, inter-tidal flats, temporal water bodies and waterways, fields of rice and reeds when harvested or slow regrowth of some vegetation covers after flooding or harvesting events. Many of these DCT often give rise to unique species assemblages and temporal shifting of species distributions and compositions (Parrott and Meyer, 2012; Watson et al., 2014). In turn, this may also affect other ecosystem functions through water and nutrient cycling.

The availability of satellite images acquired repetitively over long periods of time has allowed the proliferation of numerous change detection studies in fields such as LULC change, forest monitoring (deforestation, regeneration, forest fires, insect defoliation), urban sprawl, landscape change and crop monitoring, among many others. Lu et al. (2004) provides a wide array of examples of applications in each mentioned field. Most of these techniques make use of spectral data from optical sensors to monitor long-term changes. Despite their widely-spread use and the good results obtained, optical-based change detection methods have an important disadvantage; they are hampered by illumination effects and cloud conditions, a challenge that becomes very problematic in sub-humid to humid tropics, especially during rainy seasons or when the temporal resolution is not high.

SAR-based change detection methods are cloud and illumination independent, but have however been much less used because of their limited temporal and spatial availability, higher costs and more intensive processing requirements (Hecheltjen et al., 2014). With the recent launch of ESA's Sentinel-1 satellite and the free access to its products, SAR-based change

detection methods can now be more efficiently used to overcome some of the restrictions of optical-based methods. The high temporal resolution (six days considering Sentinel-1A and -1B at the Equator), high spatial resolution and wide swath allow for a much needed operational change detection system, cost-free, cloud-proof and illumination independent.

SAR-based change detection methods can separate LULC classes that are especially difficult to distinguish, such as rice fields from wet grasslands. Some researchers have successfully used SAR data for rice mapping using time series (Bouvet and Le Toan, 2011; Nguyen et al., 2015). Their success relies on the detection of the changes in plant morphology that take place during the three growing phases of rice per harvest, as opposed to the less frequent changes in other crops and other non-agricultural wetlands and grasslands (Nguyen et al., 2015).

The operational availability of change detection approaches will be a valuable addition to currently ongoing developments of operational wetland-monitoring services, e.g., in the European "Satellite-based Wetland Observation Service" (SWOS) Horizon 2020 project (www.swos-service.eu). Further, it is an important contribution to the development of the Global Wetland Observation Service that is currently carried out in the framework of the Group on Earth Observations together with the Ramsar Convention on Wetlands and other global stakeholders (https://www.earthobservations.org/index).

In this paper, we apply a polarimetric SAR-based time series change detection technique in two highly dynamic natural and semi-natural landscapes. We use a new method published by Conradsen et al. (2016) where change detection is carried out by performing a simultaneous test of the hypothesis of homogeneity for a series of SAR images. Our research was conducted with three specific objectives in mind. First, we show the potential of using the time series change detection algorithm presented in Conradsen et al. (2016) (referred to as S1-omnibus) and Sentinel-1 time series to capture short-term changes in highly dynamic areas. Second, we evaluate the performance of S1-omnibus vs. a pairwise comparison of consecutive images. According to Conradsen et al. (2016), it is expected that a larger proportion of change will be detected using the whole time series as opposed to the commonly-used pairwise approach. Third, we compare the performance of S1-omnibus with a Landsat-based change detection approach. Since optical and SAR instruments detect different properties of objects, it cannot be considered as a validation process, but it is still relevant to compare the performance of the new S1-omnibus algorithm with more extended and common approaches.

### 2.2. Study Areas

Many wetlands experience several short-term changes mostly related to water surface dynamics (seasonal water bodies and water ways, intertidal flats, temporarily inundated forests, among others) or related to human activities, such as agriculture or salt production. To test the capacities of the S1-omnibus method we chose two highly dynamic wetlands with different characteristics.

The first one is the Lake of Fuente de Piedra, in southern Spain: an endorheic salty water body of ~13 $km^2$ and less than 1 m deep. Its catchment occupies around 150 $km^2$, but we study all of the changes within a rectangular area of 490 $km^2$ (Figure 2.1). The lake is fed by two streams, although the most important supply of water is ground water inputs and rains (Conde-Álvarez et al., 2012). Landscapes in the uplands are dominated by olive groves and herbaceous crops (e.g., wheat and barley), and the lake was used for salt extraction during the last century. Currently, it is a Ramsar site and a nature reserve. It usually dries out at the end of spring and fills up again with the first autumn rains. Despite its small size, it is a migratory stopover for many bird species and the second largest breeding ground in Europe for the European flamingo (*Phoenicopterus roseus*) (Geraci et al., 2012).

The second study area is the largest flamingo breeding ground in Europe; the French Camargue. It is a coastal wetland of 130 $km^2$ located in the south of France, between both arms of the Rhône River Delta. It belongs to a larger and complex system of coastal wetlands and lagoons that have been flooded, dredged, canaled and cultivated during many centuries. Currently, it is a Ramsar site and a national reserve, but water is still pumped in and out for salt production and for keeping some lagoons filled during summer in certain areas. The change detection method was applied to a rectangular area of 3500 $km^2$ (Figure 2.1). Landscapes are dominated by large permanent water bodies, rice fields and other crops, salt flats and marshes near the coast and pastures for extensive cattle. The salinity of the water bodies varies depending on the rain, but it generally increases from north to south. The deepest water body, the Vaccarés lagoon, in the center of the wetland, has a maximum depth of 2 meters (Britton and Podlejski, 1981). Both study areas are test sites of the SWOS project, which allowed access to ground information, as well as to mapping products that were used for the interpretation of the results (e.g., LULC maps from Figure 2.1). In these as in many other wetlands over the world, the presence/absence and quality of their water is influenced by land uses (mainly agricultural) in their area of hydric influence. Thus, we analyze not only the areas designated as wetland in our two study sites, but also their surroundings.

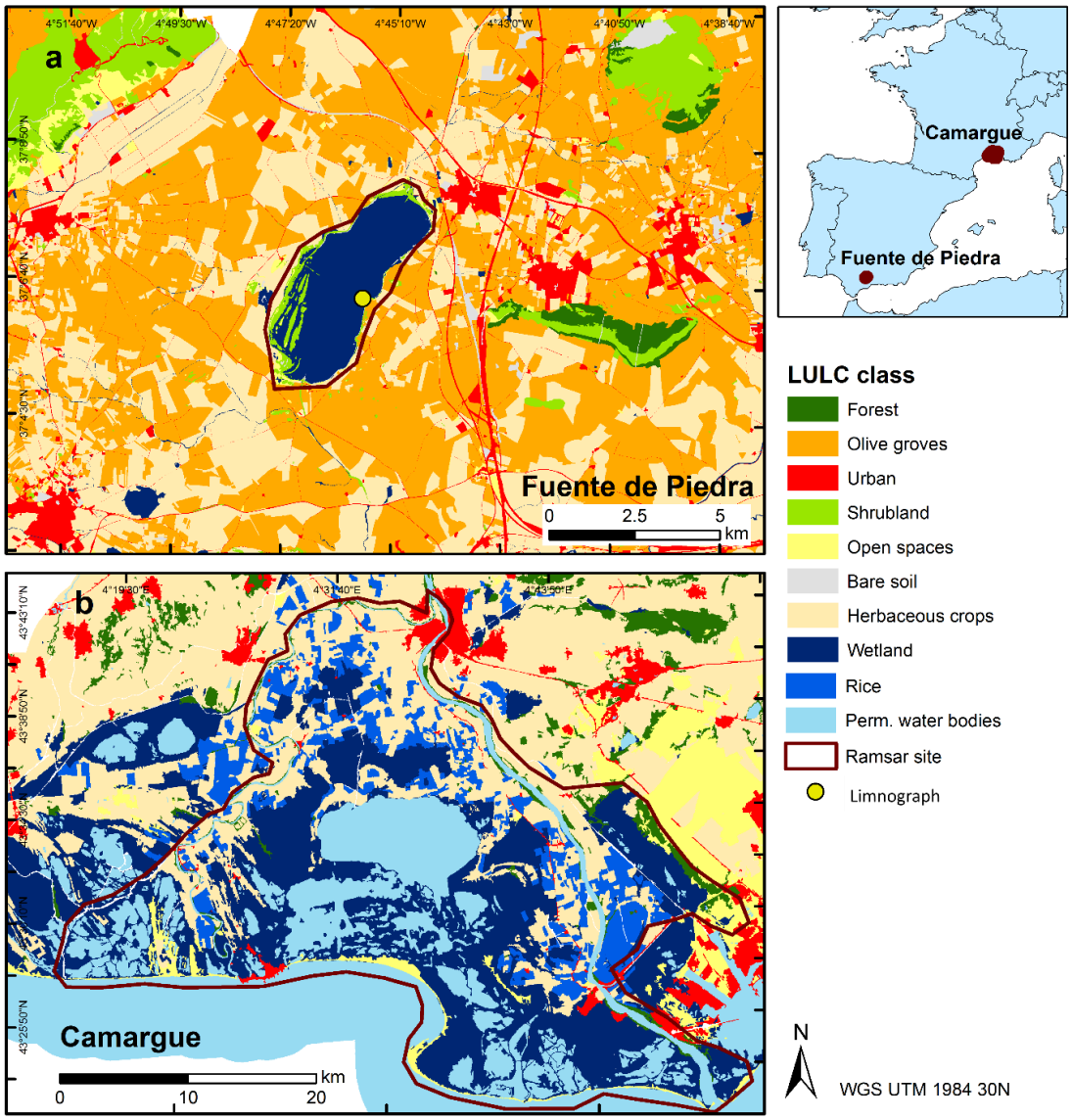


Figure 2.1. LULC maps of the study areas (a,b). In Fuente de Piedra (a), the classification has been performed using photointerpretation and field inventories by the Spanish authorities (www.siose.es). The classification in Camargue (b) is a product of the project SWOS, elaborated by Tour du Valat using Landsat images for 2015 and field inventories (www.tourduvalat.org). In order to make both classification compatible and for the sake of simplification, some classes have been merged, e.g.: the class "wetlands" includes marshlands, temporal water bodies and salt marshes; "open spaces" includes areas with little vegetation, dunes and some pastures; "urban" includes all sorts of pavement or concrete; "forests" includes coniferous, as well as broad-leaved forests.

## 2.3. Materials and Methods

### 2.3.1. Imagery and Preprocessing

We used a set of several Sentinel-1 images from the ESA Scientific Data Hub acquired for 2014/2015 at a monthly resolution and with the same orbit path (Table 2.1). Sentinel-1 imagery is offered in four different swath modes, three product types and with different polarization options. The swath mode used here is the Interferometric Wide (IW) swath, and the product type is the Single Look Complex (SLC), which consists of focused SAR data that uses the full C signal bandwidth and preserves the phase information. In the other product type for land masses, the Ground Range Detected (GRD), the phase information is lost, and thus, it cannot be used to produce the covariance matrix needed during the change detection. We used dual polarimetric images (VV-VH), which allow the measurement of the polarization properties of the terrain in addition to the backscatter that could be measured from a single polarization. The raw images were preprocessed in the Sentinel Application Platform (SNAP). The sub-swaths of the SLC image were split and de-bursted separately, and then, a 2 × 2 polarimetric matrix image was calculated. To reduce the speckle noise inherent to SAR data, a multilook spatial averaging was applied with 8 range looks and 2 azimuth looks. Finally, a terrain correction using 3 arcsec SRTM and bilinear interpolation was applied, resulting in an image with a nominal pixel size of 30 m × 30 m. The final polarimetric and multilooked matrix image that is used during the change detection has the form:

$$c2 = \begin{pmatrix} \langle |S_{vv}|^2 \rangle & \langle S_{vv} S_{vh}^* \rangle \\ \langle S_{vh} S_{vv}^* \rangle & \langle |S_{vh}|^2 \rangle \end{pmatrix}$$

where $s_{tr}$is the scattering amplitude for transmitted polarization *t* and received polarization *r*, $\langle \ldots \rangle$ denotes multilook averaging and *v* and *h* correspond to vertical and horizontal polarizations, respectively. When multiplied by the number of looks, the matrix *c2* is known to follow a complex Wishart distribution parameterized by a covariance matrix $\sum$ (Conradsen et al., 2003).

Table 2.1 Sentinel-1 and Landsat 7, 8 datasets used. Images used for the S1-omnibus and Landsat-based CVA change detection comparison are highlighted. Landsat 7 images are marked with an asterisk (*).

| Fuente de Piedra (Spain) | | Camargue (France) | |
|---|---|---|---|
| **Sentinel 1** | **Landsat** | **Sentinel 1** | **Landsat** |
| | | 11-11-2014 | |
| | | 02-12-2014 | |
| | | 31-01-2015 | |
| | | 24-02-2015 | |
| 15-03-2015 | 09-03-2015 * | 08-03-2015 | |
| 20-04-2015 | 02-04-2015 | 01-04-2015 | 15-04-2015 |
| 26-05-2015 | 12-05-2015 * | 07-05-2015 | 17-05-2015 |
| 19-06-2015 | 05-06-2015 | 12-06-2015 | 02-06-2015 |
| 25-07-2015 | 07-07-2015 | 18-07-2015 | 20-07-2015 |
| 18-08-2015 | 16-08-2015 * | 18-08-2015 | 21-08-2015 |
| 23-09-2015 | 25-09-2015 | 28-09-2015 | 06-09-2015 |
| 17-10-2015 | | | |
| 22-11-2015 | 12-11-2015 | | |
| 28-12-2015 | | | |
| 21-01-2016 | | | |
| 26-02-2016 | | | |

### 2.3.2. SAR-Based Change Detection

The change detection algorithm applied in this research takes advantage of the known distributions of the observations *c2*. It detects changes within a series of *k* uncorrelated multilooked images by testing, pixel-wise, hypotheses on the values of the parameters $\sum_i, i = 1 \ldots k$ characterizing the distributions. To test the null (no-change) hypothesis $H_0 : \sum_1 = \sum_2 = \ldots = \sum_k$ against all alternative (change) hypotheses, we use an omnibus test statistic:

$$Q = \left[ k^{2k} \frac{\prod_{i=1}^{k} |c2_i|}{|C2|^k} \right]^n$$

where n is the number of looks and where $C2 = \sum_{i=1}^{k} c2_i$. In order to set the significance for the test, the distribution of $Q$ must be known. Approximate values are given in Conradsen et al. (2016), the accuracy of which increases with the number of looks. We estimated the best equivalent number of looks to be 12, out of the total 16 (8 range × 2 azimuth). In addition, Conradsen et al. (2016) derive a factorization of the test statistic $Q$, which allows the determination of the interval in which changes occur within the time series. Thus, we test, for example, the null hypothesis that, given $\sum_1 = \sum_2 = \ldots = \sum_{j-1}$, it is also true that $\sum_1 = \sum_{j-1}$,, against the alternative that $\sum_1 \neq \sum_{j-1}$. If the null hypothesis is rejected, the

sequential testing procedure is restarted at the next observation. In this way, all time intervals in which changes occur can be identified.

To assess the capabilities of the omnibus time series change detection algorithm, we applied it to a series of consecutive Sentinel-1 images spanning one year (approximately one image per month; see Table 2.1). Using the same set of images, we compared the results of the S1-omnibus approach against the standard pairwise change detection approach, also based on the Wishart distribution (Conradsen et al., 2003). All of the changes detected between pairs of consecutive images were summed up and compared. All changes are at the 1% significance level in the per pixel change hypothesis tests.

The analysis was performed using an innovative open source software implementation available at http://mortcanty.github.io/SARDocker/. The python scripts for the change detection algorithms are encapsulated, together with all prerequisites, in a Docker container. No special software is required. The user interacts with the software in his or her browser in an Jupyter notebook served from within the Docker container.

We used data from a limnograph and pluviometer placed towards the center-east of the lake in Fuente de Piedra to interpret the results of S1-omnibus.

### 2.3.3. S1-Based and Landsat-Based Change Detection Comparison

We used a smaller set of cloud-free Landsat 7 and 8 images acquired as closely as possible in time to the Sentinel-1 imagery for comparison purposes (Table 2.1). We performed an Iteratively Re-Weighted Multivariate Alteration Detection (IR-MAD) (Canty and Nielsen, 2008) to radiometrically adapt all of the Landsat images to the last one. Using Change Vector Analysis (CVA) (Malila, 1980), we extracted the changes between each pair of consecutive images and sum them up to create a Landsat-based change mask. Since there was not always a cloud-free Landsat image per Sentinel-1 image, for this comparison we used only the Sentinel-1 images for which we had a corresponding cloudless Landsat image to create a Sentinel-1-based change mask and compare it to the Landsat-based change mask. This involved images from the period from March 2015–November 2015 for Fuente de Piedra, and from April 2015–November 2015 for Camargue. Table 2.1 shows detailed information about the images used for the different procedures. Due to the Scan Line Corrector failure in Landsat 7, images taken after June 2003 have no-data pixels along their edges, but the nadir of the scenes does not suffer such data loss. The test site of Fuente de Piedra is located

at nadir, and thus, it was possible to use Landsat 7 images there. Only Landsat 8 images were used over the Camargue.

## 2.4. Results

### 2.4.1. S1-Omnibus Approach

S1-omnibus allows one to identify in time the changes detected within the time series. The output is a raster with one band per time interval analyzed (i.e., number of images -1). Each band contains the changes detected in each time interval. Figure 2.2 shows the results obtained for Fuente de Piedra in a closer look at the lake.

The changes detected in the outer part of the lake between March and April (Figure 2.2a) suggest that it starts drying there. Between April and May (Figure 2.2b), most of the lake dries out, which matches with the reduction in the water table recorded by the limnograph. No major changes are detected until October (Figure 2.2g), when the first autumn rains occur. These precipitations are not strong enough to raise the water table levels, but they seem to be enough to cause changes in the dry soils of the wetland. Note that the image from 17 October 2016 was taken right before major precipitations during 18 October 2016 (28.5 mm). Changes detected between October and November (Figure 2.2h), November and December (Figure 2.2i) and December and January (Figure 2.2j) match the records of the limnograph.

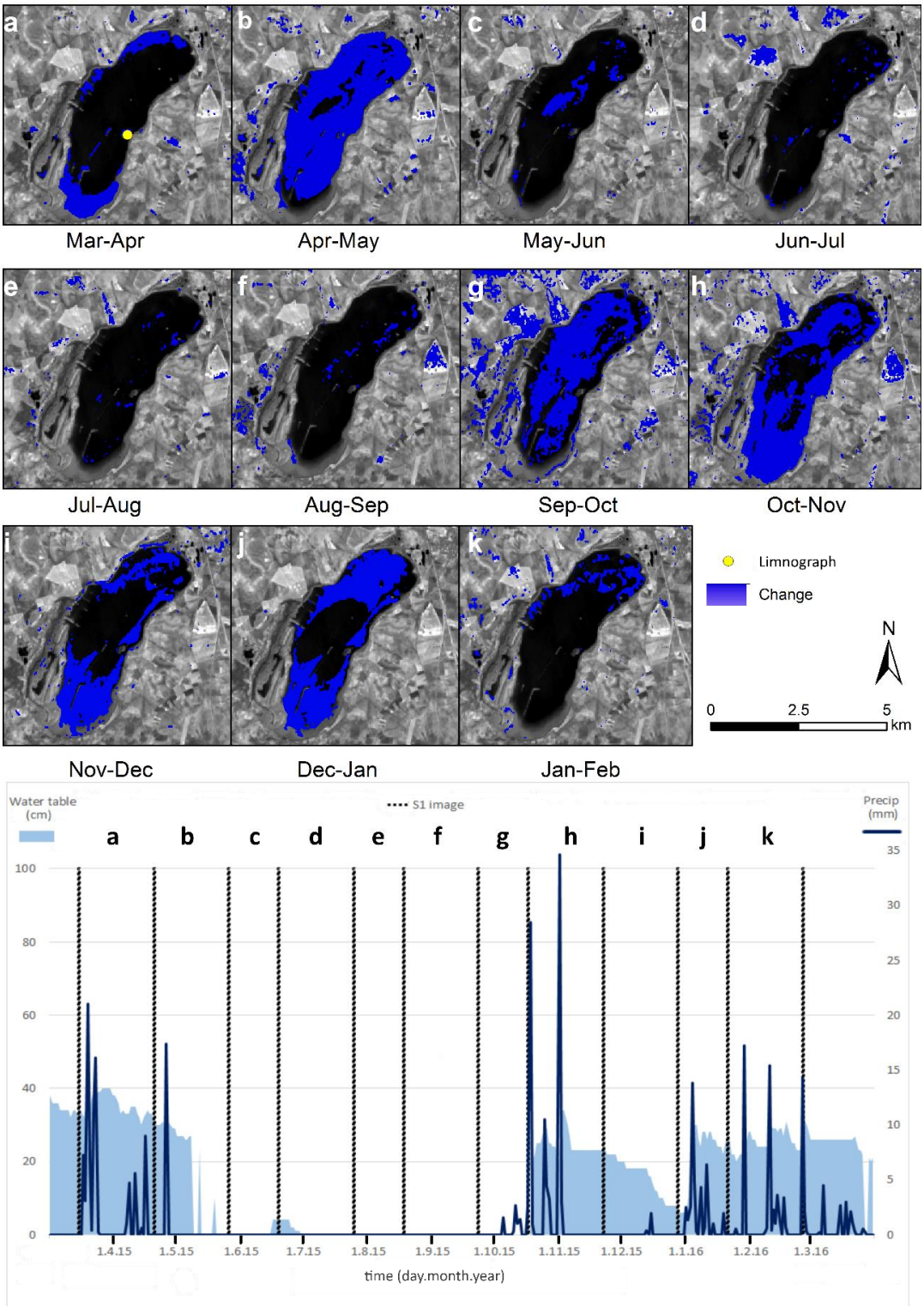


Figure 2.2 Month by month changes detected by S1-omnibus in the lake of Fuente de Piedra marked with letters a–k in the upper left corner of each image. Their corresponding water table and precipitation levels can be found in the chart. Water table and precipitations were recorded by a limnograph and pluviometer at the center of the lake, marked with a yellow circle in "a". The same Landsat 8 band 4 image has been used as the background in a–k.

A second output of S1-omnibus is the frequency of short-term change (Figure 2.3). It shows where multiple changes have been detected and how many.

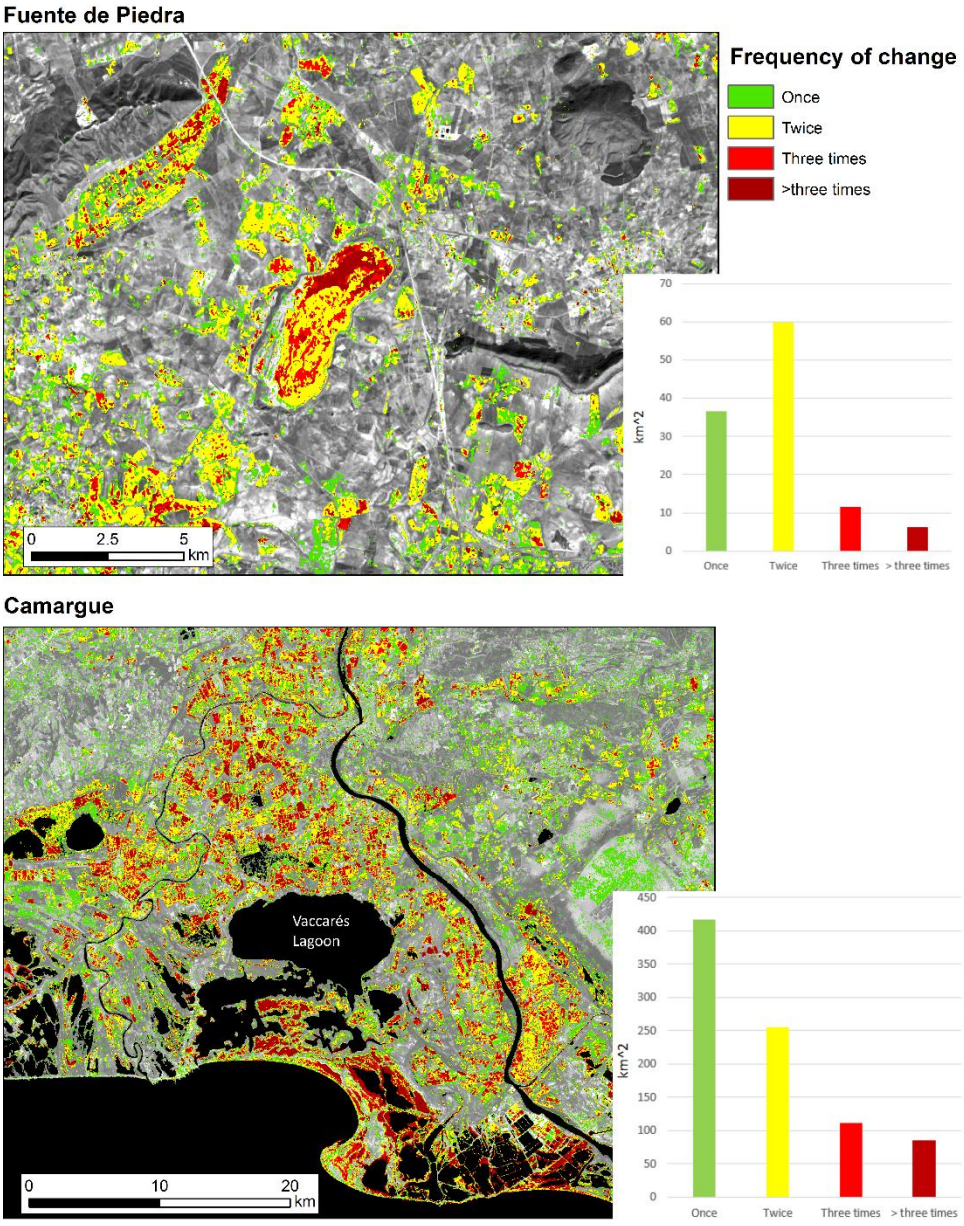


Figure 2.3 Frequency of change in Fuente de Piedra and Camargue. Colors indicate how many times a pixel has changed over the 12-month period. The charts aggregate the frequencies of change by area (Landsat 8 band 4 used as the background image)

In Fuente de Piedra, the areas more prone to suffer changes are the herbaceous crops, as well as the wetland area. The northern part of the lake has experienced several changes (up to six), most of them during the rainy period (October–April), when the lake fills up and dries out several times, until it dries completely by June. Growth and harvest patterns of the different cereals grown are also detected, and the harvest frequency can be estimated. Crops

in the northwestern corner seem to be the most intensively used. Olive groves, forests and shrublands remain unchanged through the year, as well as urban settlements. Similar change patterns can be spotted in Camargue (Figure 2.4). The marshlands to the south of the Vaccarés Lagoon exhibit multiple changes, up to eight in some areas. Some crops exhibit also very high rates of change, as well as some areas classified as urban tissue.

The rates of change found were grouped according to the LULC maps in both test sites (Figure 2.4). In Camargue, a large proportion of rice fields showed higher rates of change than other agricultural areas and also higher than wetlands. Forests, olive groves, shrublands and open spaces (areas with little or very sparse vegetation) showed the most static patterns.

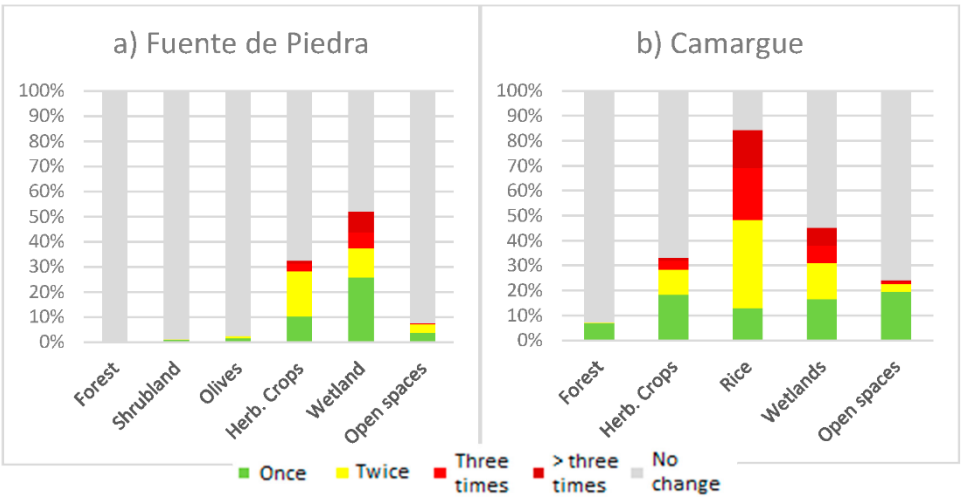


Figure 2.4 Frequencies of change aggregated in LULC classes in Fuente de Piedra (a) and Camargue (b). Each chart accounts for the proportion of pixels of each LULC class where a change was detected once, twice, three or four or more times. The gray portion of the bar corresponds to areas where no change was detected.

### 2.4.2. Comparison of S1-Omnibus Time Series and Pairwise Change Detection Approaches

The S1-omnibus method detects more changes than the pairwise approach. In Fuente de Piedra, the S1-omnibus method classified as change an area of 114 $km^2$, compared to the 79 $km^2$ detected in the pairwise method (the whole analyzed area is a rectangular extension of 490 $km^2$; Figure 2.1).

Subsets A and B of Figure 2.5 show examples of the differences found between both approaches in areas of herbaceous crops in Fuente de Piedra. No changes were detected by the pairwise approach that were not also detected by S1-omnibus.

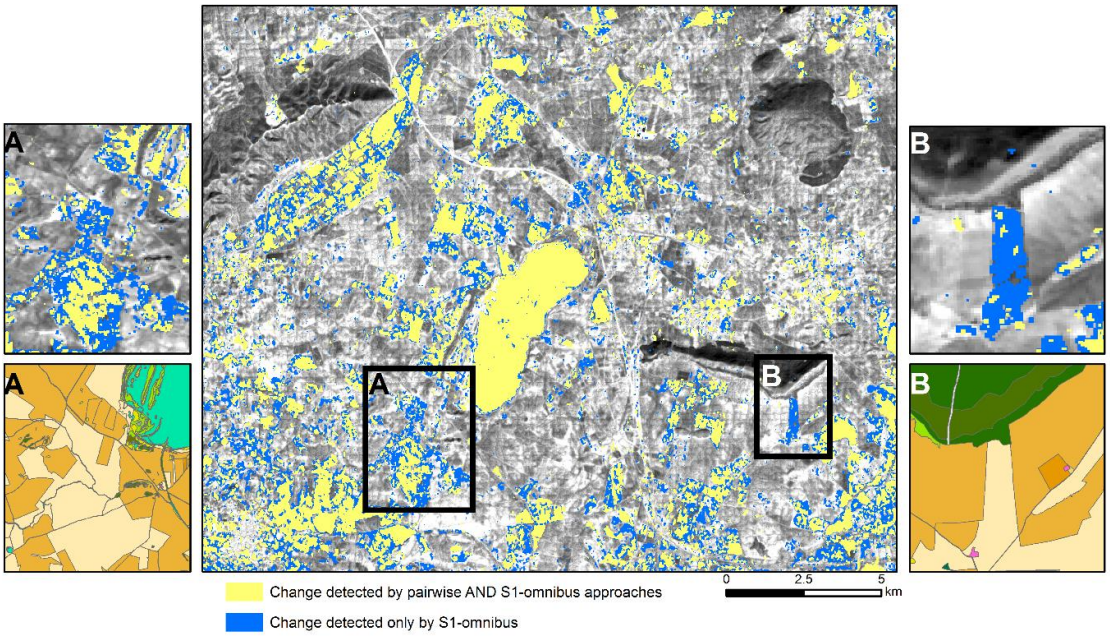


Figure 2.5 Changes detected in Fuente de Piedra by the pairwise change detection approach (yellow) overlaid on top of the S1-omnibus change detection results (blue). Changes in water level and in most crops are well detected by both approaches. Subset A shows how the S1-omnibus is capable of detecting changes in patches of crops matching the LULC map better (in the LULC map, orange is olive groves and beige herbaceous crops); Subset B shows how S1-omnibus can even detect whole patches of change that are missed with the pairwise approach (Landsat 8 band 4 used as the background image)

In Camargue, the S1-omnibus method also detected a larger proportion of change than the pairwise approach, creating more solid patches of change that correspond more to the vegetated object, whether it was a rice plot or natural herbaceous vegetation of the wetland. Other small sparse areas were reported as changed within large extensions of grasslands, changes that were not identified with the pairwise approach.

### 2.4.3. Landsat-Based and Sentinel-1-Based Change Detection Comparison

The comparison of S1-omnibus with Landsat-CVA change detection methods shows to a certain extent a good agreement (Figure 2.6), considering that optical and SAR sensors look at different properties of objects. As expected, using Sentinel-1 time series, one can detect a wider array of changes. Changes in water levels in the lake of Fuente de Piedra are detected

equally well with Landsat and Sentinel-1. However, changes in certain areas of herbaceous crops are reported only by either Landsat or Sentinel-1 (Figure 2.6, Subsets A and B). In Fuente de Piedra, the total area reported as change by both Sentinel-1 and Landsat amounts to 56 $km^2$. On the other hand, the area reported as change only by either Landsat or by Sentinel-1 is 28 $km^2$ and 52 $km^2$, respectively (bar chart in Figure 2.6).

We performed the same S1-omnibus and Landsat-CVA comparison in Camargue, and the results were slightly different. S1-omnibus flagged as change an area of 424 $km^2$, and the Landsat-CVA reported change in 557 $km^2$. The area detected as change by both methods simultaneously has an extension of 250 $km^2$. The total area covers a rectangular extension of 3500 $km^2$.

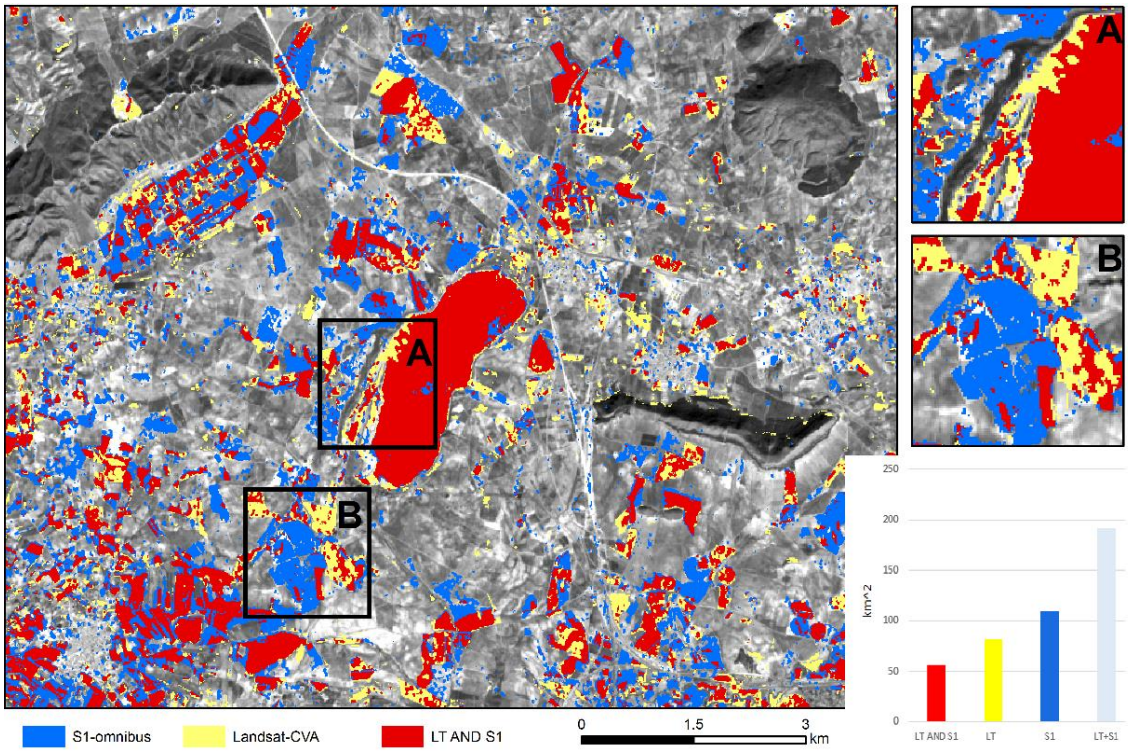


Figure 2.6 Changes detected by S1-omnibus (blue), by Landsat-CVA (yellow) and by both methods (red). Subsets A and B show a closer look at the two areas of change indicated in the main image. In chart, light blue color represents the area detected as change by either method.

## 2.5. Discussion

For effective land management and biodiversity conservation, it is essential to understand certain landscapes as mosaics of dynamic regimes rather than simplistic static cover types (Dronova et al., 2015; Parrott and Meyer, 2012; Watson et al., 2014). Temporarily-inundated wetlands belong to such category and require special approaches to assess their spatio-temporal dynamics. The statistically powerful approach we present uses free data and open source tools, which allows land planners and scientists to establish an automated and accurate monitoring service for short-term LULC change detection. We use the powerful factorization of the omnibus test statistic to perform unsupervised change analysis in two wetlands and detect areas and LULC classes of high change rates.

Locating the change patterns in space and time allows one to visualize change dynamics caused by variations in water flow or human activities. This enables us to estimate more precisely, for example, what areas dry out and when. Such estimations might be used in wetland wildlife management; breeding flamingos will abandon the single egg they lay if the wetland they are nesting in dries out too early or gets too flooded (Béchet et al., 2009).

Limnographs and gauging stations have a very good temporal resolution, but poor spatial resolution. Combining these high cadence change maps with other in situ parameters, such as the ones given by limnographs, it is possible to improve hydrological models (Wdowinski and Hong, 2015).

Maps depicting the frequency of change allow one to spot temporal and spatial patterns of short-term changes, as well as stable areas. For instance, the frequency of the change map in Fuente de Piedra shows high rates of change in the lake, as well as in some herbaceous crops, whereas olive groves, forest and natural shrublands remain mostly static throughout the year (Figure 2.3 and Figure 2.4). Most of the agricultural areas in Fuente de Piedra exhibit two changes, which suggest one harvest per year (one change from bare soil to crop and another one from crop to bare soil). Other areas of higher rates of change (three or more changes) can be spotted in agricultural areas northwest of the lake, suggesting several harvests per year.

In Camargue, high rates of change can be observed in the wetland south of the Vaccarés Lagoon, probably due to the influence of tides. False changes in permanent water bodies (e.g., the Mediterranean Sea) were reported when using Sentinel-1 in both approaches (i.e., S1-omnibus and the Sentinel-1 pairwise approach). Since these were not a real change and for a better visualization of the results, sea and other permanent water bodies were masked

out in Figure 2.3 using a permanent water mask created out of a series of Landsat images for 2015. The reasons why SAR data report changes in permanent water bodies have yet to be studied, but this might be due to variations in the water table because of the tides or due to strong winds creating waves (Bragg scattering). Such changes were not detected in the Landsat images.

Change rates were grouped into LULC classes. This revealed two groups of classes: forests, olive groves and shrublands as more "static" classes and herbaceous crops, including rice fields and wetlands, as classes prone to suffer several changes throughout a year. This allows drawing estimations of land use. For example, during the period of study (one year), no changes were reported in around 70% of the area classified as herbaceous crops of both test sites. Although a field validation would be needed, this suggests that a large portion of the area destined to grow herbaceous crops other than rice may not be actually used, but remains fallow.

The S1-omnibus method reports a larger proportion of changes in the landscape than the pairwise approach in both study areas and in both agricultural and natural landscapes. As Conradsen et al., (2016) suggested, detecting changes in consecutive pairs of images may leave undetected weak trends overtime, such as the slow growth of herbaceous vegetation after a disturbance, whether this is of anthropic origin, such as harvests, or of natural origin, like seasonal inundations. S1-omnibus seems to be able to detect these gradual changes.

The comparison of S1-omnibus and Landsat-CVA showed generally good agreement in Fuente de Piedra, with changes in some patches of herbaceous crops missed by either of the methods (Figure 2.6). In Camargue, optical and SAR methods performed more differently. Landsat-CVA flagged as change a larger extent, mainly of herbaceous crops other than rice. This might be due to phenological changes in blooming vegetation that are difficult to detect with SAR imagery.

The comparison between the water table and precipitation data and the sequence of changes detected by S1-omnibus (Figure 2.2) reveal how important it is to have a high cadence of imagery to capture all of the changes produced in such dynamic ecosystems. We limited our research to one Sentinel-1 image per month (every 24 or 36 days) for simplification purposes, but with the recent launch of Sentinel-1b, it is now possible to map these dynamics every six days. It would not be possible to reach even a similar cadence using optical data. Although both study areas are relatively cloud-free throughout the year, we could only find 6–8 cloud-free Landsat scenes for our test sites, all restricted to the dry period. The lack of suitable

optical images is greater for larger areas (the larger the area is, the more probable it is to find clouds in it), during rainy seasons and especially in the sub-humid and humid tropics. Some events, like fast floods or flooding of certain creeks or ponds, may take place only during the rainy season.

### 2.5.1. Potentials and Limitations of the Application

Although S1-omnibus cannot directly provide information on the type of change, this approach can still be useful for land managers with local knowledge or in situ data that allow them to interpret the changes and change rates. Knowing the short-term change patterns of certain land covers may aid in their classification, especially when classifying different types of wetlands, since some of them are defined by their dynamics. For instance, wet meadows are defined by seasonally- or temporally-saturated soils and brief periods of inundation (Dronova et al., 2015). Such periods of inundation can be accurately mapped using Sentinel-1 time series in order to define subclasses of wetlands and further describe the ecological status and condition of DCT. The increased temporal resolution of Sentinel-1 time series provides an information source for a better physically-based characterization of wetland types following a standardized nomenclature, e.g., Ramsar, or the Mapping and Assessment of Ecosystems and their Services (MAES). Integrating the S1-omnibus approach in operational wetland mapping activities fosters a more systematic monitoring of wetland dynamics. The broad change results thus provide a very flexible application for analyzing specific hydrological or plant phenology-driven analyses at very local scales.

Dual pol SAR data have been used before to monitor grass cutting practices for biodiversity management and subsidy control purposes, but the number of studies available is limited (Voormansik et al., 2013). In fields of tall grass, meteorological conditions such as wind can influence the backscatter signal, reporting a change when there was actually none (Voormansik et al., 2013). In a pairwise comparison of consecutive images, it is difficult to remove such influence, but it may be possible to filter that noise out by applying S1-omnibus; if using time series with a high temporal resolution, (e.g., weekly), the algorithm could be modified so that if $\sum_1 \neq \sum_2$, but $\sum_1 = \sum_3$, the change reported between $\sum_1$ and $\sum_2$ could be flagged as a false positive.

The different changes recorded by Landsat-CVA and S1-omnibus show the potential of combining optical and SAR sensors for change detection. Sentinel-1-based change detection can also be combined with other sensors to determine the direction of change and to create

a change mask to reduce error propagation in the labeling phase of the production of long-term LULCC maps (Hecheltjen et al., 2014).

Sentinel-1 does not always acquire dual-pol images, and for certain parts of the globe during certain periods, only single polarization (VV) images are available. Information on the schedule of different acquisition modes can be found at https://sentinel.esa.int/web/sentinel/missions/sentinel-1/observation-scenario. We also tested the S1-omnibus approach with single-pol VV Sentinel-1 images, and the results looked promising, but the accuracy has yet to be evaluated. An important limitation is the inherent low vegetation canopy penetration of C-band. This hinders its application for wet forests and mangroves, for which an L-band sensor would be more suitable.

It is still necessary to determine with more exactitude the change detection capabilities of S1-omnibus; e.g., how tall/thick the vegetation must be for it to be detected when it is removed or grows. Additional work to validate this change detection methodology with time series is underway using a variety of test sites where we have a higher level of control.

The open source character of our approach allows its incorporation with other tools where dense time series may be used such as GEE, which in turn may increase the number of applications of the S1-omnibus.

### 2.6. Conclusions

SAR-based change detection approaches offer a great opportunity to enhance our understanding of complex and dynamic ecosystems. S1-omnibus is capable of capturing accurately in space and time a wide array of LULC changes, and along with Sentinel-1 time series, it is possible to reach a six-day cadence at 30-m resolution. We demonstrate its potential for wetland monitoring by mapping change patterns caused by surface water dynamics and agricultural practices for a one-year period. Coupled with ground data like gauging stations, S1-omnibus and Sentinel-1 time series can be used to improve hydrological models (Wdowinski and Hong, 2015). Wetland managers can easily interpret the patterns of change and use them to locate and delineate areas of high rates of change, which are prone to have a high ecological value (Parrott and Meyer, 2012; Watson et al., 2014). Incorporating a temporal variable into the LULC classification procedures may allow the separation of land cover categories that, to this date, have proven difficult. The S1-omnibus's statistical soundness, higher control of false negatives and false positives (Conradsen et al., 2016) and the fact that it does not require complex parameterization make it an ideal method for

operational monitoring services. We also demonstrate its advantages against standard change detection approaches that use pair-wise comparisons of SAR and optical images.

# Chapter 3

## Mapping wetland dynamics with SAR-based change detection in the cloud

IEEE Geomatics and Remote Sensing Letters, Early access

March 2019

doi: 10.1109/LGRS.2019.2903596

Javier Muro, Adrian Strauch, Eleni Fitoka, Maria Tompoulidou, Frank Thonfeld

*"Big data isn't about bits, it's about talent."*

*– Douglas Merrill*

**Abstract**

Wetlands are often coupled with anthropogenic systems. This makes them highly dynamic and thus difficult to map and monitor from space. The Sentinel-1 constellation allows to monitor land changes regardless of cloud conditions and with a high frequency of pass. We use a time series of 33 Sentinel-1 dual polarized images from 2016 to map seasonal changes at the artificial Lake of Kerkini, in Greece. The images are accessed and processed in Google Earth Engine via a Flask web application. Points of change within the time series and frequency of change were determined according to an omnibus-test statistic. Results were compared to an optical-based land cover map and gauging measurements. Frequency of change patterns matched the different land cover types, indicating that frequency of change is related to the physical and structural properties of the land cover. This methodology can be used operationally to improve our understanding of ecosystems, enhance land cover maps, and to monitor wetland dynamics as well as cover changes caused by human activities.

Index Terms—Wetland dynamics, SAR, change detection, seasonality

### 3.1. Introduction

Landscapes are seldom static, with many factors that modify their structures, compositions or even their functions sometimes in the matter of days. Wetlands are ecosystems at the interface between land and water and are often coupled with anthropogenic systems, which makes them particularly dynamic. Water dynamics and moisture contents are defining characteristics of many wetlands and depend on variable factors such as precipitation and evapotranspiration rates, or water discharge from dams, agricultural fields, river network, or on human interventions like filling and drainage. This renders single image classifications inefficient to produce accurate maps and to thoroughly assess dynamic classes (Dronova et al., 2015). The use of multitemporal optical images has improved classification results, but clouds and cloud shadows often cause data gaps that impede capturing the whole range of changes. Synthetic Aperture Radar (SAR) sensors are very adequate for monitoring water surface especially under cloudy conditions, and are also not subjected to sunglint effects (White et al., 2015). Besides, most wetland types, except for some raised peatbogs, are located in flat terrains. This minimizes the slant-range distortions inherent to SAR images (i.e. foreshortening, layover, and shadowing effect).

Classification of multitemporal SAR images is often outperformed by synergistic use of SAR and optical data. However, SAR imagery has proven useful for short term change detection based on dense time series of images (Dabboor et al., 2017; Muro et al., 2016).

Incoherent SAR change detection methods measure significant changes in the backscatter intensity of one channel in pairs of images. Image rationing is a common method in which stable areas have values close to one and changed areas have either high or close to 0 values. Thresholding techniques can be applied to identify changes but the non-Gaussian distribution of the ratio image can distort the metrics and cause errors (Hecheltjen et al., 2014), which makes them unsuitable for operational systems. On the other hand, coherence change detection methods measure the correlation between the phase of pairs of images taken at different times. Stable regions show high coherence, and, when changes occur, the phases are decorrelated showing low coherence. However, vegetation or water surfaces decorrelate quickly due to motion without necessarily changing their state or condition. Coherence-based methods are better at discriminating changes within the context of multitemporal features (Hecheltjen et al., 2014). When using a time series of images, it is difficult to control the rates of false positives and negatives between all the pairs of consecutive images. Conradsen et al. (Conradsen et al., 2016) developed an algorithm that allows a higher control of these errors and can determine the points of change within in the time series (Canty and Nielsen, 2017; Muro et al., 2016).

Handling dense time series of SAR data requires high technical expertise and high computational power. Cloud processing based solutions have the capacity of overcoming these two challenges, making these applications feasible for operational use and non-specialized users. We use a Flask web application (https://github.com/mortcanty/earthengine) (Canty and Nielsen, 2017) that accesses Google Earth Engine (GEE) (Gorelick et al., 2017) and all its Sentinel-1 archive to perform change detection over the Artificial Wetland of Kerkini, in Greece. The maps of frequency of change produced are used to visualize the effect of water level fluctuations every 12 days and to improve a land cover map based on multispectral imagery.

### 3.2. Study area

Kerkini Lake (23.1418 E, 41.2204 N) is an artificial lake and a Ramsar site in Greece. It was constructed with the purpose of regulating floods, trapping sediments and irrigating the surrounding plain. Its low depth, high productivity, periodic flooding with sediments and nutrients and its position in relation to bird migration corridors have contributed to the

biological wealth of the area. Water levels are regulated by a dam since 1982 and have a seasonal variation of approximately 5 meters. This results in seasonal changes of the flooded surface from 5,000 ha up to 7,300 ha (Crivelli et al., 1995b). These seasonal changes have many effects on the wetland ecosystem such as shrinkage of feeding and nesting habitats like reed beds, wet grasslands and aquatic beds with water lilies, deterioration of riparian forests, or increase in slope erosion during dry season (Crivelli et al., 1995a). Monitoring of water fluctuation is one of the key elements in management and conservation of the Artificial Lake Kerkini. An animation showing the dynamics of the area can be found in the supplementary files.

### 3.3. Material and Methods

We used a set of 33 dual polarized (VV-VH) images in ascending orbit from the same orbit path. Images were taken usually every 12 days from 11.01.2016 to 24.12.2016. There are 3 images missing creating 3 gaps of 24 days between acquisitions due to the irregular observation scenario of Sentinel-1 (ESA, 2012a). The change detection algorithm used determines the points of change using an omnibus test statistic (Conradsen et al., 2016). It performs a simultaneous test of homogeneity over the whole time series using the components of a covariance matrix (1):

$$C2 = \begin{pmatrix} \langle |S_{vv}|^2 \rangle & \langle S_{vv} S_{vh}^* \rangle \\ \langle S_{vh} S_{vv}^* \rangle & \langle |S_{vh}|^2 \rangle \end{pmatrix} \quad (1)$$

where $S_{tr}$ the scattering amplitude for transmitted polarization *t* and received polarization *r*. $\langle \ldots \rangle$ denotes multilook averaging and *v* and *h* correspond to vertical and horizontal polarizations respectively. When this covariance matrix formulation is used for multi-look polarimetric SAR data, the complex Wishart distribution applies. However, GEE stores the Sentinel-1 images as Ground Range Detected (GRD), in which the phase information is lost during the processing. Thus, the off-diagonal elements of the matrix are 0 but the complex Wishart distribution still applies using the diagonal elements of the covariance matrix (Canty and Nielsen, 2017). The change detection is performed with an associated p-value that was set to 0.01. Once every point of change has been determined, a map of frequency of change can be generated adding up all the changes detected throughout the time series.

Open water bodies tend to present high variability in the backscatter coefficient over time due to ripples in the surface caused by wind. This effect, which is more pronounced in sensors of short wavelength such as the C-band of Sentinel-1 (Muro et al., 2016), returns

very high rates of false changes. To remove this noise, we created a permanent water mask using the percentile 95 of the VV (Figure 3.1), which corresponds to the minimum water extent (i.e. permanent water bodies).

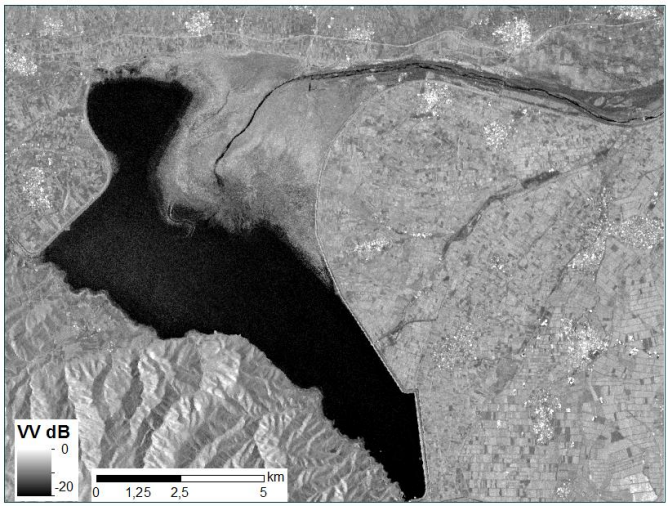


Figure 3.1 Percentile 95 of the VV backscatter signal for Kerkini Lake in 2016. Dark colors represent permanently inundated areas.

### 3.4. Results and discussion

The frequency of change map (Figure 3.2a) indicates how many times each pixel has changed during the period of study. The map shows a fringe of high values (i.e. frequent changes) along the shoreline, consequence of the fluctuations of the water table levels. This allows separating the area into regions of different frequencies of inundation, which is different from the number of days a pixel remains flooded. For instance, the intermediate area of red colors experiences changes in inundation more frequently than areas further or closer to the permanent water body, but it is not inundated as often as the areas closer to the permanent water body.

The frequency of change was compared to the Land Use/Land Cover map of Figure 3.2b. This LULC map was created within the Satellite-based Wetland Observation Service (SWOS) project and it is available at the SWOS portal (http://portal.swos-service.eu). It was produced using a hierarchical object-based analysis based on spectral, spatial and contextual features of two Sentinel-2 images; one from the dry period 12.08.2017 and another one from the rainy period 30.03.2017. An object based approach and a maximum likelihood classifier were used. Training data was collected by visual interpretation of high resolution imagery. We used a nomenclature adapted from the Millennium Assessment of Ecosystem Services

(MAES) (Finlayson et al., 2005; Fitoka et al., 2017). The MAES nomenclature is commonly used to classify different types of wetlands for reporting purposes at EU level.

Frequency of inundation drives species composition in seasonally flooded wetlands (Pétillon et al., 2010; Tyler et al., 2018; Valk, 2005). The patterns of frequency of change found corresponded with the boundaries between the classes Marshes, Seasonal water with aquatic bed, and Seasonal water of the LULC map. Thus, the frequency of change is related to the physical and structural properties of the land cover. However, the boundary between Permanent water and Seasonal water was not properly captured using only the two Sentinel-2 images from the dry and rainy periods (Figure 3.2a and b). Many studies often use images from the peak leaf-on (maximum NDVI) and leaf-off (minimum NDVI) periods (e.g. Hill et al., (2010); Li et al., (2013); Rybakov et al., (2018); Xie et al., (2019)) , and can miss dynamics occurring in between. In Mediterranean ecosystems, the lowest water table levels of reservoirs often do not correspond with the driest or hottest period, such as in this case. Highest temperatures and lowest precipitation levels are usually during June-August, but lowest water levels are at the end of September or even in January (Figure 3.3). This makes it difficult to capture the whole seasonal cycle with few images from targeted periods. As demonstrated by Pekel et al. (2016), dense time series of optical imagery are also capable of assessing water seasonality. However, delineating waterbody boundaries from multiple individual optical images is often ambiguous. Reflection on water surfaces depends on suspended matter and chlorophyll content, and can be confused with different types of bare soils (Sun et al., 2012). Confusion between bare dry soil and water in single SAR images is also common because both have very low backscatter values (Schlaffer et al., 2015). The considerable short-term dynamics of many wetlands demand the use of denser time series than the ones that optical sensors can provide. Because SAR sensors are sensitive to changes in structural properties, the frequency of change is a powerful tool to map seasonal changes and improve classifications.

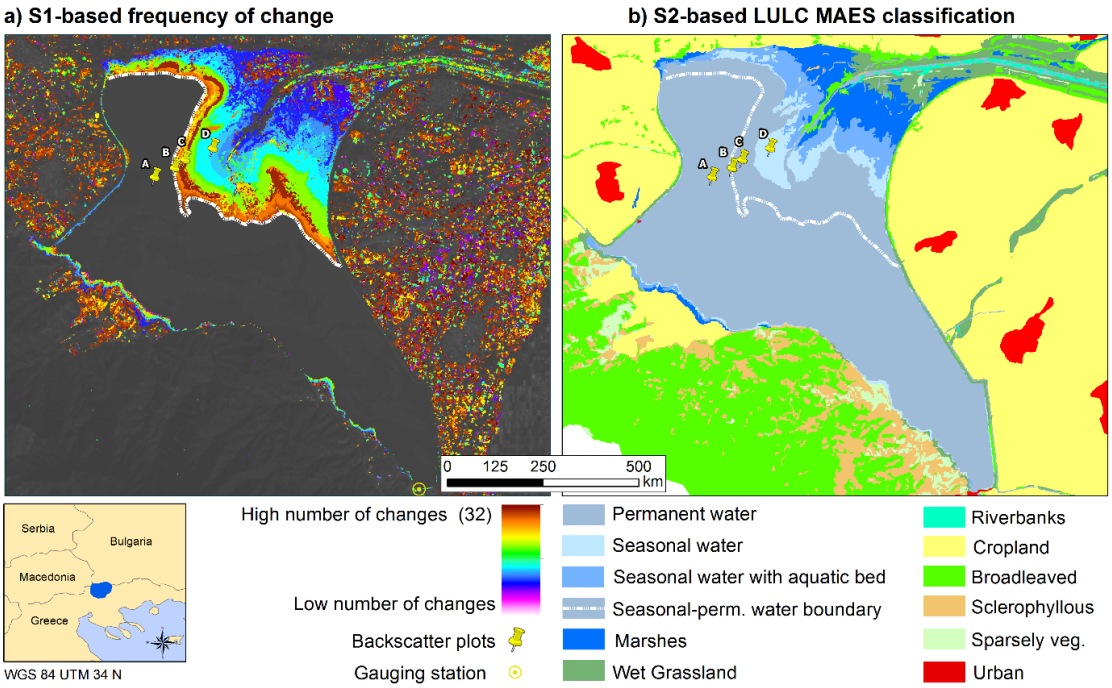


Figure 3.2 a) Frequency of change based on Sentinel-1. b) LULC map produced using multitemporal Sentinel-2 imagery and the MAES adapted nomenclature [14]. The dashed white line marks the actual boundary between permanent water and seasonal water according to the frequency of change. The gauging station is shown at the southernmost part of the wetland in Figure 3.2a. Points A-D mark the location of the plots used for the VV backscatter temporal profiles of Figure 3.3.

To characterize the area of frequent changes we analyzed the VV backscatter response across time for four points along a transect, and plotted them along with water table data taken from a gauging station (Figure 3.3). Three of the plotted points were classified as permanent water according to the LULC map; "A", "B" and "C". Only "A" shows rather consistent low backscatter values product of specular reflection, typical of water bodies. "B" and "C" present much higher backscatter values at the end and beginning of the year, when water table levels are at their lowest. These alternating high-low backscatter patterns suggest moist soil conditions alternating with water-logging after rainfalls. Point "D" was classified as seasonal water and shows even higher backscatter values under non-flooded conditions, suggesting a mix of volume scattering and double-bounce scattering (Schlaffer et al., 2015).

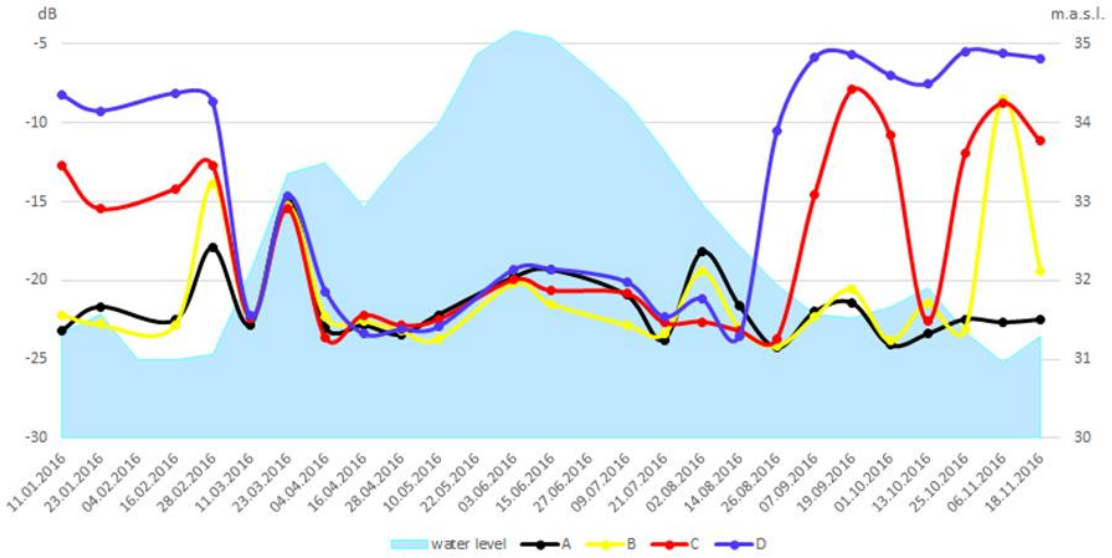


Figure 3.3. VV backscatter temporal profiles and water table levels throughout the study period. The location of points A-D is shown in Figure 3.2. The location of the gauging station is shown inFigure 3.2a, at the southernmost part of the wetland. Water table data was collected every 12 days, corresponding with the image acquisition.

Classifying optical images allows the generation of a detailed LULC map following the MAES nomenclature. Using images from dry and rainy season as input often enables to account for seasonal dynamics to some extent. However, it must be noted that these dynamics (for example water level fluctuations) cannot be specified in time with the limitations of optical data, such as reduced repetition rates due to clouds or ambiguous classification results at ecotone zones. The methodology we describe yields several advantages. It produces a clear picture of the spatio-temporal patterns of very dynamic areas. It is statistically sound, requires minimal parameterization and is computationally efficient so that it can be used in an operational way. It can be used as ancillary information to assess and improve land cover classifications, or to direct fieldwork efforts; for instance, one might want to distribute the sampling points across the gradient of change in this case. It also provides information about human actions on the landscape, such as agricultural activities. It requires, however, prior knowledge of the area to interpret the patterns of change. Unlike a standard land cover classification, the results are not thematic nor absolute, which impedes the transmission of information to unspecialized audience (e.g. decision makers).

### 3.5. Conclusion

Temporal dynamics can actually be used to improve our understanding of ecosystems and to enhance classification results. In this case, the patterns of frequency of change matched with land cover types that tend to be difficult to distinguish. Additionally, different frequencies of inundation were shown in what was thought to be permanent water. Time series of SAR images processed via cloud computing services is a very efficient way to deliver statistically sound and finalized products that can be interpreted by intermediate users. They can be successfully applied especially in cases where due to cloud cover, optical imagery cannot capture the whole year dynamics.

# Chapter 4

## Multitemporal optical and radar metrics for wetland mapping at national level in Albania

Heliyon

Submitted in July 2019

Javier Muro, Ana Varea, Adrian Strauch, Anis Guelmami, Eleni Fitoka, Frank Thonfeld, Bernd Diekkrüger, Björn Waske

*"Maps are like campfires — everyone gathers around them, because they allow people to understand complex issues at a glance, and find agreement about how to help the land."*
*— Sonoma Ecology Center, GIS/IS Program Web Site*

**Abstract**

Wetlands are highly dynamic, with many natural and anthropogenic drivers causing seasonal, periodic or permanent changes in their structure and composition. Thus, it is necessary to use time series of images for accurate classifications and monitoring. We used all available Sentinel-1 and Sentinel-2 images to produce a national wetlands map for Albania. We derived different indices and temporal metrics and investigated their impacts and synergies in terms of mapping accuracy. Best results were achieved when combining Sentinel-1 with Sentinel-2 and its derived indices. We reduced systematic errors and increased the thematic resolution using morphometric characteristics and knowledge-based rules, achieving an overall accuracy of 82%. Results were also validated against field inventories. This methodology is reproducible to other countries and can be made operational for an integrated planning that considers the food, water, and energy nexus.

## 4.1. Introduction

The value of wetlands in terms of ecosystem services is widely recognized by the scientific community (Finlayson et al., 2005; Mitsch and Gosselink, 2000; Russi et al., 2012) and policy makers (e.g. playing important roles in the Paris Agreement, the Sendai Framework for Disaster Risk Reduction, or other multilateral biodiversity related agreements (Ramsar, 2018)). However, wetlands are still being degraded at global scales, and degradation trends have increased since 2000 (Dixon et al., 2016; Ramsar, 2018). The main drivers of these trends are agricultural expansion, intensive wood, sand and gravel harvesting, dam building, agricultural and urban waste, drainage and salinization (Finlayson et al., 2005; Ramsar, 2018). This case study focuses on Albania, a country that hosts one of the few last systems of large and undammed rivers of Europe. Some segments of these rivers are biodiversity hotspots for fish and mollusks and harbor high rates of endemisms (Weiss et al., 2018). However, many other rivers in Albania are heavily dammed. Over 90% of its electricity is already provided by hydropower and authorities are planning to increase investment in it. Besides, another 3000 hydropower projects are planned in the Balkan region (Weiss et al., 2018). Some of these projects have been financed by European public banks (Sikorova and Gallop, 2015), but they are facing strong social opposition from academic, conservation, and local organizations (Sikorova and Gallop, 2015; Vejnovic and Gallop, 2018; Weiss et al., 2018).

For instance, 37% of the planned projects are located in protected areas, and opponents argue lack of disclosure and negative environmental and social impacts caused by some of these projects (Vejnovic and Gallop, 2018).

According to the Global Outlook on Wetlands (Ramsar, 2018), from the Ramsar Secretariat, properly managed wetlands can directly and indirectly contribute to most of the Sustainable Development Goals (SDGs). This puts wetlands in a central position in the debate about sustainable development. The Ramsar Convention as well as UN Environment are two major stakeholders when it comes to assessing the status and trends of wetland ecosystems and their changes over time. Within the framework of the SDGs, especially indicator 6.6.1 "Change in the extent of water-related ecosystems over time" directly requires countries to report on their national wetlands regularly ("UN stats Metadata repository," 2018). Earth Observation (EO) can generate the information that policy makers need to make and justify decisions, and can also support efficiently the implementation of the SDGs (Paganini et al., 2018). The GEO-Wetlands Initiative is a collaborative partnership aiming to make this step as easy as possible for countries by providing methods, tools, guidelines, training and knowledge [www.geowetlands.org]. This case study is one example of how state-of-the-art EO technology can efficiently support wetland mapping and monitoring at national scale.

The last official inventory of wetlands of Albania is from 2003 and it was part of the MedWet Inventory System initiative (Marieta et al., 2003; Perennou et al., 2012). Since then, the paradigm in EO has experienced a revolution with an increasing number of freely available data sets, fusion of Synthetic Aperture Radar (SAR) and optical sensors, general advances in algorithms for classification and modelling, and ultimately, the cloud computing platforms (Gorelick et al., 2017; Joshi et al., 2016; Stefanski et al., 2014; Waske and Benediktsson, 2007). Mapping large areas that include dynamic cover types such as wetlands, with sufficient thematic resolution and accuracy, requires the use of large numbers of images from different sensors. This poses a challenge in terms of available computing power and on technical capacity, both factors considered as bottlenecks that hinder development and the implementation of informed land management policies and plans of developing countries. Cloud computing platforms offer new opportunities to bypass these bottlenecks and to process large amounts of information on an operational basis. They have prompted a number of studies that use time series of images for classification of either specific land cover types classes (e.g. rice mapping (Dong et al., 2016), open water bodies (Hardy et al., 2019), cropland extent (Xiong et al., 2017) or settlements (Patel et al., 2015)), or more complex land cover maps at national (Mack et al., 2017) or even at continental scale (Pflugmacher et al., 2019).

Mapping at national scales is a more practical approach, since monitoring and reporting tasks are often needed at national level. Time series of images can be processed using data fusion techniques (Gevaert and García-Haro, 2015), data interpolation (Inglada et al., 2017) best pixel selection (Griffiths et al., 2013), fitting time series functions (Zhu and Woodcock, 2014), or aggregation of data into meaningful multitemporal metrics (Carrasco et al., 2019; Mack et al., 2017; Mahdianpari et al., 2018; Pflugmacher et al., 2019). These metrics (e.g. maximum, mean and minimum) can be applied to the bands directly or to indices derived from them. They are representative of the different seasonal stages of the land cover caused by phenological, land use, or inundation regimes. Time series of SAR imagery are instrumental in covering the complete seasonality of wetlands (Muro et al., 2019; White et al., 2015), especially in areas of persistent cloud cover where images from the dry period and rainy (and therefore cloudy) period are needed. Using both, SAR and multispectral imagery has proven to achieve higher classification accuracies (Joshi et al., 2016; Stefanski et al., 2014; Waske, 2014).

Even when using the full spectral and temporal resolution, there are limitations to the classification power of EO. Coupling EO data with other spatial information can return higher accuracies and increase the thematic resolution (Manandhar et al., 2009; Stefanov et al., 2001; Van der Voorde et al., 2007). Examples of the use of ancillary spatial information in mapping tasks include: topographic information (Hird et al., 2017), spatial explicit metrics (size, shape, edge length) (Herold et al., 2003), precipitation distribution (Pflugmacher et al., 2019) or distance to water bodies and elevation ranges (Long and Skewes, 1996) among many others.

We use the cloud computing platform Google Earth Engine (GEE), to map the wetlands of Albania at national scale by using the whole archive of Sentinel-1 and Sentinel-2 imagery for the period June 2015 – June 2018, and a set of flexible knowledge-based rules.

The purpose of this study is to:

- Assess whether the combination of multispectral and SAR data enhances the classification of wetlands.
- Apply the methodology and demonstrate how it can help to fulfill reporting commitments at national level.
- Update the inventory of Albanian wetlands for the target year 2017.

## 4.2. Material and Methods

### 4.2.1. Study area

Albania (Figure 4.1) has an extension of 28.784 km$^2$. It has a steep orography in the east, with most rivers flowing westwards across extensions of floodplains used for agriculture. Several segments of many rivers have been channelized and there are abundant small dams used to store water and produce hydropower scattered over the country. However, there are still several large rivers that remain in pristine conditions (Weiss et al., 2018). Agriculture, energy and tourism are three of its strongest economic sectors (EcoAlbania, 2017; FAO, 2015).

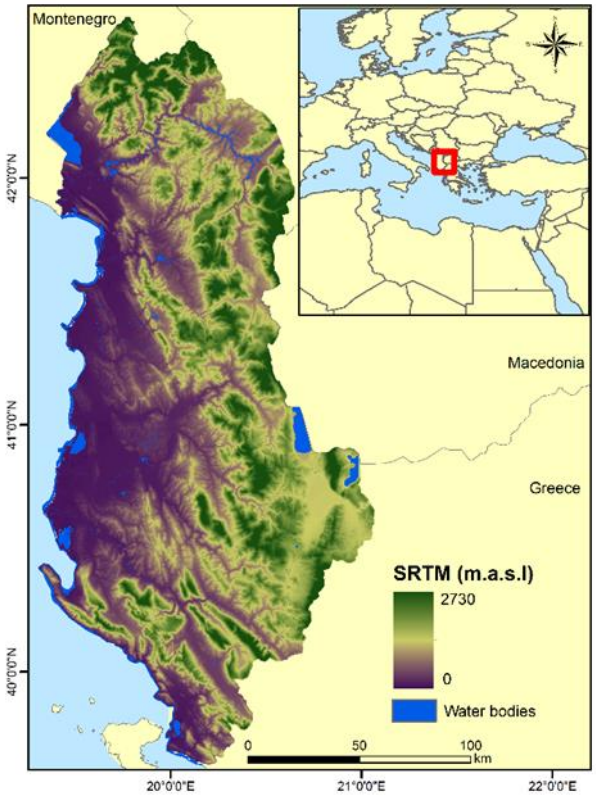


Figure 4.1 Location of Albania with its Digital Elevation Model and water bodies.

### 4.2.2. Datasets

We used all the Sentinel-1A and 2A images from June 2015 to June 2018. This implied imagery from around 100 overpasses for Sentinel-2, and 264 overpasses for Sentinel-1. Out of all the Sentinel-2 imagery acquired we created a median composite (dataset S2 henceforth). Clouds were masked using the quality band of the Level-1C products (ESA, 2012b), and cloud shadows were masked using azimuth and zenith angles to estimate the position of the shadow. Out of the same Sentinel-2 images we created another multitemporal composite

using the 90th and 50th percentiles of three indices; the normalized difference vegetation index (NDVI) (Tucker, 1979), the normalized difference water index (NDWI) (Mc Feeters, 1996), and the normalized difference built-up index (NDBI) (Zha et al., 2003). The 90th and 50th percentiles of these indices represent the maximum and median conditions of vegetation and water. Minimum metrics were not used because they were too affected by cloud and shadow noise, and the maxima of the NDBI already correspond to the minima of NDWI and NDVI. We refer to this dataset as NDIs (normalized difference indices).

Out of the Sentinel-1A images accessed, we created another multitemporal composite (dataset S1 henceforth) using the 99th, 50th, and 5th percentiles of both polarizations and in ascending orbit. We used the 5th percentile instead of the 1st to eliminate outliers occurring in the seams between images. Currently, Sentinel-1 data from GEE is already clamped to the 99th and 1st percentiles. The data is processed by GEE in the Sentinel Application Platform (SNAP) using the following steps: Apply orbit file, noise removal, thermal noise removal, radiometric calibration, terrain correction using SRTM 30, and conversion to dB via log scaling (GEE, 2018). All datasets, multispectral and SAR, were resampled to 20 meters.

#### 4.2.3. Classification

We based our classification scheme on the Millenium Assessment of Ecosystem Services (MAES), modified to include Ramsar wetland types (Fitoka et al., 2017), mapping the following ten classes: Bare soil, Permanent water bodies, Intermittent water bodies, Marshlands, Cropland, Grassland, Heathland and scrubland, Deciduous forest, Coniferous forest and Built-up. "Intermittent water bodies" refer to areas that are bare when not inundated (e.g. intertidal mudflats and the water spread area of many water reservoirs). "Marshlands" are areas that have vegetation and water, at least temporarily. "Heathland and scrubland" are areas dominated by shrub-like vegetation. The other 7 classes are self-explanatory.

We applied a Random Forest (Breiman, 2001) classifier using 500 trees in GEE and collected a set of 300 polygons for training and validation. The polygons were delineated using aerial imagery of 2015 at 20 m and 8 m resolution, available at the portal of the State Authority for Geospatial Information (ASIG) (https://geoportal.asig.gov.al). Each class had circa 30 polygons about the same size except for the class "Cropland" which were twice larger. This was necessary because it was the class with the largest extension and variability due to the different crops and rotation patterns. For each dataset and combination of datasets we

performed a cross-validation in which 2/3 of the polygons within each class were randomly selected for training and 1/3 for validation.

### 4.2.4. Post-classification processing

The different datasets used have their own inherent noise and errors. For example, SAR data is prone to slant-range distortions (foreshortening and layover) in areas with a complex relief (White et al., 2015). Thus, we used morphological constrains to create a Potential Wetlands Mask (PWM) to mask out these artifacts that would cause classification errors. Out of the SRTM digital elevation model we calculated a set of 3 derivatives: Topographic Wetness Index (TWI) (Böhner and Selige, 2006), a Multiresolution Index of Valley Bottom Flatness (MrVBF) (Gallant and Dowling, 2003), and a Terrain Surface Convexity Index (TSC) (Iwahashi and Pike, 2007). These datasets were combined with the Global Surface Water (GSW) product (Pekel et al., 2016) and then normalized to values from 0 to 1. The result was a map showing the likelihood of each pixel of being a wetland. A histogram-based threshold method (Otsu, 1979) was set to mask out areas unlikely to be a wetland, producing the PWM (Figure 4.2). Training, classification and validation was limited to areas within the PWM. This way, artifacts produced by the terrain on SAR (slant-range) and in optical data (illumination angles) were reduced.

Statistical mapping (e.g. Random Forest) can seldom produce accurate results on its own. Knowledge-based criteria and ancillary information can be used to produce outputs with the thematic resolution and mapping accuracy needed (Connolly and Holden, 2009; Long and Skewes, 1996; Perennou et al., 2018; Van der Voorde et al., 2007). To that end, we applied an additional set of knowledge-based rules to further separate the land cover classes. These rules are based on theoretical considerations and observations, and are common practice to enhance the result of remote sensing-based classifications (Manandhar et al., 2009; Stefanov et al., 2001; Van der Voorde et al., 2007). To separate "Riverbanks" from other bare surfaces we applied a 120 m buffer to the river network. All "Heathland and scrubland" areas within this buffer were as well reclassified as "Riverine scrubs". An additional class of "Beaches and coastal dunes" was created for all bare surfaces within 50 m from the shoreline. Figure 4.2 shows the classification and post-classification workflow used. The final result is a classification of 6 wetlands classes (counting "Beaches and coastal dunes" as a wetlands) and 7 non-wetland classes.

For validating this dataset, we performed a stratified random sampling of 527 points using the platform Laco-wiki (See et al., 2017). The platform gives access to Google, Bing and

satellite imagery enabling a visual interpretation of the validation samples and generates accuracy reports. Additionally, we compared our results with the last inventory of wetlands, carried out in 2001-2003 (Marieta et al., 2003). Through visual inspection we discarded from the inventory the wetlands that were not visible in current high resolution imagery.

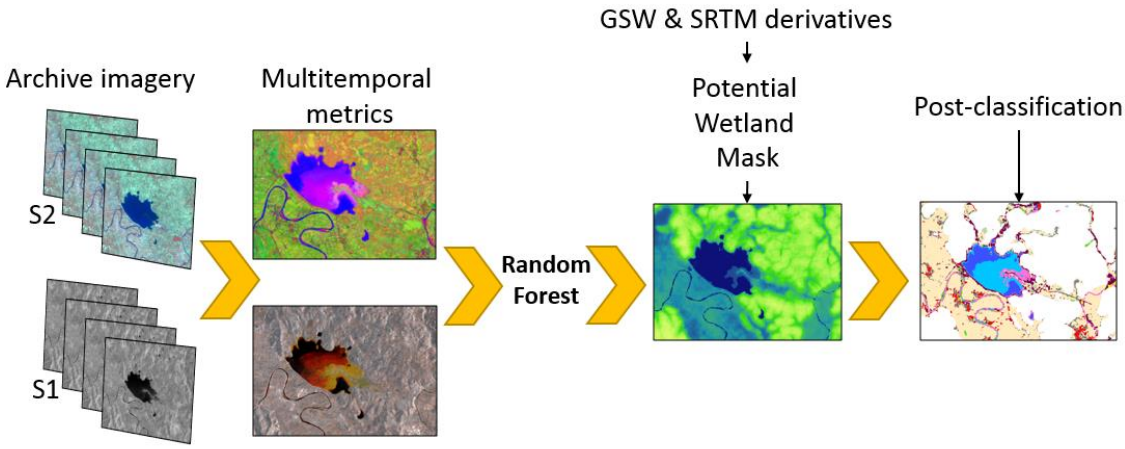


Figure 4.2 Classification workflow. S1 and S2 are the Sentinel-1 and Sentinel-2 image collections, out of which the different multitemporal metrics are calculated. RF is the Random Forest classifier, and PWM is the Potential Wetlands Mask. During the post-classification phase we removed systematic errors using the PWM and added 3 new wetland classes using knowledge-based rules. The PWM was generated out of the Global Surface Water (GSW) layer and SRTM digital elevation model derivatives.

## 4.3. Results

### 4.3.1. Impact of the different datasets on the mapping accuracy

This analysis was carried out with the 10 initial land cover classes and the results of the cross-validation; overall accuracy (OA), producers' accuracy (PA) and users' accuracy (UA). The classifications produced using the three datasets (S1, S2 and NDIs) or combining S1 and NDIs achieved the highest accuracies, followed by the combination of S1 and S2, and the combination of S2 and NDIs (Figure 4.3). When using each dataset separately, accuracies were significantly lower than any combination of multiple datasets.

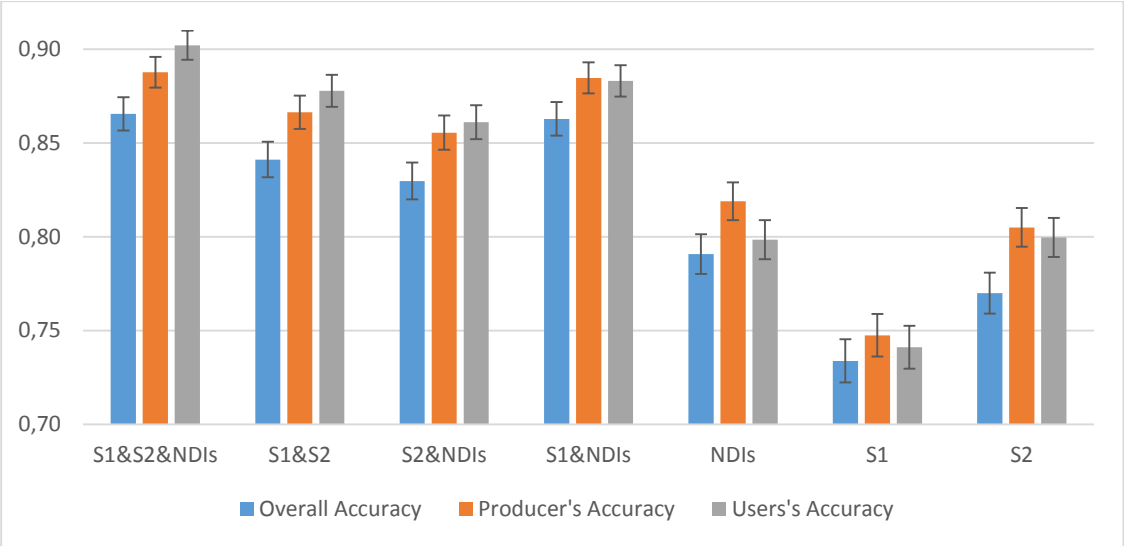


Figure 4.3 Overall, and average producers' and users' accuracies of individual and combined datasets. Error bars indicate the standard deviation at 95% confidence interval.

When using S1 and NDIs for classification, the class "Marshlands" occupied larger extensions at the expense of "Cropland" and "Heathland and scrubland" (Table 4.1). When using S1 and S2, the class "Intermittent water bodies" was overestimated at the expense of "Permanent water", mostly at the sea. When using only the optical datasets (i.e. NDIs and S2) the class "Built-up" was greatly overestimated at the expense of "Bare soil" and "Heathland and scrubland" (UA of Built-up 69%, Appendix A).

Table 4.1 Number of hectares per class with each combination of multiple predictors before post-classification processing

| | S1&S2&NDI (ha) | S1 & S2 (ha) | S2 & NDI (ha) | S1 & NDI (ha) |
|---|---|---|---|---|
| Bare soil | 15,749 | 18,642 | 7,714 | 15,104 |
| Permanent Water | 77,972 | 74,165 | 78,672 | 75,124 |
| Built-up | 30,782 | 30,440 | 54,033 | 32,955 |
| Marshlands | 30,803 | 22,848 | 25,732 | 41,794 |
| Intermittent water | 7,636 | 15,980 | 11,563 | 6999 |
| Deciduous forest | 32,144 | 33,859 | 30,388 | 30,364 |
| Coniferous forest | 12,771 | 17,674 | 13,879 | 13,858 |
| Cropland | 256,310 | 246,606 | 260,065 | 262,866 |
| Grassland | 28,378 | 26,792 | 35,259 | 27,426 |
| Heathland and scrubland | 105,883 | 111,420 | 81,121 | 91,935 |

Areas of steep slope oriented towards the Sentinel-1 satellite returned very high backscatter values, which made them to be misclassified as "Built-up" regardless of their true class. Despite the PWM excluded most of these errors, some remained along small rivers and creeks between steep mountains.

The distinction between "Coniferous forest" and "Deciduous forest" was equally good regardless of the combination of datasets used, as long as more than one were used. The confusion between "Heathland and scrubland" and "Grassland" was high for all combinations of datasets (e.g. UA of "Heathland and scrubland" 52% and PA of "Grasslands" 41% when using the three datasets, Appendix A).

The class "Cropland" occupied the largest extent, and thus had a larger number of inconsistencies. For instance, some croplands were classified as "Heathland and scrubland" and others as "Bare Soil". Many of them correspond to rather dry areas with high content in salt that are not actively farmed (Figure 4.4 A and B).

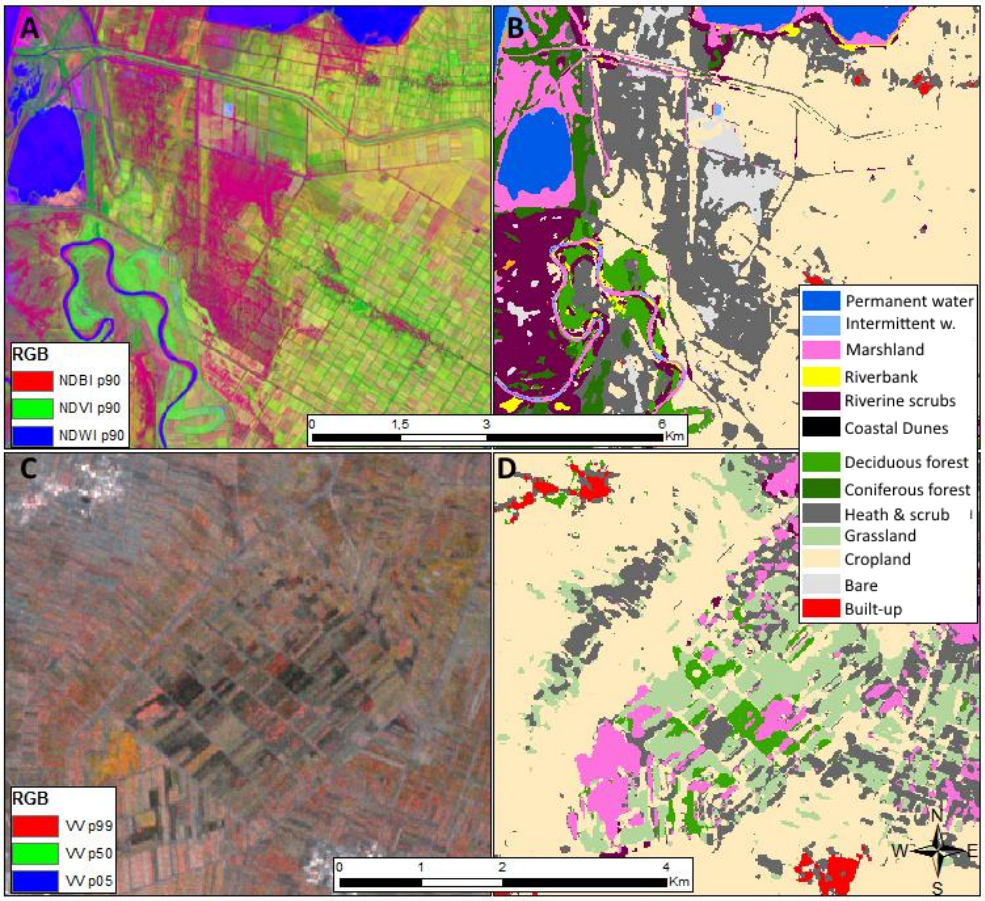


Figure 4.4 "Cropland" misclassified as "Bare soil" and "Heathland and Scrub" (A and B) and as "Marshlands" (C and D). "A" shows an RGB composite of NDBI, NDVI and NDWI. Red areas represent high NDBI values. "C" shows a Sentinel-1 RGB composite of percentiles 99, 50 and 05 of a former marshland, now used for agriculture. The brighter areas correspond to the extremely high backscatter values of slopes oriented towards the sensor. "B" and "D" shows the classification results of "A" and "C" respectively.

Other croplands showed higher frequencies of inundation and were thus misclassified as "Marshlands" (Figure 4.4 C and D). These were very localized cases easy to correct manually. The area shown in Figure 4.4 C and D actually corresponds to the former Maliqui freshwater marsh, recently drained and now used for agriculture.

### 4.3.2. Post-processing classification

Post-classification processing was applied only to the results of the combination of S1, S2 and NDIs datasets. Using knowledge-based criteria we incorporated three classes: "Riverbanks", "Riverine scrubs" and "Dunes" increasing the wetland-related classes from 3 to 6 (Figure 4.5). This generated an inevitable trade-off between thematic resolution and classification accuracy, and some errors were introduced. For instance, a few bare soil areas of industrial use (e.g. ports or salt pans) were classified as "Dunes" or "Riverbanks".

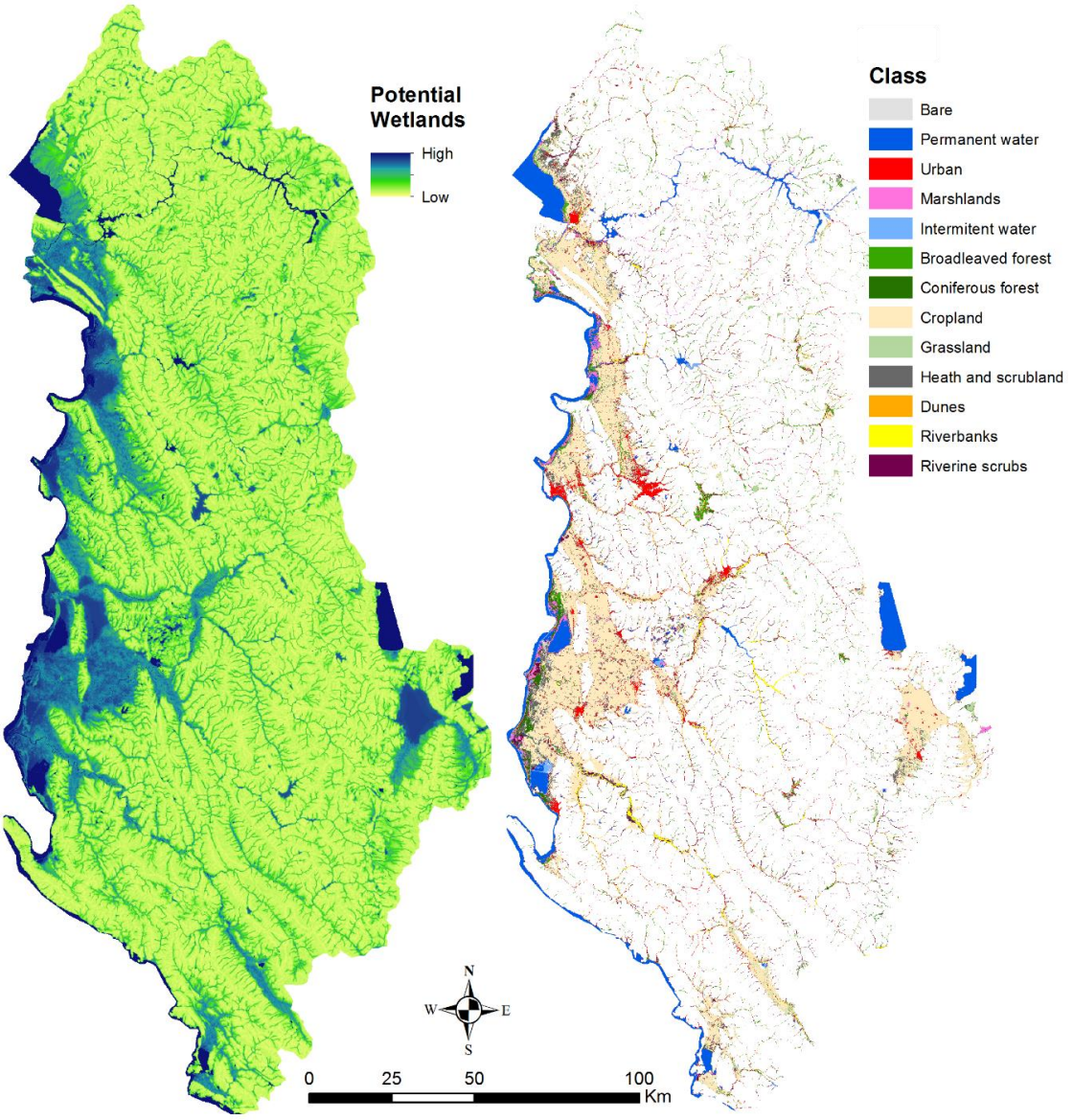


Figure 4.5 Map of potential wetlands (left) and post-classification map with the 13 final classes (right). The map of potential wetlands indicates the probability of each pixel of being a wetland according to morphological criteria. Only areas above a histogram-based threshold (Otsu, 1979) were mapped.

The accuracy analysis with independent samples returned an overall accuracy of 82%. The detailed accuracy matrix (Appendix A) shows that most conflicting classes were "Bare soil" and "Riverine scrubs" that were often mixed up with "Heathland and scrub". In addition, "Heathland and scrub" was sometimes misclassified as "Cropland", and "Marshland" was sometimes confused with "Intermittent water bodies".

Because the aim of this study is to apply the methodology at national scale, we compared our results with the last inventory of Albanian wetlands (Marieta et al., 2003). It was carried out

in 2003 using field information and satellite and aerial image interpretation. Out of 694 inventoried wetlands, we eliminated 18 that we couldn't find through visual inspection of current imagery, and are assumed to have disappeared. Fourteen of them were artificial water reservoirs, 3 marshes and 1 lake. For the remaining 676 wetlands we analyzed their correspondence with our results. The PWM excluded 99 wetlands. Thirty-three of those were small artificial water reservoirs, and 54 were very small glacial lakes (circa 1 ha).

## 4.4. Discussion

### 4.4.1. Impact of the different datasets on the mapping accuracy

Fusing the datasets from different sensors (Sentinel-1 and Sentinel-2) and the different indices (NDBI, NDVI, NDWI), provided the highest accuracies (Figure 4.3), in agreement with other studies (Blaes et al., 2005; Brisco and Brown, 1995; Chatziantoniou et al., 2017; Stefanski et al., 2014; Waske, 2014; White et al., 2017). SAR signals are sensitive to structure and biomass, dielectric properties of vegetation and soil (inundation patterns) and roughness (White et al., 2017, 2015). This makes SAR data essential to distinguish certain land cover classes such as "Built-up" and "Bare soil", or classes with a different levels moisture and inundation such as "Intermittent water bodies" (Figure 4.6). Other studies using multitemporal metrics have reported high accuracies using only optical data (Inglada et al., 2017; Mack et al., 2017; Pflugmacher et al., 2019), but they only have one or two classes for wetlands, and therefore very high accuracies in their class "water".

Despite the fact that the normalized difference indices were calculated from the same Sentinel-2 images, when combining both NDIs and S2 dataset, the accuracy increased significantly with respect to using only the S2 dataset. The NDIs dataset contains information on the temporal variation of physical and biological characteristics of the land cover (e.g. maximum inundation, vegetation peak, and minimum inundation and vegetation), while the S2 datasets contains only spectral information. The combination S2&NDIs even approached the performance accuracy levels of the combination S2&S1. This highlights the importance of the temporal dimension when mapping dynamic cover types.

"Cropland" is also a very dynamic class due to management practices that are not constant across time nor space, making this class prone to errors. In our case, this caused a high rate of omission errors (i.e. "Cropland" classified as something else, Figure 4.4 C and D). For instance, some croplands are harvested once, others twice (e.g. winter wheat) or not at all

(i.e. fallow land and permanent crops), and other times are used for temporary grasslands, increasing the error rate (Mack et al., 2017; Stefanski et al., 2014).

Systematic and standardized sampling campaigns such as the ones carried out at EU level within the LUCAS (Land Use-Cover Area frame Survey) project can be used to produce more accurate classifications including crop types (Mack et al., 2017; Pflugmacher et al., 2019). Unfortunately, such datasets are currently not available for Albania. It would be possible to use cadastral information to leave out areas used for agriculture and eliminate these uncertainties. However, many agricultural areas act as habitat for wetland species when the natural wetlands are dried out or disturbed, and should be included in wetland mapping activities (Czech and Parsons, 2002). Besides, for an integrated management that considers the water-food-and energy nexus it is important to include agricultural areas, whether they are in use or not (fallow).

Yearly water level fluctuations are common in artificial wetlands used as water reservoirs. These water bodies are often classified as one single class of permanent water, whereas they are composed of areas that are either permanently or temporarily inundated. The use of multitemporal statistics allowed us to separate these two categories (Figure 4.6). Mapping the intermittent water bodies is especially important in the case of water reservoirs. These areas are often steep and local mountainous vegetation cannot grow there due to the flood recurrence. This makes these areas prone to erosion, increasing the sediment deposition rate on the water reservoir and thus decreasing its life span. Mapping the water spread area (i.e. intermittent water) have been used before in sedimentation models to predict the life span of the dam (Foteh et al., 2018).

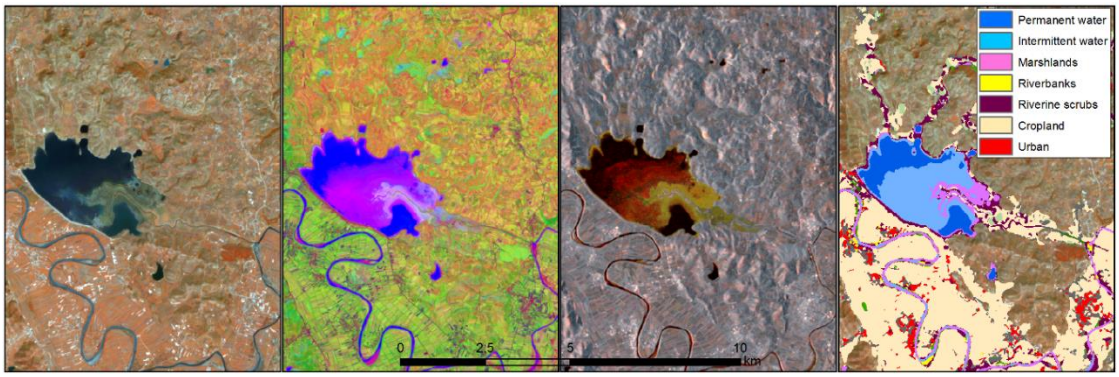


Figure 4.6 From left to right, an example of the datasets S2, NDIs, S1 and result of classification. NDIs and the S1 metrics allow to separate the parts of the wetland that are permanently and temporarily flooded.

### 4.4.2. Post-classification processing

Often, land managers need higher accuracies and thematic resolutions, especially for quantitative analyses (Chatziantoniou et al., 2017; Manandhar et al., 2009). Using knowledge-based rules based on spatial, environmental, geomorphologic or ecological criteria can improve accuracies and the separability of classes that are spectrally similar but ecologically very different (Manandhar et al., 2009). For instance, the mapping exercise of Pflugmacher et al. (Pflugmacher et al., 2019) was carried out at continental scale. This implied mapping the same land cover types across climatic regions, where a same land cover type can display different spatiotemporal patterns (e.g. boreal coniferous forests vs. Mediterranean coniferous forests). To account for this, they implemented auxiliary variables that exploited the relationship between climate, topography and vegetation (precipitation, temperature, and latitude and longitude). The addition of these variables had the highest effect on model performance, higher even than adding other temporal metrics. Although they did not used knowledge-based rules, their results show the relevance of adding environmental information rather than just more remotely sensed data. The knowledge-based rules we set were based on theoretical considerations and observations. Their addition increased the thematic resolution, but also introduced some classification errors. This is something to be expected and good knowledge of the area is necessary to balance the trade-off between thematic resolution and classification accuracy (Knight et al., 2013). Knowledge-based rules require ecological rather than remote sensing expertise and are specific for each case study (Perennou et al., 2018). Thus, they should be modified according to the needs and conditions of other environments when replicating the methodology somewhere else. This, in turn, could pose an issue of lack of standardization. Regardless, our results provide supporting evidence of the benefits of including ancillary information based on logic and expert knowledge in mapping activities (Chatziantoniou et al., 2017; Long and Skewes, 1996; Manandhar et al., 2009), so that mapping products can be better suited for decision making.

The comparison of our final product with the 2003 inventory revealed that our workflow missed 99 of the 676 wetlands inventoried. Almost half of these were artificially created water reservoirs located in areas with a topography unsuitable to store water without building a dam, and therefore not regarded as potential wetland areas. However, there were 54 small glacial lakes (circa 1 ha) that were also masked out. Almost all of these omission errors were initially classified as some wetland type before the PWM was applied. Omission errors can be avoided by applying a more conservative manual threshold to the PWM, but that can increase the number of errors related to the terrain artifacts. Trade-offs between omission

and commission errors are often unavoidable and a histogram-based thresholding method is still recommended. Other types of wetlands such as raised peatbogs could be as well excluded when located on a slope.

### 4.5. Conclusions

Landscape temporal dynamics are traits that have often hampered mapping activities, and in consequence delayed spatially-based decisions. Using a combination of multitemporal SAR and optical metrics we can use such traits to distinguish spectrally similar but ecologically different cover types. Including additional knowledge-based rules can remove artifacts and increase the thematic resolution. Cloud computing platforms can facilitate the handling of large amounts of spatial data and allow to deliver ready to use products in an operational way.

The demanding monitoring and reporting requirements of the Ramsar Convention on Wetlands and the Sustainable Development Goals create a need for countries to improve their capabilities for wetland mapping, inventorying, monitoring and assessment. Earth Observation plays a very important role in increasing these capabilities, and our results demonstrate the usefulness of multitemporal optical and radar metrics in combination with knowledge-based rules for wetland mapping at national level.

# Chapter 5

## Land Surface Temperature trends as indicator of land use changes in wetlands

International Journal of Applied Earth Observation and Geoinformation, 70, 62-71

August 2018

doi:10.1016/j.jag.2018.02.002

Javier Muro, Adrian Strauch, Sascha Heinemann, Stefanie Steinbach, Frank Thonfeld, Björn Waske, Bernd Diekkrüger

*"Time is the only thing we truly have."*

*– Anonymous*

**Abstract**

The impacts of agricultural expansion on wetlands are diverse and complex. Land surface temperature (LST) has a great potential to act as a global indicator of the status of wetlands and changes in their hydrological and evapotranspiration regimes, which are often linked to land use and cover changes. We use the whole MODIS LST archive (2000–2017) to perform time series analysis in the Kilombero catchment, Tanzania; a large wetland that has experienced major land conversions to agriculture during the last two decades. We estimated pixel based trends using three models: a seasonal trend model, and aggregated time series using annual means and percentile 90. We characterized the trends found by using land cover change maps derived from Landsat imagery and a post-classification comparison. The relation between Normalized Difference Vegetation Index (NDVI) and LST trends was also studied ($r = -0.56$). The results given by the seasonal trend model and annual means were similar ($r = 0.81$). Fewer significant trends were found using the percentile 90, and these had larger magnitudes. Positive LST trends (i.e. increasing) corresponded to deforestation and farmland expansion into the floodplain, while forestation processes resulted in negative LST trends. Moderate increases of LST in natural wetlands suggest that the impacts of human activities extend also into non-cultivated areas. We provide evidence of how time series analysis of LST data can be successfully used to monitor and study changes in wetland ecosystems at regional and local scales.

## 5.1. Introduction

Wetlands are multiple value ecosystems, providing a wide variety of services (Tiner, 2015). In some cases, wetlands are almost the only source of natural resources sustaining rural economies. Their plant communities have widely varying vegetation type, density and water demand and availability. Their water requirements and impacts on streamflows are complex and uncertain, and agriculture practices have a large impact on their functioning. Remote sensing imagery has been widely used for monitoring wetlands and provide spatially distributed and temporally frequent information on their environmental state (Amler et al., 2015; Guo et al., 2017; Jones et al., 2009).

Most monitoring approaches are based on bi-temporal land use land cover (LULC) change techniques, or on mapping the water surface dynamics with optical (Díaz-Delgado et al.,

2016) or radar time series (Betbeder et al., 2015). Thermal infra-red data has been less frequently used, but it can nonetheless be essential to understand the spatial distributions of evapotranspiration in ground water dependent ecosystems. Land surface temperature (LST) based evapotranspiration estimations using thermal data have proven useful in practical applications in water management and water rights conflict solving (Anderson et al., 2012; McVicar and Jupp, 1998). It has been suggested that it is also possible to use LST variations to detect changes in land management practices, even when they are not associated with any direct change in land cover types (Luyssaert et al., 2014), or to map wetlands under aquatic vegetation (Leblanc et al., 2011). An additional advantage is that LST reacts to drought conditions earlier than Normalized Difference Vegetation Index (NDVI) (McVicar and Jupp, 1998).

A challenge encountered when using LST data is its high temporal variability; it greatly depends on climatic and illumination conditions, and measuring the change in LST between two single points in time is ecologically uninformative (McVicar and Jupp, 1998). Analyses of dense LST time series can reveal landscape change trends affecting water balances and energy fluxes. This is especially relevant in highly dynamic and water dependent ecosystems such as wetlands. Despite having a coarse resolution (1 km), the daily MODIS LST products are ideal for time series analysis, providing daily LST data at global scale since 2000 (Neteler, 2010).

A second challenge to overcome when analyzing LST time series is separating the seasonal, gradual, and abrupt changes that are combined in time series data (Ghazaryan et al., 2016; Verbesselt et al., 2010), in addition to the noise generated by atmospheric effects. Time series analysis can be performed by extracting and aggregating the data into statistical parameters (Forkel et al., 2013), performing harmonic analysis (Forkel et al., 2013; Verbesselt et al., 2010) or applying change detection algorithms and unsupervised classification of the changes (Hecheltjen et al., 2014). Methods such as Breaks For Additive Seasonal and Trend (BFAST) (Verbesselt et al., 2010), BFAST-monitor (Verbesselt et al., 2012), or greenbrown (Forkel et al., 2015, 2013) have been developed to deal with such challenges. They analyze data decomposing it into three components: the seasonal variation, trend, and a remainder (Verbesselt et al., 2010). Break points caused by sudden changes in the land cover properties are flagged.

A third challenge is caused by the irregular time steps caused by gaps due to clouds and other effects that result in poor pixel quality and are flagged as such in the quality band.

The open source R package Greenbrown (Forkel et al., 2013) has been designed to analyze trends, trend changes, and phenology events in gridded time series of vegetation indices interpolating missing values. These indices are indicative of vegetation cover and health status, and widely used in time series analysis to assess changes in vegetation (Forkel et al., 2013; Ghazaryan et al., 2016; Yengoh et al., 2015). However, due to the highly variable surface water dynamics of some wetlands, vegetation indices are less suited to study their long term trends. Decreases in NDVI can be a result of a loss of vegetation, or consequence of an increase in flooding. On the other hand, both decreases in vegetation cover and water content will produce increases in LST and vice versa. In spite of that, we find fewer examples of the use of LST to monitor long term changes. When LST is used for monitoring, it is often in combination with NDVI (Julien et al., 2011) or is mainly focused on climatology (Jiménez-Muñoz et al., 2016). The relationship between NDVI and LST has also been previously studied; when energy is the limiting factor NDVI and LST have a positive correlation, but when water is the limiting factor LST and NDVI are negatively correlated (Karnieli et al., 2010). To our knowledge, despite its well-recognized potentials, LST has not yet been thoroughly employed to analyze temporal trends in water based ecosystems.

The objective of this research is to investigate the potential of LST as indicator of land use changes using the Kilombero Valley as a study area. The Kilombero Valley is a large complex of wetlands that has experienced major land conversions to agriculture during the last two decades, and the consequences of such conversions are not well understood. The spatio-temporal variations of LST and NDVI in Kilombero were analyzed and assessed against these land conversions using the full MODIS archive (2000–2017) of LST and NDVI products and a set of Landsat-based LULC change maps. Three different time series models were compared (annual means, annual maxima and a seasonal trend model), and the existence of break points in the time series was explored.

## 5.2. Materials and methods

### 5.2.1. Study area

The Kilombero valley is a pilot site of the European Horizon 2020 project Satellite-based Wetlands Observation Service (SWOS) and the largest seasonal wetland in East Africa. The basin covers an area of 4,023,025 ha and the floodplain of the main river covers about 796,700 ha (Mombo et al., 2011). The elevation ranges between 200 and 2500 m.a.s.l. and the regional climate is sub-humid tropical with average daily temperatures around 22–23 °C, and

annual precipitation of about 1200–1400 mm. The bimodal rainy pattern comprises a short rainy season (November–January) and a long rainy season (March–May) with a distinct dry season from July until October (Koutsouris et al., 2016). The Kilombero River discharge is very variable (92–3044 $m^3/s$) and regularly floods the floodplain during the long rainy season.

The landscape consists of periodically inundated grasslands, swampy areas, Miombo woodlands, evergreen forest fragments, teak plantations, and an increasing farmed surface (Figure 5.1) (Leemhuis et al., 2017). Most of the agriculture is for subsistence and consists of maize and rice among other products. In the floodplain, there are two industrialized farms that produce sugar cane (Figure 5.1). The grasslands of the floodplain are periodically inundated, and during the dry season they are burnt to boost grass growth after the onset of the rainy season. Kilombero is a Ramsar site and home to several endangered and endemic species such as the puku antelope (*Kobus vardonii*), which inhabits these frequently flooded grasslands. The floodplain also acts as a vital natural corridor between the Udzungwa Mountains National Park to the northwest and the Selous Game reserve in the east, and two of these wildlife corridors have recently ceased to function (Figure 5.1) (Wilson et al., 2017). The floodplain is also an important source of clean water for the downstream area (Wilson et al., 2017). Despite its long history of human occupation, the rapid increase in human population over the last decades (TNBS, 2012) along with uncontrolled farming practices have led to intensive land use conversion, wildlife decline and habitat fragmentation. A recent game census confirmed a strong decrease of large mammal populations (TWRI, 2013), and anecdotal evidence suggests decline in productivity of fisheries (Wilson et al., 2017). Furthermore, the agricultural expansion is altering the hydrological regime of the rivers, decreasing evapotranspiration and baseflow and increasing runoff (Leemhuis et al., 2017). The western part of the basin has a higher altitude and its vegetation cover has been degraded through frequent anthropogenic caused fires. As compensatory action, a few sites are being subjected to reforestation for climate change mitigation (GLR, 2009). Human population and industrialized agriculture are expected to increase due to plans for large scale agricultural development within the frame of Southern Agricultural Growth Corridor of Tanzania (SAGCOT) (Leemhuis et al., 2017).

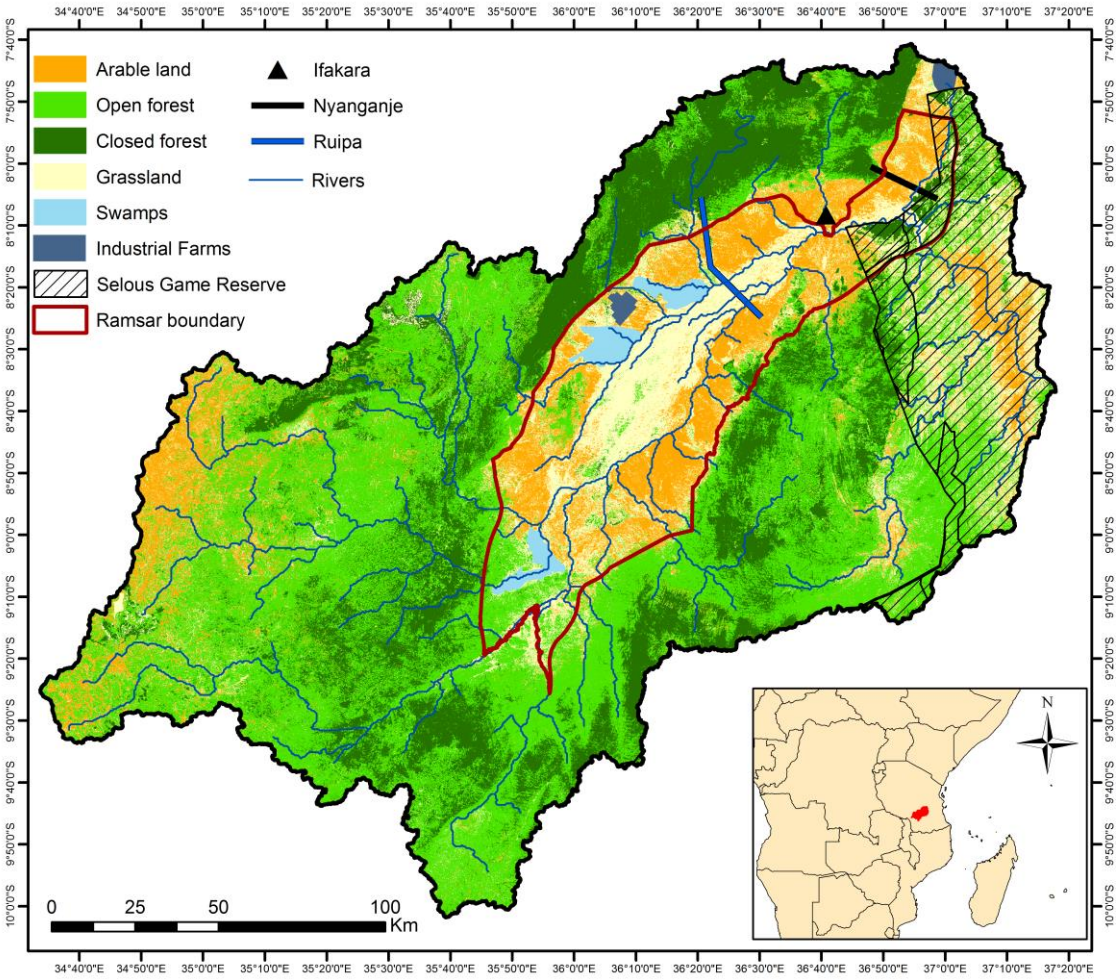


Figure 5.1 Kilombero catchment with its main LULC classes. Ifakara, is the main urban center. The map also shows the Nyanganje and Ruipa wildlife corridors, (modified from Wilson et al., (2017)) and the Selous Game reserve.

### 5.2.2. Datasets

We used the full archive (2000–2017) of the 8-day LST product (MOD11A2) from the Terra satellite. It is composed of the daily 1-kilometer LST product (MOD11A1) and stored on a 1-kilometer grid as the average values of clear-sky LSTs during an 8-day period. It uses the generalized split-window algorithm, optimized to separate ranges of atmospheric column water vapor and lower boundary air surface temperatures into tractable sub-ranges. Surface emissivities are estimated from land cover types and clouds are masked with the MODIS Cloud Mask data product (MOD35 L2). LST products are validated through field campaigns and radiance-based validation studies and are ready to use in science applications and publications. Errors are within ±1 K in most cases, but larger errors may occur in desert

regions due to the presence of aerosols. Further details regarding the validation are available at Wan, (2014, 2008); Wan et al., (2004).

The NASA Land Processes Distributed Active Archive Center provides mainly 2 versions of the LST MOD11A2 product: V005 and V006. V006 seems to offer better estimates for arid areas (Wan, 2014), but V005 has been suggested to offer good quality data for inland water pixels (Neteler, 2010). Since our study area is a wetland, we used V005.

The NDVI dataset MOD13A1 from the Terra satellite is delivered every 16 days at 500 m resolution. It is retrieved from daily atmospherically corrected bidirectional surface reflectance products where low quality pixels are removed (Didan et al., 2017). The algorithm chooses the best available pixel value from all the acquisitions from the 16-day period.

We acquired Landsat Surface Reflectance Level-2 Science Products from the USGS downloading platform Earth Explorer and performed cloud masking using the Fmask algorithm (Zhu et al., 2015).

### 5.2.3. LULC change analysis

Multi-temporal statistical metrics (Mack et al., 2017) were calculated for the tasseled cap components of Wetness, Greenness, and Brightness (Crist and Cicone, 1984) from all available Landsat scenes of two three-year time spans; (2003–2005 and 2014–2016). A Land Use Land Cover (LULC) classification for each of these two time spans was performed using a Random Forest classifier, the Tasseled Cap components and the SRTM DEM and derivatives (slope, surface roughness, and Topographic Wetness Index (Beven and Kirkby, 1979)). Field observations and data from flight campaigns and Google Earth were used as reference for training and validation. Further information can be found in Leemhuis et al., (2017). The initial classification results were aggregated into coarser classes: Closed Forest, Open forest, Grasslands, Arable land and Water. A post classification comparison was performed between both LULC maps and error propagation was reduced by using a change-no change mask. This mask was produced applying a threshold (Otsu, 1979) on the magnitude component of a Change Vector Analysis of the tasseled cap 85 percentiles. Pixels labeled as "no change" in the mask were discarded from the post classification comparison. These pixels are assumed to be unchanged as changing labels of those pixels can be attributed to errors of the individual classifications. Further, LULC changes were clustered into three categories to facilitate the analysis and interpretation of results: Farmland Expansion on Grasslands (from Grasslands and Water to Arable Land), Deforestation (from Forest and

Open Forest to Grasslands and Arable Land) and Forestation (from any class to Forest and Open Forest, and from Open Forest to Forest). We use the term "Forestation" to include "afforestation" (forest growth in previously non-forested areas) as well as "reforestation" (forest growth in previously vegetated areas). Changes in other directions were minimal and thus discarded. The overall accuracy of this LULC change map was estimated to be 60% (Table 5.1). It was evaluated using 200 points (of which only 158 were valid) randomly distributed and Google Earth, Bing, and Landsat imagery via Collect Earth (Bey et al., 2016).

Table 5.1. Accuracies of the LULC change map derived from Landsat scenes of two three-year time spans: 2003–2005 and 2014–2016.

| Accuracies | Deforestation | Forestation | Farmland expansion | No change | Total |
|---|---|---|---|---|---|
| **Overall** | – | – | – | – | 60% |
| **Users** | 60% | 31% | 58% | 95% | 61% |
| **Producers** | 99% | 100% | 42% | 13% | 64% |

### 5.2.4. Time series analysis

The trend estimation of satellite data is usually performed in three ways (Forkel et al., 2013; Frey and Kuenzer, 2015); aggregating the data using multitemporal metrics, using an additive decomposition model, or via de-seasonalization of the data. Different methods might be used depending on the circumstances. We used three methods provided within the greenbrown R package (Forkel et al., 2015, 2013):

- Seasonal Trend Model (STM): Linear and harmonic terms are fitted to the original time series using ordinary least squares (OLS) regression. It is based on the classical additive decomposition model and follows the implementation of BFAST (Verbesselt et al., 2010) (Verbesselt et al., 2010). The significance of the trend is estimated using a t-test.
- Annual Aggregated Trends by annual means (AATmean). It calculates trends on annual aggregated time series using the annual mean and an OLS regression. The significance of the trend is estimated using the Mann–Kendall test.
- Annual Aggregated Trends using the percentile 90 (AAT90). It uses the annual 90 percentile and performs an OLS regression. The significance of the trend is also estimated using the Mann–Kendall test.

Trends were divided on a pixel basis into positive, negative or non-significant at 90% confidence level. Pixels with no significant trends were masked out (Figure 5.2). Our focus was to study the variation of LST with farmland expansion rather than the number of break points. Thus, we assumed monotonic trends and set the number of break points to 0. Additionally, to explore the influence of the number of breaks in the analysis we re-run the STM model setting the maximum number of break points to 1 (Figure 5.3). The break point detection algorithm searches for structural changes in a regression and estimates their position by minimizing the residual sum of squares (Forkel et al., 2013). When a break point is detected, the trend is divided into two segments whose slope may or may not be significant. To better estimate the position of a break point it is necessary to specify a minimum length of the segments. We set it to 2.5 years which represents 15% of the study period.

Records from complete years are needed when aggregating the data by annual means. Thus, data from 2000 and 2017 were excluded when comparing AATmean, AAT90 and STM models. However, further analyses were run using the STM and data from 2000 (from March 2000) and 2017 (to March 2017). To facilitate interpretation, the slopes of the trends were rescaled into ΔLST in Kelvin (K) using a linear regression;

$$\Delta LST = slope * t$$

where *t* is the length of the time period (or of each segment) in years.

We extracted LST data for homogeneous subsets of pixels representative of the spatial and temporal patterns of the area marked in Figure 5.3a–g (industrial farmland expansion, swamp partially surrounded by agriculture, reforestation, subsistence farmland expansion, undisturbed wetland, seasonally inundated grassland and deforestation). To remove the influence of remaining unscreened clouds we eliminated the 5% of the lowest values, since clouds display lower LST. We plotted the LST data and calculated the times of break (Figure 5.4).

NDVI is widely used in time series analyses. However, LST is better suited to monitor changes in seasonally inundated areas since a drop in NDVI may be caused by an increase in surface water or by a decrease in vegetation. On the other hand, a drop in LST will be caused by a decrease of vegetation or water content (or both) and vice versa. To study the difference between NDVI and LST trends we compared the ΔLST map with a ΔNDVI map generated using the MODIS MOD13A1 product and the STM model.

## 5.3. Results

### 5.3.1. Models' performances

We compared the three models using only data from the period 2001–2016 to exclude years of incomplete data. AATmean and STM returned similar results regarding direction and magnitude of ΔLST (correlation coefficient r = 0.81, Table 5.2). AAT90 reported fewer significant trends. These were generally in line with the other two models in terms of direction, but magnitude ranges had a greater amplitude (higher minimum and maximum values, Figure 5.2).

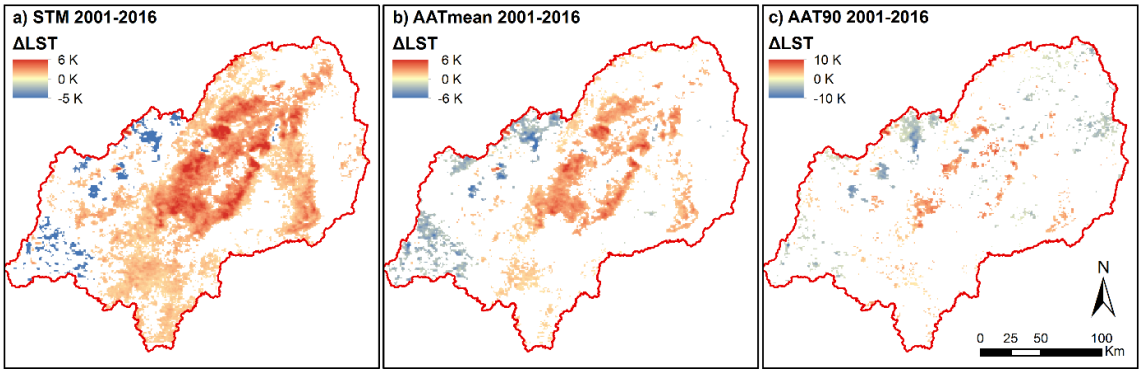


Figure 5.2 Results of the comparison of the three trend models used: (a) seasonal trend model (STM), (b) aggregated time series by annual means (AATmean), and (c) by percentile 90 (AAT90) at 90% confidence level. Monotonic trends were assumed for this analysis (i.e. break points were not searched for).

Table 5.2 Comparison of the results of the three trend models and their correlation to each other.

| *r* | STM | AATmean | AAT90 | SD |
|---|---|---|---|---|
| **STM** | 1 | 0.81 | 0.52 | 1.17 |
| **AATmean** | – | 1 | 0.56 | 1.72 |
| **AAT90** | – | – | 1 | 4.1 |

### 5.3.2. LST trends in Kilombero catchment

We found average monotonic increases in LST of 2–3 K in the core of the Ramsar site (Figure 5.3A). Major increases of up to 6 K were found along the Ramsar boundary. The southern and northern parts of the Ramsar site showed lesser or no LST trends, as well as other areas further away from the Ramsar site. Mild decreases were found in a permanent swamp inside the Ramsar site ("b" in Figure 5.3, Figure 5.4), and stronger decreases in some

areas north-center and west of the basin that have been reforested with tree plantations during the study period ("c" in Figure 5.3, Figure 5.4). When a break point was detected it was usually placed close to the start and end of the time series, except for a few areas to the east of the basin (red colors in Figure 5.3B).

We calculated and plotted the trend and break points for the points marked in Figure 5.3A as "a–g" and the results are shown in Figure 5.4. Point "a" corresponds to the expansion of a large scale farm of sugarcane on wetland area producing a break point. Point "b" is a permanent swamp that has not experienced land use changes during the study period, but it is surrounded by agriculture. Here LST decreases after a break point in 2013 whose cause is unknown. Point "c" has been reforested with plantations, which has caused a break point and a very significant decreasing trend afterward ($p \leq 0.001$). Point "d" is an area where unorganized small scale farming has been developed during the study period. No break points are detected here, although the trend is increasing and very significant ($p \leq 0.001$). Point "e" is an undisturbed swamp that shows a very mild increasing trend significant only at 90% confidence interval. Point "f' is a seasonally inundated grassland that shows a similar temporal pattern than "e". Point "g" is an upland forest that has been partly and slowly converted to small scale agriculture. A break point is detected in 2008 followed by a very significant increasing trend ($p \leq 0.001$).

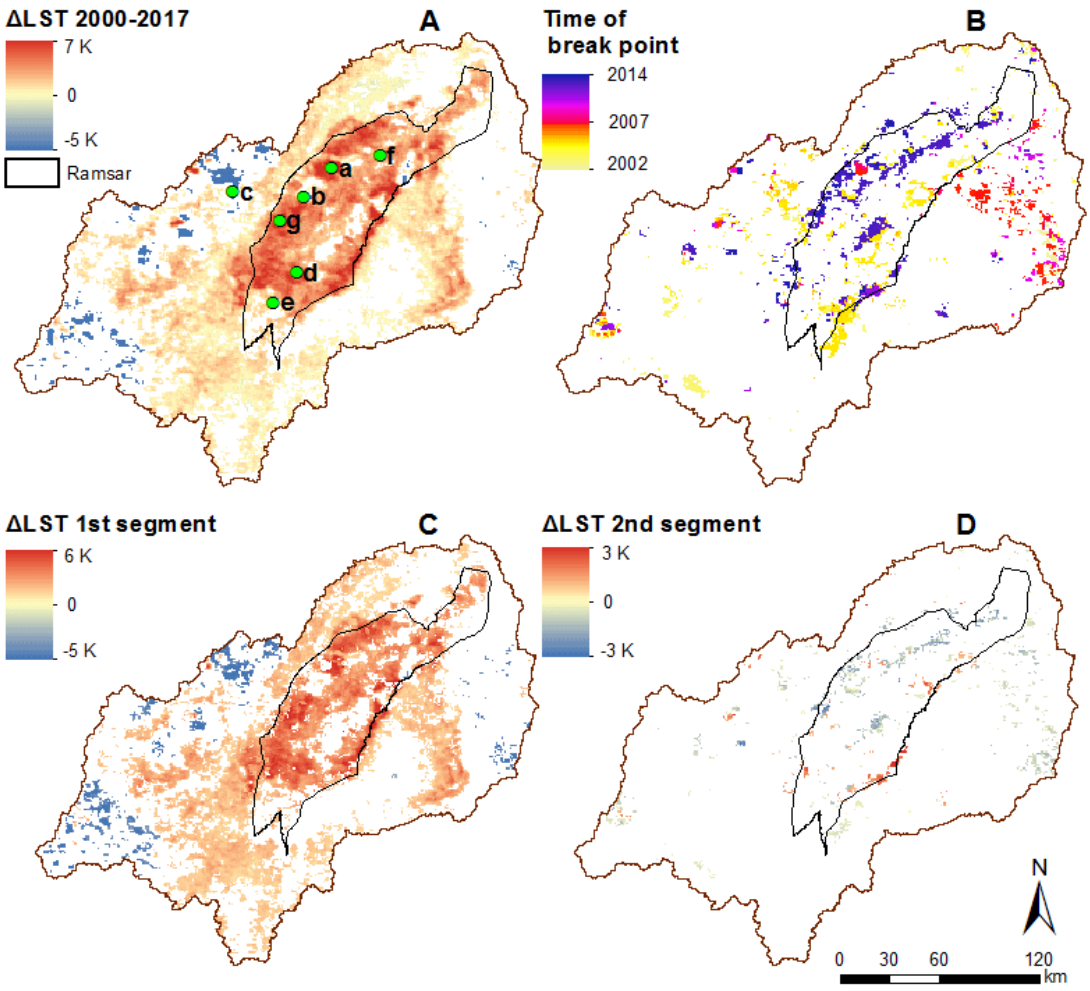


Figure 5.3 Results of the trend analysis using the STM model for the period March 2000–March 2017. In map A, monotonic trends are assumed (i.e. break points = 0). In maps B, C and D the maximum number of break points was set to 1. B indicates the time of break, and C and D show the ΔLST before and after the break point respectively (i.e. first and second segment). Letters "a–g" mark the location of the pixels plotted in Figure 5.4.

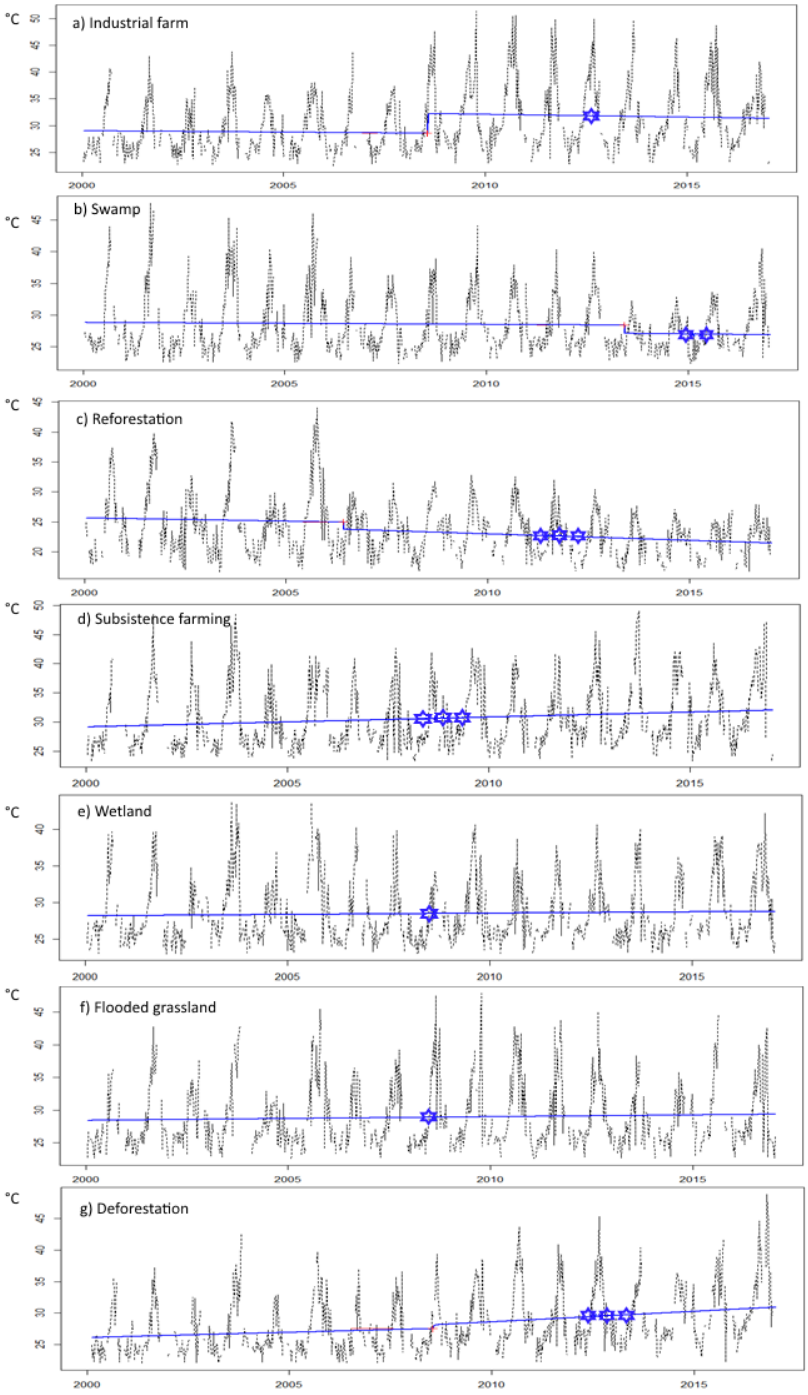


Figure 5.4 LST trends for the points marked in Figure 5.3A "a–g". Number of stars indicate the p-values of each segment at which the trend is significant: *** ($p \leq 0.001$), ** ($p \leq 0.01$), * ($p \leq 0.05$), and no symbol if $p > 0.1$."a" is an industrial farm developed on the wetland during the study period; "b" is a swamp partially surrounded by agriculture; "c" is a reforested area; "d" is an area where small scale and unorganized farming has developed during the study period; "e" is a wetland up the river that is still mostly undisturbed; "f" is a seasonally inundated grassland; "g" was a forest upland area that has been converted to small scale agriculture.

### 5.3.3. LST, NDVI and LULC changes

The correlation analysis between ΔLST and ΔNDVI returned a correlation coefficient of −0.56. Only pixels with significant trends in both data sets were used ($p \leq 0.1$). Table 5.3 shows the statistics of both parameters. The mean and standard deviation of ΔLST and ΔNDVI per LULC change class are shown in the charts of Figure 5.5.

Table 5.3 Statistics of the ΔLST and ΔNDVI products

| | Min | Max | Mean | SD |
|---|---|---|---|---|
| **ΔLST** | −5.3 | 6.9 | 1.68 | 1.12 |
| **ΔNDVI** | −0.4061 | 0.4553 | −0.0151 | 0.09 |

Despite the differences in spatial resolution between datasets (1 km for ΔLST, 500 m for ΔNDVI and 30 m for the LULC maps) Deforestation and Farmland Expansion patterns were related to significant increases in LST (Figure 5.5 lower right chart). Overall, Farmland Expansion on grasslands was responsible for an increase of almost 3 K (±1), and Deforestation caused increases of more than 2 K (±1.5). Areas labeled as "No change" also experienced overall increases in LST. Pixels showing decreasing LST trends corresponded mostly to Forestation processes (Figure 5.3and Figure 5.4c). However, the overall patterns of Forestation found in the LULC change maps could not be associated with trends in LST (Figure 5.5). On the other hand, increases in NDVI were related to the change class Forestation, and decreases to Farmland Expansion.

The results of the trend analysis using the MODIS NDVI product revealed spatial patterns similar to those shown by the LST (Figure 5.5). The largest increases in LST and decreases in NDVI took place inside or close to the Ramsar site. There were, however, some differences between ΔLST and ΔNDVI. For instance, there were no significant trends of NDVI in the core of the Ramsar site, whereas the LST trend analysis indicated positive and significant monotonic trends ("f" in Figure 5.3 and Figure 5.4)

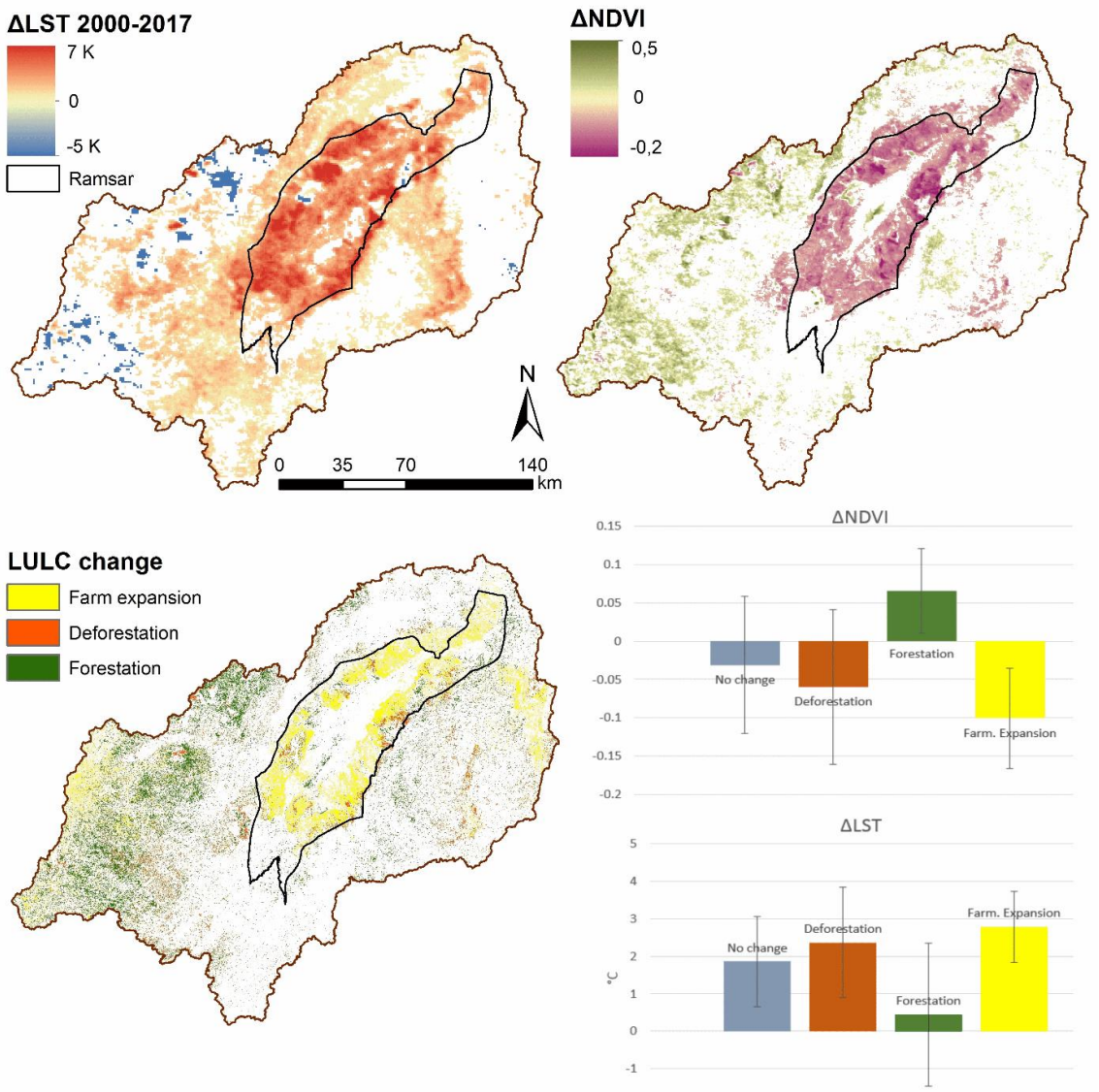


Figure 5.5 Variation of LST and NDVI in Kilombero using the STM model at 90% confidence interval for the period 2000–2017. Lower left map shows the LULC change map. ΔLST and ΔNDVI are grouped into the LULC change classes in the lower right charts.

## 5.4. Discussion

### 5.4.1. Models' performances

The three models (STM, AATmean and AAT90) agree in the vast concentric area at the outer limits of the Kilombero river floodplain (Figure 5.2). There is also a common area of LST decrease in the northern central part of the catchment product of forestation projects. AATmean and STM produced similar results in terms of magnitude and direction of ΔLST (Figure 5.2 and Table 5.2), but the number of pixels with significant trends was larger using

the STM model. Aggregating time series data is a common way to account for the seasonality and it is resilient against overestimation of trends (Forkel et al., 2013). However, it reduces the number of observations which may result in an underestimation of the trend significance. It will also prevent us from studying intra-annual dynamics such as beginning, end or length of the season (Forkel et al., 2013; Frey and Kuenzer, 2015; Ghazaryan et al., 2016).

The AAT90 model reported fewer pixels with significant trends but with much larger amplitudes (Table 5.2). The AAT90 method, by its definition, has a focus on the trend of the annual peak LST which is when changes in vegetation cover or water content are expected to have a more pronounced effect in the LST. STM and AATmean (directly or indirectly) account for the same time an area is left bare without vegetation (e.g. after a harvest). Hence, STM and AAT mean are more sensitive the LULC changes than AAT90. This does not necessarily mean that AAT90 is less accurate. Wetlands are crucial during the dry periods in many parts of the world serving as refuge and source of water in moments of scarcity. Mapping ΔLST only during the LST peak season can still have relevant applications for specific cases, such as inferring the availability of water or vegetation during breeding periods of fish, amphibians, or vectors of diseases (Metz et al., 2014), or during migrations of birds and other animals. These three time series analysis methods involve advantages and constraints that will be more or less relevant depending on the application (Forkel et al., 2013). In general, we recommend the use of seasonal trend models rather than aggregation methods because the seasonal trend models allow using data for incomplete years and at full temporal resolution.

Break points represent abrupt changes either due to conversion of one land cover type to another or due to changes in land management (Forkel et al., 2013; Verbesselt et al., 2010), e.g., through implementation or abandonment of irrigation systems (Hentze et al., 2017). However, land use changes often have long-term impacts on biophysical variables such as productivity or LST rather than abrupt ones. Hence, long-term monitoring and a combination of break point detection and trend estimation is required to characterize LULC changes and their impact on LST. Whether break points are detected or not, partly depends on the parameters set. For instance, the minimum length of a segment determines the shortest length of time necessary for a break point to be detected. If it is a large value (e.g. 40% of the study period), break points towards the beginning or end of the time series will not be detected, or will be placed somewhere else in the time line. On the other hand, a small minimum length might return false break points at the beginning or end of the time series. The use of different trend models also had an effect on where a break point was set for some

of the sampling sites "a–g" (Figure 5.4). This is expected since we are measuring the trends of different properties (e.g. extreme or average values). Since the focus of the paper is to evaluate the effect of land changes on LST and due to the relatively short length of the study period, a thorough study of the break points was not carried out.

### 5.4.2. LST trends in Kilombero catchment

Disturbances like deforestation cause a break point in the time series, increasing the LST abruptly. It would be expected that LST showed a decreasing trend during the years after deforestation as vegetation begins to regrow. However, in cases of substitution of natural vegetation (whether it is forest or wetland) for agriculture, LST tended to keep increasing after the break point (Figure 5.4g and d). In our case, Farmland Expansion was also related to increases in LST, contributing to create an agricultural heat island (Raymond et al., 1994). Most of the trends found were monotonic, and most of the break points identified were close to the end or beginning of the time series (Figure 5.3B).

The large increase in population in the area along with lack of property rights have caused uncontrolled farmland expansion as well as deforestation (Connors, 2015; Jones et al., 2009; Wilson et al., 2017). Most of the increases in LST and agricultural expansion patterns took place along the borders of the Ramsar area where many natural resources are found (mainly water, wood, and fertile lands). Areas of permanent swamps (Figure 2.3) and at the south of the Ramsar site are still not heavily used and showed no major increases in LST (nor decreases in NDVI). The seasonally inundated grasslands of the core of the Ramsar site have remained unoccupied, mostly because recurrent floods limit agricultural expansion. However, they present moderate increases in LST (although not in NDVI), which suggests that farming activities might be affecting the water balance in these seasonally inundated areas. This is in agreement with the results obtained in Leemhuis et al. (Leemhuis et al., 2017), where hydrological models determined that the land cover changes are decreasing evapotranspiration and baseflow and increasing runoff. This is also supported by the fact that the Selous Game Reserve (Figure 5.1) is the only larger region without a significant LST trend. As a game reserve it is not foreseen to host humans, limiting human impact compared to the regions outside protected areas. Climate change processes could also be affecting the evapotransporation regimes of the floodplain, but 17 years is too short time for such conclusions.

When transforming the continuous patterns of the land surface into discrete classes, errors are bound to occur. In our case, the Forestation class was overestimated (Table 5.2). Because

of that and the large difference in spatial resolution between the LULC change map (30 m) and the LST data-set (1 km), overall changes in LST for the Forestation class were not conclusive. However, in areas where the ground truth data showed actual forestation of grasslands the LST decreased considerably (Figure 5.4c). For the other classes of land change the results were clearer: LST increased in areas of Deforestation and Farmland Expansion, and areas without LULC changes also reported significant increments in LST.

It is to be noted that the recently released annual LULC products from the Climate Change Initiative still consider a large part of the floodplain as flooded grasslands, despite that it is rather heavily used for agriculture and its ecological functions have been degraded (Leemhuis et al., 2017) (Leemhuis et al., 2017). The concepts of "Ecological Character" and "Wise Use" of wetlands defined by the Ramsar Convention imply that wetland ecosystem services may be exploited to a certain extent, as long as the integrity and health of the wetland system remain uncompromised (Verhoeven and Setter, 2010). Our results, along with those of other researches (Connors, 2015; Leemhuis et al., 2017; Willcock et al., 2016; Wilson et al., 2017) indicate that agricultural expansion might be compromising the wetland's ecological character. The uncontrolled use of the wetland for agriculture might even have repercussions on areas that are still mostly natural, such as the core of the floodplain (Figure 5.5).

The upcoming plans to modernize the agriculture in the area by SAGCOT should consider the water balance and the preservation of the ecosystem services that the wetland provides (Leemhuis et al., 2017). For instance, modernizing the energy sources that farmers use might stop or reduce the deforestation caused by the use of timber for fuel. One of the main ecological functions of the Kilombero floodplain was to serve as a corridor for wildlife between the Udzungwa Mountains National Park to the northwest, and the Selous Game reserve to the east (Figure 5.1). That function has been recently lost, leaving animal populations isolated (Wilson et al., 2017). Two of these now defunct corridors (Ruipa and Nyanganje, Figure 5.1) used to go through the areas where LST has increased. Restoring Ruipa and Nyanganje corridors would be a straight forward solution regarding the connectivity function. There are a few areas that show no increase in LST, suggesting that they are not yet heavily used by agriculture and could be subjected to some regime of protection. Evidence suggests that protection regimes in the area have succeeded in stopping deforestation and farmland expansion to some extent (Brink et al., 2016; Willcock et al., 2016). However, if migration continues, different approaches might be needed to provide sustainable strategies for the wise use of the wetland.

### 5.4.3. Potentials and limitations of LST time series

MODIS LST time series can be useful for local and regional scale applications despite its coarse spatial resolution. ΔLST maps would not be useful for wetlands smaller than 1 km × 1 km, but single pixel trend analysis can still produce meaningful results. Besides, there is also room for improvements in spatial resolution. For instance, future efforts could be directed towards combining MODIS with Landsat (Weng et al., 2014) or ASTER data (Yang et al., 2016) for time series analysis at higher spatial resolution.

Despite the MODIS cloud mask, intermittent cloudiness and low quality pixels might still affect the surface temperature. In this study area, high mountain ridges are almost always cloudy, and trends there are questionable. Using only the high quality pixels of MODIS might be advisable in very arid areas where the cloud mask tends to fail, although it might reduce the number of observations considerably. Recent studies also show that other cloud mask schemes perform better (Gomis-Cebolla et al., 2016).

Trend analyses carry a risk of over- and underestimation, and quantitative results should be treated with care. STM models offer the possibility of using data from incomplete years, but are prone to overestimation. Aggregated time series are more resilient against overestimation, but the data used is reduced, generating a risk of underestimation.

## 5.5. Conclusions

The impacts of agricultural expansion and deforestation on wetlands are diverse and complex. Sometimes, certain impacts will not affect the classification of a land cover (e.g., wood extraction of single trees rather than stand replacing clear-cuts), but will have an impact on its biophysical variables (productivity, spectral indices or LST). The spatial and temporal distribution of such impacts in wetlands can be analyzed by using LST dense time series. These analyses can also be particularly useful in large areas with high rates of expansion and difficult access to field data, delivering quantitative information in a timely manner.

Analyses based on annual means (AATmean) and the seasonal trend model (STM) performed similarly in our case, with the STM identifying more pixels with significant trends. The analysis based on peak temperatures (AAT90) detected areas of extreme change. Overall increases in LST matched farmland expansion and deforestation patterns, and LST and NDVI were negatively correlated. We observed increases of LST also in unoccupied areas of the Ramsar site, where agriculture and the number of cattle herders have rapidly increased during the last decade, suggesting that their impact extends into the still natural areas.

The time period studied here is too short to consider the influence of climate change. However, we do provide evidence on how the agricultural expansion on wetlands increases the surface temperature, which in turn determines the atmospheric temperature.

Operational production of LST trend maps and time series charts can provide wetland managers with a quick and reliable single indicator of the effect of land processes on water and energy fluxes.

# Chapter 6

# Synthesis

## 6.1. Objectives

### 6.1.1. Objective 1: Evaluation of Sentinel-1 to monitor short-term wetland dynamics

Sentinel-1 characteristics make it ideal to monitor changes in most types of wetlands. It is freely available, it rarely has positional errors, and it has a high spatial and temporal resolution. When positional errors occur, these are often solved a few weeks after acquisition when precise orbit files are accessible via https://qc.sentinel1.eo.esa.int/doc/api/. Sentinel-1 is a C-band sensor, which means that it has a penetration range of 5 cm. This makes it sensitive to small changes in low laying vegetation such as wet grasslands or reeds, but unable to detect changes under the canopy. It doesn't seem to be sensitive neither to phenological changes in deciduous trees (leaf-on, leaf-off). In chapters 2 and 3 I showed how using the S1-omnibus test, an algorithm for change detection in time series, Sentinel-1 data proved to be sensitive to changes in wetlands' physical and structural properties. When compared to multispectral images (chapter 2), Sentinel-1 performed better; i.e. a larger proportion of changes were detected and false positives were reduced. False positives in multispectral images are often caused by atmospheric noise or changes in illumination conditions. Sentinel-1 was also sensitive to changes in agricultural fields of annual crops, mainly cereals. The S1-omnibus algorithm allows for a better control of the rates of false positives and negatives. This is a very important advantage when compared to commonly used image rationing methods with either multispectral or SAR imagery. Such thresholds can be biased by the subjectivity of the image interpreter. Although there are other histogram-based thresholding techniques like Otsu (Otsu, 1979), Coudrey (Coudray et al., 2010) or Rosin (Rosin, 2001), their application is image specific, and thus depend on factors like the histogram distribution or level of noise (Davier, 2012).

I found evidence on how the patterns of frequency of change can match the typology of land cover classes (chapter 3). This happens because the different inundation regimes that are detected in the frequency of change determine the composition of vegetation (e.g. via seed dispersal). At the Kerkini Lake, I focused on 4 wetland classes: Permanent water bodies, Marshlands, Seasonal water bodies with aquatic bed, and Seasonal water bodies without aquatic bed. By aquatic bed it is meant plants that grow on or below the water's surface during part of the growing season in most years. These 4 classes had significant different frequencies of change, consequence of different inundation regimes. On the other hand, certain wetland classes are often difficult to discriminate due to their spectral similarity and dynamics, and due to the continuous character of natural landscapes. This is, boundaries

between classes are often not "hard", but smooth, creating patches of mixed pixels (Foody, 1997). Using the frequency of change one can estimate better the boundary between two fuzzy and dynamic classes, as demonstrated in chapter 3 at Lake Kerkini. These results also suggest that the frequency of change is inversely proportional to the coherence. The coherence measures how similar the phases are between consecutive pairs of SAR images. Leaving aside true land cover/use changes, urban areas have very high coherence and very low frequencies of change. Forests tend to have high coherence, but not as high as urban areas, and low frequencies of change. Other cover types such as grasslands, crops, or wetlands have lower coherence, and high frequencies of change due to harvesting or inundation regimes.

Besides the frequency of change, the S1-omnibus method allows to identify when the change took place within the time series. This can be used to determine the nature of the change and even the land cover type. For instance, knowing that certain crops are harvested earlier or later in the season we can infer the crop type. An additional advantage of this method is that it can be used to plan fieldwork; for instance, by limiting the field visits to areas that show change, or distribute the training points across gradients of change.

The major disadvantage of SAR-based change detection methods in general is that the results demand interpretation by the user. Land cover classifications offer a categorical and discrete result with which managers and non-experts in remote sensing can easily work, even though natural landscapes are often continuous (Foody, 1997). NDVI or NDWI maps are usually also well received by non-experts in remote sensing. Variations in these indices have straightforward physical meaning: increases or decreases in vegetation and water. On the other hand, the frequency of change and the coherence are properties with a temporal component that although they add relevant information, they require to think in more abstract terms; i.e. what does it mean that a change was flagged in place *x* at time *y*? What do variations in coherence throughout the year represent? What does a high frequency of change mean? We can find this interpretation challenge also in thresholding methods, especially in SAR imagery. Decreases in backscatter intensity can be due to inundation, loss of soil moisture, or deforestation. For all change detection methods, knowledge about the local dynamics and landscape composition is necessary for the interpretation of results. One advantage of the S1-omnibus methodology used in chapters 2 and 3 is that it can be applied systematically for monitoring without local knowledge. In other words, local knowledge would be necessary for the interpretation of the results, not for the implementation of the methodology.

In chapter 4 I fused Sentinel-1 temporal information along with Sentinel-2 derived metrics to map different cover types. The results showed the improvement in accuracy when using both with respect to using either. Cover types like built up and bare soil are often difficult to distinguish using multispectral imagery. In SAR, cities showed constant high backscatter values, whereas the bare soil of riverbanks showed relatively constant mid-low values. Marshlands had high maximum and low minimum. Seasonal water bodies without vegetation presented similar profiles to Marshlands, but with lower maximum (Figure 6.1).

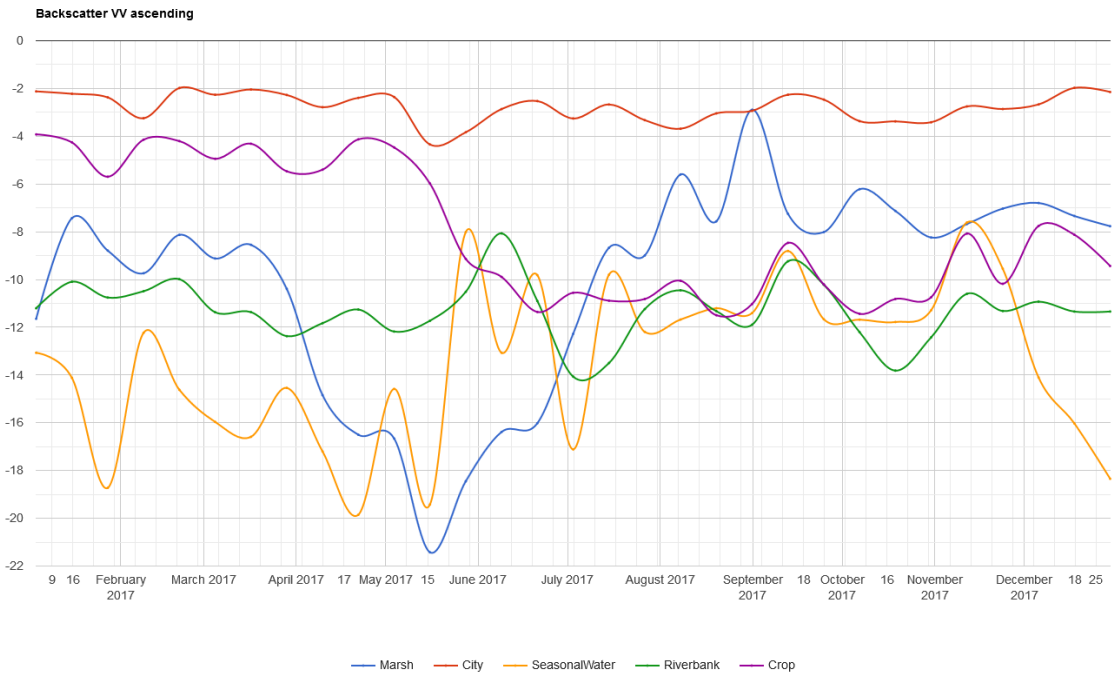


Figure 6.1 Representative temporal VV profiles of Marshes, City, Seasonal water body without vegetation, Riverbank and an annual Crop in Albania.

Although a steep orography does not pose a problem for change detection, the Sentinel-1 based multitemporal metrics presented artifacts in steep slopes, even after ortorectification. Those slopes oriented towards the sensor were over illuminated (very high max. and min. backscatter). Those slopes on the opposite direction were under-illuminated. Since we limited the study to flat areas (where most wetlands are) using geomorphological criteria, geometric distortions didn't affect our classification. Slopes affect backscatter in complex ways depending on their aspect, polarization, steepness and land cover (Hoekman and Reiche, 2015). For SAR multitemporal metrics to be applied on rough terrain, very precise terrain correction and terrain flattening procedures are necessary.

### 6.1.2. Objective 2: Develop and test cloud computing methodologies for wetland mapping and monitoring

Preprocessing of Sentinel-1 images can be challenging. Common errors I encountered and others reported in forums are: computational memory issues, errors in geo-registration, and border noise and topographic deformations that require complex corrections. Handling large amounts of multispectral imagery is also challenging. One single Sentinel-2 tile occupies around 900 Mb of memory, a size that grows exponentially if we need long temporal time series at the highest resolution (10 m) for a large area (resampling 20 m bands to 10 m bands, *times* more tiles *times* longer time series). Most wetland practitioners, even if they are proficient in remote sensing, do not have access to supercomputers. However, only internet is required to access cloud computing platforms. In chapter 3 I used the same algorithm than in chapter 2, but within Google Earth Engine (GEE). Although the dataset it uses is slightly different, the same principles apply (coherence based, Wishart distribution and omnibus test) (Canty and Nielsen, 2017). I was spared from downloading and preprocessing Sentinel-1 images and could replicate the experiment with a few clicks.

In chapter 4 I was able to preprocess and use several hundreds of Sentinel-1 and Sentinel-2 images for classifying all the wetlands of Albania. Without GEE I would have had to download and process an estimated minimum of 1700 Gb of information (1636 Sentinel-2 tiles *times* 0,8 Gb *equals* ~1300 Gb, plus 264 images for Sentinel-1 *times* 1,6 Gb *equals* ~420 Gb).

Wetland management requires accurate spatial and temporal information, which often involves high technical expertise and equipment (e.g. advanced programming skills, licensed software or computing power). Moreover, wetlands are disappearing faster in countries with lower management capacities. The community built around GEE (GEE forums, stackexchange, users summits) has made it possible for non-programmers (like me) to develop scripts capable of deriving accurate spatiotemporal statistics, representative models of the surface dynamics, and national scale inventories for any part of the world without hitting computational barriers. Cloud computing is also increasing the number of applications that use multisensory approaches, that although they were recognized to improve classification results, they were seldom applied until recently (Waske, 2014).

Cloud computing platforms are also having repercussions on global policies for sustainable development, with several initiatives already relaying on GEE such as the Center for International Forest Research, Food and Agriculture Organization, or the Global Forest

Watch. More recently, the Group on Earth Observation and Amazon Web Services (AWS) have formed a partnership to promote the use of remote sensing for sustainable development, offering credits to government agencies and research institutions for using the AWS in sustainable development initiatives.

### 6.1.3. Objective 3: Use time series of EO imagery to understand wetlands dynamics, the effects of human actions on them, and support decision making

As previously mentioned, wetlands are disappearing faster in countries with lower management capacities (i.e. low and middle income countries), because they have still a larger proportion of natural areas, and because their populations and economies are growing faster. The most common causes for wetland degradation are agricultural expansion and dam building (Ramsar, 2018). Population and economic growth put pressure on authorities to secure their food and energy supply without relying on other nations. This pressure is then transferred to ecosystems. The study sites of chapter 4, Albania, and chapter 5, Kilombero, are good examples of this. In them, wetlands have been or are at immediate risk of being degraded by anthropogenic actions; dam building in the case of Albania, and farmland expansion in the case of Kilombero. Using dense time series of multispectral and SAR imagery, I created an inventory of wetlands at national scale for Albania (chapter 4). And with thermal imagery, I analyzed the trends and impacts of farmland expansion on the Kilombero wetland (chapter 5). These products are aimed to support wetland monitoring and decision making. In the following lines I develop both chapters in the context of objective 3.

Albania is seeking to increase its energy production in order to supply its increasing demand of energy without depending on imports. Over 90% of its energy production already comes from hydropower, and many advocate for increasing it further. Promoters of hydropower have faced opposition from conservation organizations, scientists and local populations. Albania has one of the few remaining systems of unregulated (i.e. undammed) large rivers of Europe. These large wild rivers host a large number of endemisms and species that have only recently been discovered. Opponents of hydropower argue that these projects, even though financed by developing institutions such as the World Bank, they are sometimes executed without enough information about their environmental and social impacts (Sikorova and Gallop, 2015; Vejnovic and Gallop, 2018; Weiss et al., 2018). Chapter 4 was aimed at creating an accurate and updated inventory of wetlands for Albania as a contribution to the spatial information that any hydropower project should count on before it is implemented. The final

product was a land cover map of 13 classes, with 6 of those being wetland classes: Permanent water bodies, Intermittent water bodies (without aquatic bed), Marshlands, Riverbanks, Riverine scrubs and Coastal Dunes. Remote sensing has some limitations that can be partially overcome with other spatial analyses depending on the situation. Although the addition of SAR metrics to the multispectral metrics improved accuracies, it was still necessary to incorporate knowledge-based decision rules to further separate some wetland classes that cannot be distinguished accurately with only satellite imagery. Using distance to rivers and to the sea we separated Riverbanks and Coastal Dunes from other non-wetland bare surfaces. These are cover types that are spectrally very similar. We also separated Riverine from non-riverine Scrublands using the same distance criteria. The results showed a distinct configuration of riverine ecosystems between East and West. To the East, undammed rivers flow through and create wide extensions of Riverbanks and Riverine scrubs. This changes drastically once rivers reach the western part of the country, where some have been channelized (Figure 6.2), and the Riverbanks and Riverine scrubs are substituted by croplands.

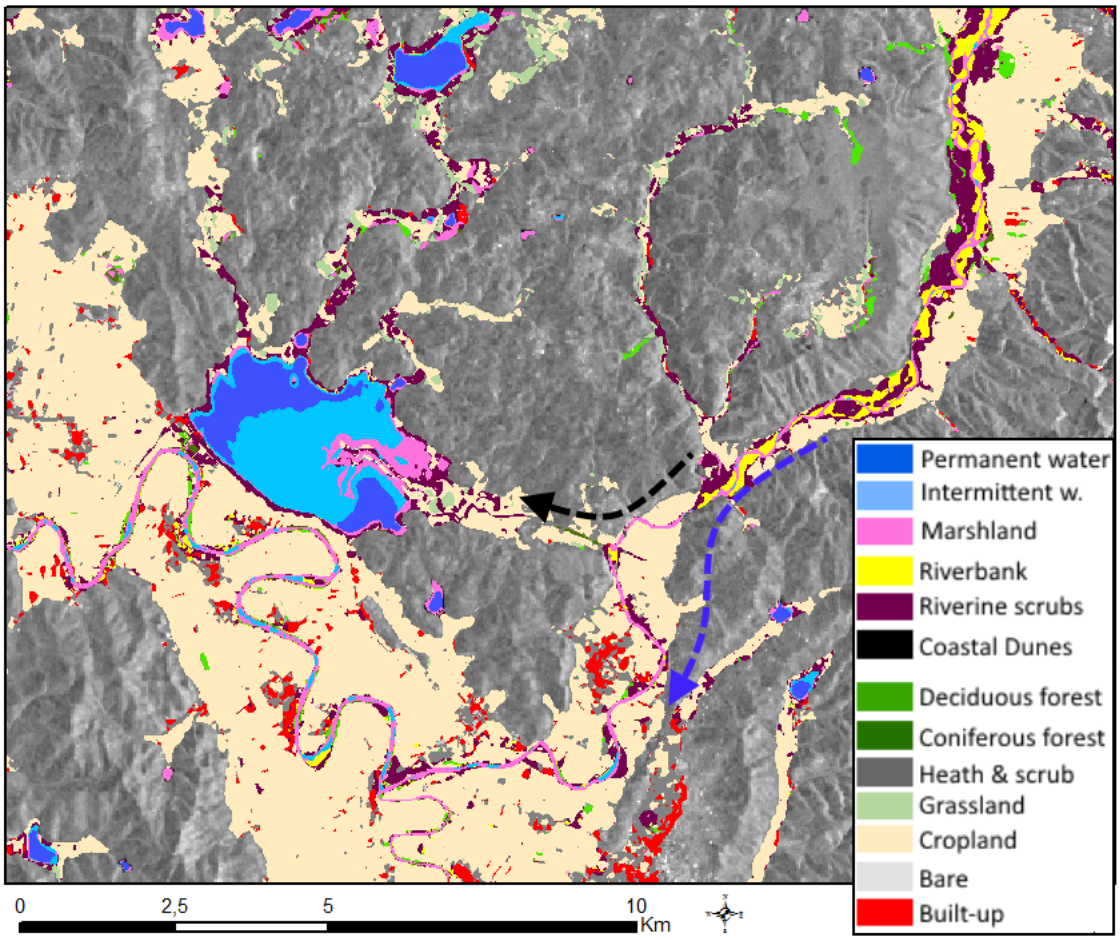


Figure 6.2: Murrizit reservoir in Albania. The blue arrow indicates the natural flow of the river. The black arrow indicates the deviation of water towards the reservoir. Upstream, (upper right corner) the river forms wide extensions of riverbanks and riverine scrubs. Once its flow is deviated towards the reservoir, it becomes narrower and the presence of riverbanks and riverine scrublands is reduced in favor of agricultural land. Background image is a Sentinel-1 VV.

Currently, the indicator 6.3.2 for the SDG 6 (clean water and sanitation), is based on the proportion of water bodies, ignoring vegetated wetlands. Paradoxically, increasing the number dams in Albania would have a positive result for indicator 6.3.2 by increasing the proportion of water bodies, but at the expense of riverine forest, riverbanks, marshlands and other valuable ecosystems that harbor greater levels of biodiversity and contribute to clean water more than water reservoirs (Maavara et al., 2017). Therefore, wetland inventories of sufficient spatial and thematic resolution are needed in the development of national energy and environmental policies.

The case of the Kilombero wetland is somewhat different. In it, the weak land management systems could not cope with the increasing demand of resources. This prompted the destruction of several natural corridors, deforestation, soil erosion, and a decrease in fish stocks (Wilson et al., 2017), along with social conflicts between sugar companies, farmers and pastoralists (Chachange, 2010; Hakiardhi and LHRC, 2009; IWGIA, 2016). Its remote location, difficult access and large extension made it difficult for authorities to monitor the situation and act on time. In chapter 5 I used 3 different statistical methods to model the variation of the Land Surface Temperature (LST) in the wetland with the land cover changes. Two models performed Annual Aggregations of the Trends (AAT) using the maxima (AAT90) and the mean temperatures (AATmean). The third model (STM, Season Trend Model) used a detrending technique to remove the effect of seasonality. The three models differed to some extent, which does not necessarily mean that one is better than the others. The AAT90 model detected less changes, but of higher amplitude, which is expected. For instance, an area reforested during the study period will show a higher difference in temperature if we look at the maximum values (hottest period) than if we look at the average values. The same applies if an area is drained or deforested. It is generally acknowledged that aggregating time series (what AAT90 and AATmean do) is resilient to the overestimation of trends, but because aggregation reduces the number of observations the method is also prone to underestimate the significance of trends (Forkel et al., 2013). As expected, the STM reported more areas with positive trends (increase in LST) than the other two models. STM is a more statistically robust model, and thus recommended instead of aggregation methods.

Agricultural expansion and deforestation proved to be major drivers for the increase in LST. Therefore, LST can be a good indicator to study the consequences of land cover changes in wetlands. NDVI is much more commonly used than LST for trend analysis. NDVI is a good parameter to study deforestation or vegetation degradation trends, but in wetlands, LST is more appropriate. While an increase in NDVI can be caused by an increase in vegetation (something usually desired, conservation wise) it can also be caused by a loss of water (something usually undesired). Similarly, a decrease in NDVI can be caused by a loss of vegetation, or by an increase in water extent. LST increases will always be related to the loss of vegetation and/or water, and decreases in LST will be related to gains in vegetation and/or water.

The LST trend analysis also showed how the LST increased at the center of the Ramsar site, an area which is still not farmed. This suggests a low evapotranspiration, product of a decrease in water content. This is supported by the results of Näschen et al., (2018).

According to the authors, the land cover changes in Kilombero have decreased the baseflow (minimum stream flow during the dry season) while increasing the maximum flow during the flood season. When vegetation cover is removed, the soil loses retention capacity. As a consequence, more water leaves the basin during flood season, and less water is retained for the dry season. With less water retained during dry season, evapotranspiration decreases and temperature increases.

After the partnership we formed with the projects GlobE and KILOWREMP and along with the Ramsar advisory mission, Tanzanian authorities have started to take measures. An integrated management plan based on an ecosystems-based approach was developed at the end of 2018 (Daconto et al., 2018). It depicts three scenarios:

- a zero action scenario where wetland is seen only as a wildlife conservation area,
- a short term scenario with no external funding and focused on coordination of existing resources (public awareness, local, regional and central government),
- an extended scenario that counts on external investment and support for habitat restoration, sustainable agricultural development, and strengthening of coordination mechanisms between stakeholders.

Other literature suggests that there is potential for improving the agricultural production in Kilombero without increasing the farmed extent. Such improvements would come from agricultural credits, new seeds, storage and planting methods, information on weather conditions and pest control (Bernd et al., 2014; Kalimang´asi et al., 2014). However, an increase in yield often implies an increase in water consumption, which might have still an effect on water availability in the wetland. The increasing demand in water could be met by building dams upstream, causing negative impacts in the wetlands downstream. Technological advances provide alternatives that can maintain the ecosystem services of the wetland while securing agriculture. Drought tolerant crops, fog harvesters or paludiculture are alternatives to be at least considered. Despite progress made with our partnership, the Ramsar advisory mission and the SAGCOT improvements, the future of Kilombero is still very uncertain. The president of Tanzania has recently signed a bill to revise the Stiegler's Gorge dam project in the Selous Game reserve (BBC, 2018; Daconto et al., 2018). The dam might affect the water dynamics of the wetland, depending on the level of flooding (WWF, 2017). Also, concessions for gas exploitation in the core of the wetland were under review in 2018 (Daconto et al., 2018).

### 6.2. Final remarks and outlook

The wide array of imagery freely available from different sensors allows us to gather different types of land surface data: reflectance values, vegetation or water indices, temperature, backscatter, and their multitemporal metrics. These parameters are representative of the physical, structural and biological properties of the wetlands and their dynamics, and we can use them to create models that help us understand their functioning and the impacts of human activities on them. Cloud computing platforms are speeding up the development of methodologies, allowing us to create mapping products tailored to specific management needs. These mapping efforts should take place at national level, the same way that energy and food security policies are developed at national scale. Or, if possible, at an even coarser scale. For instance, the LST trend analyses carried out in chapter 5 took place at regional scale and were performed in a desktop computer. With many Sub-Saharan countries experiencing similar trends in agricultural expansion, deforestation, and land degradation, continental-level analyses are necessary. GEE does not allow the direct implementation of customized algorithms for time series analysis, but it is possible to perform an ordinary least squares linear regression across mean annual values, similar to the AATmean model of chapter 5. Figure 6.3 shows the result of this regression for the entire African continent. The southeastern part of the continent is experiencing increasing trends in LST, similar to the ones we saw in Kilombero. While the Congo Basin and the Sahara Desert remain mostly stable, the area between them that crosses the continent from East to West shows patterns of decreasing LST. This area matches the location of the African Great Green Wall; a massive reforestation effort by African nations aimed at reclaiming desert lands and stopping desertification. The greatest significant decreases found correspond to the Eastern part of South Sudan, an area that has seen multiple armed conflicts during the last years. It is possible that these decreases in LST are due to revegetation processes, consequence of land abandonment in the area. These and the other LST patterns shown should be studied on a case by case basis, but this map offers a general view of the trends in water and energy fluxes that have taken place in Africa during this century.

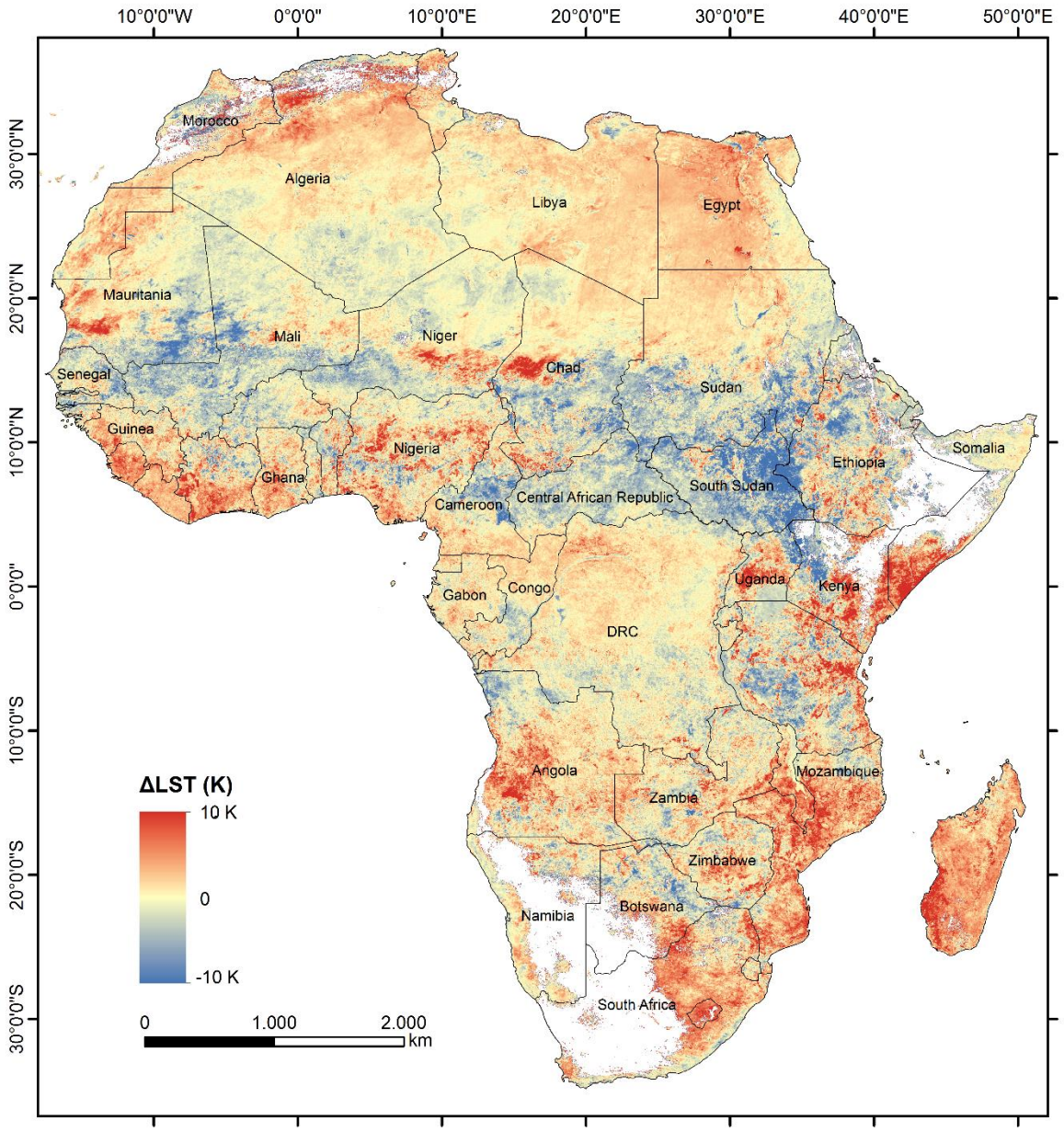


Figure 6.3 Land Surface Temperature trend in Africa between 2001 and 2018. Null values occur in areas of high root mean square error.

Despite the dam building spree of the Balkan peninsula and other large hydro-projects in Africa and Asia, most of the European continent along with USA are slowly removing old dams (Schiermeier, 2018). Here, remote sensing will be once again crucial in monitoring the effects of human action on the landscape; whether and how the rivers will recover their natural flows.

Preserving wetlands functionality can only be achieved with integrated resources management that can account for the needs of food security, energy supply and water resources. New EO technologies are contributing to lower the barrier between experts'

knowledge and people's needs. Wetland practitioners have now a much better access to Earth's surface data with a global and systematic coverage, ready-to-use products, and statistically sound methodologies that can be reproduced in other areas, or even upscaled at continental or global levels. Time series mapping is giving us a picture of where we are, how we got here, and where are we going towards.

## 7. Apendices

Appendix 4.1: Error matrix of the classification of Albanian wetlands using Sentinel-1, Sentinel-2 and Normalized Difference indices as input, and knowledge-based decision rules.

| | | Reference | | | | | | | | | | | | | |
|---|---|---|---|---|---|---|---|---|---|---|---|---|---|---|---|
| | | Bare Soil | Permanent water | Urban | Marshlands | Intermittent water | Deciduous | Coniferous | Cropland | Grassland | Heath & scrub | Dunes | Riverbanks | Riverine scrubs | UA |
| Classification result | Bare Soil | 13 | 0 | 2 | 0 | 0 | 2 | 0 | 5 | 2 | 6 | 0 | 0 | 0 | 43% |
| | Permanent water | 0 | 76 | 0 | 1 | 0 | 0 | 0 | 0 | 0 | 0 | 0 | 0 | 0 | 99% |
| | Urban | 0 | 0 | 19 | 0 | 0 | 3 | 0 | 2 | 0 | 4 | 0 | 2 | 0 | 63% |
| | Marshland | 0 | 0 | 0 | 16 | 6 | 4 | 2 | 0 | 1 | 0 | 0 | 1 | 0 | 53% |
| | Intermittent water. | 0 | 2 | 0 | 0 | 27 | 0 | 0 | 0 | 0 | 0 | 1 | 0 | 0 | 90% |
| | Deciduous | 0 | 0 | 0 | 0 | 0 | 30 | 0 | 1 | 0 | 1 | 0 | 0 | 0 | 94% |
| | Coniferous | 0 | 0 | 0 | 1 | 0 | 0 | 27 | 0 | 0 | 1 | 0 | 0 | 1 | 90% |
| | Cropland | 0 | 0 | 1 | 0 | 0 | 2 | 0 | 91 | 4 | 0 | 0 | 0 | 2 | 91% |
| | Grassland | 0 | 0 | 0 | 0 | 0 | 2 | 0 | 4 | 23 | 1 | 0 | 0 | 0 | 77% |
| | Heath & scrub | 1 | 0 | 3 | 0 | 0 | 1 | 0 | 16 | 1 | 22 | 0 | 0 | 0 | 50% |
| | Dunes | 2 | 1 | 0 | 0 | 0 | 0 | 1 | 1 | 0 | 0 | 25 | 0 | 0 | 83% |
| | Riverbanks | 1 | 0 | 0 | 0 | 1 | 1 | 0 | 0 | 0 | 1 | 0 | 26 | 0 | 87% |
| | Riverine scrubs | 0 | 0 | 4 | 0 | 0 | 3 | 0 | 4 | 2 | 5 | 0 | 2 | 14 | 41% |
| | PA | 59% | 99% | 66% | 90% | 55% | 62% | 88% | 90% | 56% | 63% | 83% | 72% | 71% | |

## 8. References


Amler, E., Schmidt, M., Menz, G., 2015. Definitions and Mapping of East African Wetlands: A Review. Remote Sens. 7, 5256–5282. https://doi.org/10.3390/rs70505256

Anderson, M.C., Allen, R.G., Morse, A., Kustas, W.P., 2012. Use of Landsat thermal imagery in monitoring evapotranspiration and managing water resources. Remote Sens. Environ. 122, 50–65. https://doi.org/10.1016/j.rse.2011.08.025

Arnold, S., Kosztra, B., Banko, G., Smith, G., Hazeu, G., Bock, M., Valcarcel Sanz, N., 2013. The EAGLE concept - A vision of a future European Land Monitoring Framework, in: Towards Horizon 2020. Presented at the EARSeL Symposium, Matera, Italy.

Banskota, A., Kayastha, N., Falkowski, M.J., Wulder, M.A., Froese, R.E., White, J.C., 2014. Forest Monitoring Using Landsat Time Series Data: A Review. Can. J. Remote Sens. 40, 362–384. https://doi.org/10.1080/07038992.2014.987376

BBC, 2018. Tanzania dam: Power plant planned in Selous Game Reserve.

Béchet, A., Germain, C., Sandoz, A., Hirons, G.J.M., Green, R.E., Walmsley, J.G., Johnson, A.R., 2009. Assessment of the impacts of hydrological fluctuations and salt pans abandonment on Greater flamingos in the Camargue, South of France. Biodivers. Conserv. 18, 1575–1588. https://doi.org/10.1007/s10531-008-9544-8

Bernd, R., Frankwell, D., Nagalpa, H., 2014. Assessment of information needs of rice farmers in Tanzania; A case study of Kilombero District, Morogoro. Library Philosophy and Practice.

Betbeder, J., Rapinel, S., Corgne, S., Pottier, E., Hubert-Moy, L., 2015. TerraSAR-X dual-pol time-series for mapping of wetland vegetation. ISPRS J. Photogramm. Remote Sens. 107, 90–98. https://doi.org/10.1016/j.isprsjprs.2015.05.001

Beven, K.J., Kirkby, M.J., 1979. A physically based, variable contributing area model of basin hydrology / Un modèle à base physique de zone d'appel variable de l'hydrologie du bassin versant. Hydrol. Sci. Bull. 24, 43–69. https://doi.org/10.1080/02626667909491834

Bey, A., Sánchez-Paus Díaz, A., Maniatis, D., Marchi, G., Mollicone, D., Ricci, S., Bastin, J.-F., Moore, R., Federici, S., Rezende, M., Patriarca, C., Turia, R., Gamoga, G., Abe, H., Kaidong, E., Miceli, G., 2016. Collect Earth: Land Use and Land Cover Assessment through Augmented Visual Interpretation. Remote Sens. 8, 807. https://doi.org/10.3390/rs8100807

Blaes, X., Vanhalle, L., Defourny, P., 2005. Efficiency of crop identification based on optical and SAR image time series. Remote Sens. Environ. 96, 352–365. https://doi.org/10.1016/j.rse.2005.03.010

Böhner, J., Selige, T., 2006. Spatial Prediction of Soil Attributes Using Terrain Analysis and Climate Regionalisation, in: SAGA. Anal. Model. Appl. Verl. Erich Goltze GmbH 13–27.

Bouvet, A., Le Toan, T., 2011. Use of ENVISAT/ASAR wide-swath data for timely rice fields mapping in the Mekong River Delta. Remote Sens. Environ. 115, 1090–1101. https://doi.org/10.1016/j.rse.2010.12.014

Breiman, L., 2001. Random Forests. Mach. Learn. 45, 5–32. https://doi.org/10.1023/A:1010933404324

Brink, A., Martínez-López, J., Szantoi, Z., Moreno-Atencia, P., Lupi, A., Bastin, L., Dubois, G., 2016. Indicators for Assessing Habitat Values and Pressures for Protected Areas—An Integrated Habitat and Land Cover Change Approach for the Udzungwa Mountains National Park in Tanzania. Remote Sens. 8, 862. https://doi.org/10.3390/rs8100862

Brisco, B., Ahern, F., Murnaghan, K., White, L., Canisus, F., Lancaster, P., 2017. Seasonal Change in Wetland Coherence as an Aid to Wetland Monitoring. Remote Sens. 9, 158. https://doi.org/10.3390/rs9020158

Brisco, B., Brown, R.J., 1995. Multidate SAR/TM Synergism for Crop Classification in Western Canada. Photogramm Eng Remote Sensing 61, 1009–1014.

Brisco, B., Schmitt, A., Murnaghan, K., Kaya, S., Roth, A., 2013. SAR polarimetric change detection for flooded vegetation. Int. J. Digit. Earth 6, 103–114. https://doi.org/10.1080/17538947.2011.608813

Britton, R.H., Podlejski, V.D., 1981. Inventory and classification of the wetlands of the Camargue (France). Aquat. Bot. 10, 195–228. https://doi.org/10.1016/0304-3770(81)90024-3

Canty, M.J., Nielsen, A.A., 2017. Spatio-temporal Analysis of Change with Sentinel Imagery on the Google Earth Engine, in: Proceedings of the 2017 Conference on Big Data from Space (BiDs'2017). Presented at the ESA Conference on Big Data from Space, P. Soille and P. G. Marchetti, Toulouse, France, pp. 126–129. https://doi.org/10.2760/383579

Canty, M.J., Nielsen, A.A., 2008. Automatic radiometric normalization of multitemporal satellite imagery with the iteratively re-weighted MAD transformation. Remote Sens. Environ. 112, 1025–1036. https://doi.org/10.1016/j.rse.2007.07.013

Carrasco, L., O'Neil, A., Morton, R., Rowland, C., 2019. Evaluating Combinations of Temporally Aggregated Sentinel-1, Sentinel-2 and Landsat 8 for Land Cover Mapping with Google Earth Engine. Remote Sens. 11, 288. https://doi.org/10.3390/rs11030288

Chachange, C., 2010. Land acquisition and accumulation in Tanzania, The case of Morogoro,Iringa and Pwani Regions.

Chatziantoniou, A., Psomiadis, E., Petropoulos, G., 2017. Co-Orbital Sentinel 1 and 2 for LULC Mapping with Emphasis on Wetlands in a Mediterranean Setting Based on Machine Learning. Remote Sens. 9, 1259. https://doi.org/10.3390/rs9121259

Condé, R., Martinez, J.-M., Pessotto, M., Villar, R., Cochonneau, G., Henry, R., Lopes, W., Nogueira, M., 2019. Indirect Assessment of Sedimentation in Hydropower Dams Using

MODIS Remote Sensing Images. Remote Sens. 11, 314. https://doi.org/10.3390/rs11030314

Conde-Álvarez, R.M., Bañares-España, E., Nieto-Caldera, J.M., Flores-Moya, A., Figueroa, F.L., 2012. Submerged macrophyte biomass distribution in the shallow saline lake Fuente de Piedra (Spain) as function of environmental variables. An. Jardín Botánico Madr. 69, 119–127. https://doi.org/10.3989/ajbm.2305

Connolly, J., Holden, N.M., 2009. Mapping peat soils in Ireland: updating the derived Irish peat map. Ir. Geogr. 42, 343–352. https://doi.org/10.1080/00750770903407989

Connors, J.P., 2015. Agricultural Development, Land Change, and Livelihoods in Tanzania's Kilombero Valley. Arizona State University.

Conradsen, K., Nielsen, A.A., Schou, J., Skriver, H., 2003. A test statistic in the complex wishart distribution and its application to change detection in polarimetric SAR data. IEEE Trans. Geosci. Remote Sens. 41, 4–19. https://doi.org/10.1109/TGRS.2002.808066

Conradsen, K., Nielsen, A.A., Skriver, H., 2016. Determining the Points of Change in Time Series of Polarimetric SAR Data. IEEE Trans. Geosci. Remote Sens. 54, 3007–3024. https://doi.org/10.1109/TGRS.2015.2510160

Coppin, P., Jonckheere, I., Nackaerts, K., Muys, B., Lambin, E., 2004. Digital change detection methods in ecosystem monitoring: a review. Int. J. Remote Sens. 25, 1565–1596. https://doi.org/10.1080/0143116031000101675

Coudray, N., Buessler, J.-L., Urban, J.-P., 2010. Robust threshold estimation for images with unimodal histograms. Pattern Recognit. Lett. 31, 1010–1019. https://doi.org/10.1016/j.patrec.2009.12.025

Cowardin, L.M., Carter, V., Golet, F.C., LaRoe, E.T., 1979. Classification of wetlands and deepwater habitats of the United States. U.S. Department of the Interior, Fish and Wildlife Service, Northern Prairie Wildlife Research Center, Washington, D.C. Jamestown.

Crist, E.P., Cicone, R.C., 1984. A Physically-Based Transformation of Thematic Mapper Data---The TM Tasseled Cap. IEEE Trans. Geosci. Remote Sens. GE-22, 256–263. https://doi.org/10.1109/TGRS.1984.350619

Crivelli, A.J., Grillas, P., Jerrentrup, H., Nazirides, T., 1995a. Effects on fisheries and waterbirds of raising water levels at Kerkini Reservoir, a Ramsar site in northern Greece. Environ. Manage. 19, 431–443. https://doi.org/10.1007/BF02471984

Crivelli, A.J., Grillas, P., Lacaze, B., 1995b. Responses of vegetation to a rise in water level at Kerkini Reservoir (1982–1991), a Ramsar site in northern Greece. Environ. Manage. 19, 417–430. https://doi.org/10.1007/BF02471983

Czech, H.A., Parsons, K.C., 2002. Agricultural Wetlands and Waterbirds: A Review. Waterbirds Int. J. Waterbird Biol. 25, 56–65.

Dabboor, M., Brisco, B., Banks, S., Murnaghan, K., White, L., 2017. Multitemporal monitoring of wetlands using simulated radarsat constellation mission compact polarimetric SAR data. Presented at the IGARSS, IEEE, Fort Worth, Texas, USA, pp. 4586–4589. https://doi.org/10.1109/IGARSS.2017.8128022

Daconto, G., Games, I., Lukumbuzya, K., Raijmakers, F., 2018. Integrated Management Plan for the Kilombero Valley Ramsar Site (Technical Report No. TAN 11 027 11). Enabel.

Davidson, N.C., 2014. How much wetland has the world lost? Long-term and recent trends in global wetland area. Mar. Freshw. Res. 65, 934. https://doi.org/10.1071/MF14173

Davier, E.R., 2012. Thresholding Techniques, in: Computer and Machine Vision. Theroy, Algorithms and Practicalities. Academic Press, pp. 108–109.

de Jong, R., de Bruin, S., de Wit, A., Schaepman, M.E., Dent, D.L., 2011. Analysis of monotonic greening and browning trends from global NDVI time-series. Remote Sens. Environ. 115, 692–702. https://doi.org/10.1016/j.rse.2010.10.011

DeFries, R.S., Rudel, T., Uriarte, M., Hansen, M., 2010. Deforestation driven by urban population growth and agricultural trade in the twenty-first century. Nat. Geosci. 3, 178.

Di Gregorio, A., 2016. Land Cover Classification System.

Díaz-Delgado, R., Aragonés, D., Afán, I., Bustamante, J., 2016. Long-Term Monitoring of the Flooding Regime and Hydroperiod of Doñana Marshes with Landsat Time Series (1974–2014). Remote Sens. 8, 775. https://doi.org/10.3390/rs8090775

Didan, K., Barreto Munoz, A., Solano, R., Huete, A., 2017. MODIS Vegetation Index Users Guide.

Dixon, M.J.R., Loh, J., Davidson, N.C., Beltrame, C., Freeman, R., Walpole, M., 2016. Tracking global change in ecosystem area: The Wetland Extent Trends index. Biol. Conserv. 193, 27–35. https://doi.org/10.1016/j.biocon.2015.10.023

Dong, J., Xiao, X., Menarguez, M.A., Zhang, G., Qin, Y., Thau, D., Biradar, C., Moore, B., 2016. Mapping paddy rice planting area in northeastern Asia with Landsat 8 images, phenology-based algorithm and Google Earth Engine. Remote Sens. Environ. 185, 142–154. https://doi.org/10.1016/j.rse.2016.02.016

Dronova, I., Gong, P., Wang, L., Zhong, L., 2015. Mapping dynamic cover types in a large seasonally flooded wetland using extended principal component analysis and object-based classification. Remote Sens. Environ. 158, 193–206. https://doi.org/10.1016/j.rse.2014.10.027

EcoAlbania, 2017. Mapping of hydropower plant in Albania, using GIS. EcoAlbania.

ECOWAS, 2017. GIS Hydropower Resource Mapping and Climate Change Scenarios for the ECOWAS Region - Technical Report on Methodology and Lessons Learnt for ECOWAS Countries. ECOWAS.

ESA, 2012a. Sentinel-1: ESA's Radar Observatory Mission for GMES Operational Services.

ESA, 2012b. Sentinel-2: ESA's Optical High-Resolution Mission for GMES Operational Services (ESA SP-1322/2 March 2012).

FAO, 2018. The State of the World's Forests 2018 - Forest pathways too sustainable development. FAO, Rome.

FAO, 2015. FAO Country programming framework.

FAO, 2003. World agriculture: towards 2015/2030.

Fensholt, R., Horion, S., Tagesson, T., Ehammer, A., Ivits, E., Rasmussen, K., 2015. Global-scale mapping of changes in ecosystem functioning from earth observation-based trends in total and recurrent vegetation: Mapping of ecosystem functioning change from EO data. Glob. Ecol. Biogeogr. 24, 1003–1017. https://doi.org/10.1111/geb.12338

Finlayson, M., D'Cruz, R., Davidson, N., 2005. Ecosystems and human well-being: wetlands and water, in: Millenium Ecosystem Assessment. World Resources Institute.

Fitoka, E., Poulis, G., Perennou, C., Thulin, S., Malak, D.A., Franke, J., Guelmami, A., Schröder, C., 2017. The wetland ecosystems in MAES nomenclature: SWOS modifications.

Foody, G.M., 1997. Fully fuzzy supervised classification of land cover from remotely sensed imagery with an artificial neural network. Neural Comput. Appl. 5, 238–247. https://doi.org/10.1007/BF01424229

Forkel, M., Carvalhais, N., Verbesselt, J., Mahecha, M., Neigh, C., Reichstein, M., 2013. Trend Change Detection in NDVI Time Series: Effects of Inter-Annual Variability and Methodology. Remote Sens. 5, 2113–2144. https://doi.org/10.3390/rs5052113

Forkel, M., Migliavacca, M., Thonicke, K., Reichstein, M., Schaphoff, S., Weber, U., Carvalhais, N., 2015. Codominant water control on global interannual variability and trends in land surface phenology and greenness. Glob. Change Biol. 21, 3414–3435. https://doi.org/10.1111/gcb.12950

Foteh, R., Garg, V., Nikam, B.R., Khadatare, M.Y., Aggarwal, S.P., Kumar, A.S., 2018. Reservoir Sedimentation Assessment Through Remote Sensing and Hydrological Modelling. J. Indian Soc. Remote Sens. 46, 1893–1905. https://doi.org/10.1007/s12524-018-0843-6

Frey, C.M., Kuenzer, C., 2015. Analysing a 13 Years MODIS Land Surface Temperature Time Series in the Mekong Basin, in: Kuenzer, C., Dech, S., Wagner, W. (Eds.), Remote Sensing Time Series. Springer International Publishing, Cham, pp. 119–140. https://doi.org/10.1007/978-3-319-15967-6_6

Gallant, A., 2015. The Challenges of Remote Monitoring of Wetlands. Remote Sens. 7, 10938–10950. https://doi.org/10.3390/rs70810938

Gallant, J.C., Dowling, T.I., 2003. A multiresolution index of valley bottom flatness for mapping depositional areas: Multiresolution Valley Bottom Flatness. Water Resour. Res. 39. https://doi.org/10.1029/2002WR001426

Gärtner, P., 2018. This Landsat project would cost... URL https://philippgaertner.github.io/2018/06/landsat-cost-estimator/

GEE, 2018. Sentinel-1 algorithms in Google Earth Engine [WWW Document]. URL https://developers.google.com/earth-engine/sentinel1

Geraci, J., Béchet, A., Cézilly, F., Ficheux, S., Baccetti, N., Samraoui, B., Wattier, R., 2012. Greater flamingo colonies around the Mediterranean form a single interbreeding population and share a common history. J. Avian Biol. 43, 341–354. https://doi.org/10.1111/j.1600-048X.2012.05549.x

Gevaert, C.M., García-Haro, F.J., 2015. A comparison of STARFM and an unmixing-based algorithm for Landsat and MODIS data fusion. Remote Sens. Environ. 156, 34–44. https://doi.org/10.1016/j.rse.2014.09.012

Ghazaryan, G., Dubovyk, O., Kussul, N., Menz, G., 2016. Towards an Improved Environmental Understanding of Land Surface Dynamics in Ukraine Based on Multi-Source Remote Sensing Time-Series Datasets from 1982 to 2013. Remote Sens. 8, 617. https://doi.org/10.3390/rs8080617

GLR, 2009. Reforestation in Grassland Areas of Uchindile, Kilombero, Tanzania and Mapanda, Mufindi, Tanuania. Tanzania.

Gomis-Cebolla, J., Jiménez-Muñoz, J., Sobrino, J., 2016. MODIS-Based Monthly LST Products over Amazonia under Different Cloud Mask Schemes. Data 1, 2. https://doi.org/10.3390/data1020002

Gorelick, N., Hancher, M., Dixon, M., Ilyushchenko, S., Thau, D., Moore, R., 2017. Google Earth Engine: Planetary-scale geospatial analysis for everyone. Remote Sens. Environ. 202, 18–27. https://doi.org/10.1016/j.rse.2017.06.031

Griffiths, P., van der Linden, S., Kuemmerle, T., Hostert, P., 2013. A Pixel-Based Landsat Compositing Algorithm for Large Area Land Cover Mapping. IEEE J. Sel. Top. Appl. Earth Obs. Remote Sens. 6, 2088–2101. https://doi.org/10.1109/JSTARS.2012.2228167

Guo, M., Li, J., Sheng, C., Xu, J., Wu, L., 2017. A Review of Wetland Remote Sensing. Sensors 17, 777. https://doi.org/10.3390/s17040777

Hakiardhi, LHRC, 2009. Facts finding mission report on the prevailing land dispute at Namwawala village in Kilombero District, Morogoro Region.

Hansen, M.C., Stehman, S.V., Potapov, P.V., 2010. Quantification of global gross forest cover loss. Proc. Natl. Acad. Sci. 107, 8650–8655. https://doi.org/10.1073/pnas.0912668107

Hardy, A., Ettritch, G., Cross, D., Bunting, P., Liywalii, F., Sakala, J., Silumesii, A., Singini, D., Smith, M., Willis, T., Thomas, C., 2019. Automatic Detection of Open and Vegetated Water Bodies Using Sentinel 1 to Map African Malaria Vector Mosquito Breeding Habitats. Remote Sens. 11, 593. https://doi.org/10.3390/rs11050593

Hecheltjen, A., Thonfeld, F., Menz, G., 2014. Recent Advances in Remote Sensing Change Detection – A Review, in: Land Use and Land Cover Mapping in Europe. Springer, Netherlands, pp. 145–178.

Henderson, F.M., Lewis, A.J., 2008. Radar detection of wetland ecosystems: a review. Int. J. Remote Sens. 29, 5809–5835. https://doi.org/10.1080/01431160801958405

Hentze, K., Thonfeld, F., Menz, G., 2017. Beyond trend analysis: How a modified breakpoint analysis enhances knowledge of agricultural production after Zimbabwe's fast track land reform. Int. J. Appl. Earth Obs. Geoinformation 62, 78–87. https://doi.org/10.1016/j.jag.2017.05.007

Herold, M., Liu, X., Clarke, K.C., 2003. Spatial Metrics and Image Texture for Mapping Urban Land Use. Photogramm. Eng. Remote Sens. 69, 991–1001. https://doi.org/10.14358/PERS.69.9.991

Hess, L.L., Melack, J.M., Affonso, A.G., Barbosa, C., Gastil-Buhl, M., Novo, E.M.L.M., 2015. Wetlands of the Lowland Amazon Basin: Extent, Vegetative Cover, and Dual-season Inundated Area as Mapped with JERS-1 Synthetic Aperture Radar. Wetlands 35, 745–756. https://doi.org/10.1007/s13157-015-0666-y

Hill, R.A., Wilson, A.K., George, M., Hinsley, S.A., 2010. Mapping tree species in temperate deciduous woodland using time-series multi-spectral data. Appl. Veg. Sci. 13, 86–99. https://doi.org/10.1111/j.1654-109X.2009.01053.x

Hird, J., DeLancey, E., McDermid, G., Kariyeva, J., 2017. Google Earth Engine, Open-Access Satellite Data, and Machine Learning in Support of Large-Area Probabilistic Wetland Mapping. Remote Sens. 9, 1315. https://doi.org/10.3390/rs9121315

Hoekman, D.H., Reiche, J., 2015. Multi-model radiometric slope correction of SAR images of complex terrain using a two-stage semi-empirical approach. Remote Sens. Environ. 156, 1–10. https://doi.org/10.1016/j.rse.2014.08.037

Inglada, J., Vincent, A., Arias, M., Tardy, B., Morin, D., Rodes, I., 2017. Operational High Resolution Land Cover Map Production at the Country Scale Using Satellite Image Time Series. Remote Sens. 9, 95. https://doi.org/10.3390/rs9010095

Iwahashi, J., Pike, R.J., 2007. Automated classifications of topography from DEMs by an unsupervised nested-means algorithm and a three-part geometric signature. Geomorphology 86, 409–440. https://doi.org/10.1016/j.geomorph.2006.09.012

IWGIA, 2016. Tanzanian Pastoralists Threatened: Evictions, Human Rights and Loss of Livelihood. Copenhagen, Denmark.

Jiménez-Muñoz, J.C., Mattar, C., Sobrino, J.A., Malhi, Y., 2016. Digital thermal monitoring of the Amazon forest: an intercomparison of satellite and reanalysis products. Int. J. Digit. Earth 9, 477–498. https://doi.org/10.1080/17538947.2015.1056559

Jones, K., Lanthier, Y., van der Voet, P., van Valkengoed, E., Taylor, D., Fernández-Prieto, D., 2009. Monitoring and assessment of wetlands using Earth Observation: The GlobWetland project. J. Environ. Manage. 90, 2154–2169. https://doi.org/10.1016/j.jenvman.2007.07.037

Joosten, H., Clarke, D., 2002. Wise use of Mires and Peatlands. Saarijärvi, Finland.

Joshi, N., Baumann, M., Ehammer, A., Fensholt, R., Grogan, K., Hostert, P., Jepsen, M., Kuemmerle, T., Meyfroidt, P., Mitchard, E., Reiche, J., Ryan, C., Waske, B., 2016. A Review of the Application of Optical and Radar Remote Sensing Data Fusion to Land Use Mapping and Monitoring. Remote Sens. 8, 70. https://doi.org/10.3390/rs8010070

Julien, Y., Sobrino, J.A., Mattar, C., Ruescas, A.B., Jiménez-Muñoz, J.C., Sòria, G., Hidalgo, V., Atitar, M., Franch, B., Cuenca, J., 2011. Temporal analysis of normalized difference vegetation index (NDVI) and land surface temperature (LST) parameters to detect changes in the Iberian land cover between 1981 and 2001. Int. J. Remote Sens. 32, 2057–2068. https://doi.org/10.1080/01431161003762363

Kalimang´asi, N.N., Kihombo, A., Kalimang´asi, N., 2014. Technical Efficiency of Cocoa Production through Contract Farming: Empirical Evidence from Kilombero and Kyela Districts. Int. J. Sci. Res. Publ. 4.

Karnieli, A., Agam, N., Pinker, R.T., Anderson, M., Imhoff, M.L., Gutman, G.G., Panov, N., Goldberg, A., 2010. Use of NDVI and Land Surface Temperature for Drought Assessment: Merits and Limitations. J. Clim. 23, 618–633. https://doi.org/10.1175/2009JCLI2900.1

Kennedy, R.E., Yang, Z., Cohen, W.B., 2010. Detecting trends in forest disturbance and recovery using yearly Landsat time series: 1. LandTrendr — Temporal segmentation algorithms. Remote Sens. Environ. 114, 2897–2910. https://doi.org/10.1016/j.rse.2010.07.008

Knight, J.F., Tolcser, B.P., Corcoran, J.M., Rampi, L.P., 2013. The Effects of Data Selection and Thematic Detail on the Accuracy of High Spatial Resolution Wetland Classifications. Photogramm. Eng. Remote Sens. 79, 613–623. https://doi.org/10.14358/PERS.79.7.613

Koutsouris, A.J., Chen, D., Lyon, S.W., 2016. Comparing global precipitation data sets in eastern Africa: a case study of Kilombero Valley, Tanzania: Comparing global precipitation data sets in Tanzania, East Africa. Int. J. Climatol. 36, 2000–2014. https://doi.org/10.1002/joc.4476

Künzer, C., Dech, S., Wagner, W., 2015. Remote Sensing Time Series: Revealing Land Surface Dynamics, Remote Sensing and Digital Image Processing. Springer, Netherlands.

Leblanc, M., Lemoalle, J., Bader, J.-C., Tweed, S., Mofor, L., 2011. Thermal remote sensing of water under flooded vegetation: New observations of inundation patterns for the 'Small' Lake Chad. J. Hydrol. 404, 87–98. https://doi.org/10.1016/j.jhydrol.2011.04.023

Leemhuis, C., Thonfeld, F., Näschen, K., Steinbach, S., Muro, J., Strauch, A., López, A., Daconto, G., Games, I., Diekkrüger, B., 2017. Sustainability in the Food-Water-Ecosystem Nexus: The Role of Land Use and Land Cover Change for Water Resources and Ecosystems in the Kilombero Wetland, Tanzania. Sustainability 9, 1513. https://doi.org/10.3390/su9091513

Li, M., Im, J., Beier, C., 2013. Machine learning approaches for forest classification and change analysis using multi-temporal Landsat TM images over Huntington Wildlife Forest. GIScience Remote Sens. 50, 361–384. https://doi.org/10.1080/15481603.2013.819161

Liu, Y., Li, Y., Li, S., Motesharrei, S., 2015. Spatial and Temporal Patterns of Global NDVI Trends: Correlations with Climate and Human Factors. Remote Sens. 7, 13233–13250. https://doi.org/10.3390/rs71013233

Long, B.G., Skewes, T.D., 1996. A Technique for Mapping Mangroves with Landsat TM Satellite Data and Geographic Information System. Estuar. Coast. Shelf Sci. 43, 373–381. https://doi.org/10.1006/ecss.1996.0076

Lu, D., Mausel, P., Brondízio, E., Moran, E., 2004. Change detection techniques. Int. J. Remote Sens. 25, 2365–2401. https://doi.org/10.1080/0143116031000139863

Luyssaert, S., Jammet, M., Stoy, P.C., Estel, S., Pongratz, J., Ceschia, E., Churkina, G., Don, A., Erb, K., Ferlicoq, M., Gielen, B., Grünwald, T., Houghton, R.A., Klumpp, K., Knohl, A., Kolb, T., Kuemmerle, T., Laurila, T., Lohila, A., Loustau, D., McGrath, M.J., Meyfroidt, P., Moors, E.J., Naudts, K., Novick, K., Otto, J., Pilegaard, K., Pio, C.A., Rambal, S., Rebmann, C., Ryder, J., Suyker, A.E., Varlagin, A., Wattenbach, M., Dolman, A.J., 2014. Land management and land-cover change have impacts of similar magnitude on surface temperature. Nat. Clim. Change 4, 389–393. https://doi.org/10.1038/nclimate2196

Maavara, T., Lauerwald, R., Regnier, P., Van Cappellen, P., 2017. Global perturbation of organic carbon cycling by river damming. Nat. Commun. 8, 15347.

Mack, B., Leinenkugel, P., Kuenzer, C., Dech, S., 2017. A semi-automated approach for the generation of a new land use and land cover product for Germany based on Landsat time-series and Lucas *in-situ* data. Remote Sens. Lett. 8, 244–253. https://doi.org/10.1080/2150704X.2016.1249299

Maes, J., Liquete, C., Teller, A., Erhard, M., Paracchini, M.L., Barredo, J.I., Grizzetti, B., Cardoso, A., Somma, F., Petersen, J.-E., Meiner, A., Gelabert, E.R., Zal, N., Kristensen, P., Bastrup-Birk, A., Biala, K., Piroddi, C., Egoh, B., Degeorges, P., Fiorina, C., Santos-Martín, F., Naruševičius, V., Verboven, J., Pereira, H.M., Bengtsson, J., Gocheva, K., Marta-Pedroso, C., Snäll, T., Estreguil, C., San-Miguel-Ayanz, J., Pérez-Soba, M., Grêt-Regamey, A., Lillebø, A.I., Malak, D.A., Condé, S., Moen, J., Czúcz, B., Drakou, E.G., Zulian, G., Lavalle, C., 2016. An indicator framework for assessing ecosystem services in support of the EU Biodiversity Strategy to 2020. Ecosyst. Serv. 17, 14–23. https://doi.org/10.1016/j.ecoser.2015.10.023

Mahdianpari, M., Salehi, B., Mohammadimanesh, F., Homayouni, S., Gill, E., 2018. The First Wetland Inventory Map of Newfoundland at a Spatial Resolution of 10 m Using Sentinel-1 and Sentinel-2 Data on the Google Earth Engine Cloud Computing Platform. Remote Sens. 11, 43. https://doi.org/10.3390/rs11010043

Malila, W.A., 1980. Change vector analysis: an approach for detecting forest changes with Landsat, in: LARS Symposia. p. 385.

Manandhar, R., Odeh, I., Ancev, T., 2009. Improving the Accuracy of Land Use and Land Cover Classification of Landsat Data Using Post-Classification Enhancement. Remote Sens. 1, 330–344. https://doi.org/10.3390/rs1030330

Marieta, M., Fitoka, E., Bego, F., 2003. Inventory of Albanian Wetlands. ECAT and Greek Biotope/Wetland Centre (EKBY). Thermi, Greece.

Massom, R., Lubin, D., 2006. Polar Remote Sensing, Volume II: Icesheets. Springer Praxis Books.

Mc Feeters, S.K., 1996. The use of the Normalized Difference Water Index (NDWI) in the delineation of open water features. Int. J. Remote Sens. 17, 1425–1432. https://doi.org/10.1080/01431169608948714

McVicar, T.R., Jupp, D.L.B., 1998. The current and potential operational uses of remote sensing to aid decisions on drought exceptional circumstances in Australia: a review. Agric. Syst. 57, 399–468. https://doi.org/10.1016/S0308-521X(98)00026-2

Metz, M., Rocchini, D., Neteler, M., 2014. Surface Temperatures at the Continental Scale: Tracking Changes with Remote Sensing at Unprecedented Detail. Remote Sens. 6, 3822–3840. https://doi.org/10.3390/rs6053822

Mitsch, W.J., Gosselink, J.G., 2000. The value of wetlands: importance of scale and landscape setting. Ecol. Econ. 35, 25–33. https://doi.org/10.1016/S0921-8009(00)00165-8

Mombo, F., Speelman, S., Van Huylenbroeck, G., Hella, J., Pantaleo, M., Moe, S., 2011. Ratification of the Ramsar convention and sustainable wetlands management: situation analysis of the Kilombero Valley wetlands in Tanzania. J. Agric. Ext. Rural Dev 3, 153–164.

Muro, J., Canty, M., Conradsen, K., Hüttich, C., Nielsen, A., Skriver, H., Remy, F., Strauch, A., Thonfeld, F., Menz, G., 2016. Short-Term Change Detection in Wetlands Using Sentinel-1 Time Series. Remote Sens. 8, 795. https://doi.org/10.3390/rs8100795

Muro, J., Strauch, A., Fitoka, E., Tompoulidou, M., Thonfeld, F., 2019. Mapping Wetland Dynamics With SAR-Based Change Detection in the Cloud. IEEE Geosci. Remote Sens. Lett. 1–4. https://doi.org/10.1109/LGRS.2019.2903596

Näschen, K., Diekkrüger, B., Leemhuis, C., Steinbach, S., Seregina, L., Thonfeld, F., van der Linden, R., 2018. Hydrological Modeling in Data-Scarce Catchments: The Kilombero Floodplain in Tanzania. Water 10, 599. https://doi.org/10.3390/w10050599

Neteler, M., 2010. Estimating Daily Land Surface Temperatures in Mountainous Environments by Reconstructed MODIS LST Data. Remote Sens. 2, 333–351. https://doi.org/10.3390/rs1020333

Nguyen, D., Clauss, K., Cao, S., Naeimi, V., Kuenzer, C., Wagner, W., 2015. Mapping Rice Seasonality in the Mekong Delta with Multi-Year Envisat ASAR WSM Data. Remote Sens. 7, 15868–15893. https://doi.org/10.3390/rs71215808

Nielsen, A.A., Canty, M.J., Skriver, H., Conradsen, K., 2017. Change detection in multi-temporal dual polarization Sentinel-1 data. IEEE, pp. 3901–3908. https://doi.org/10.1109/IGARSS.2017.8127854

Otsu, N., 1979. A Threshold Selection Method from Gray-Level Histograms. IEEE Trans. Syst. Man Cybern. 9, 62–66. https://doi.org/10.1109/TSMC.1979.4310076

Paganini, M., Petiteville, I., Ward, S., Dyke, G., Steventon, M., Harry, J., Kerblat, F., 2018. Satellite Earth observations in support of the sustainable development goals. ESA.

Parrott, L., Meyer, W.S., 2012. Future landscapes: managing within complexity. Front. Ecol. Environ. 10, 382–389. https://doi.org/10.1890/110082

Patel, N.N., Angiuli, E., Gamba, P., Gaughan, A., Lisini, G., Stevens, F.R., Tatem, A.J., Trianni, G., 2015. Multitemporal settlement and population mapping from Landsat using Google Earth Engine. Int. J. Appl. Earth Obs. Geoinformation 35, 199–208. https://doi.org/10.1016/j.jag.2014.09.005

Pekel, J.-F., Cottam, A., Gorelick, N., Belward, A.S., 2016. High-resolution mapping of global surface water and its long-term changes. Nature 540, 418–422. https://doi.org/10.1038/nature20584

Perennou, C., Guelmami, A., Paganini, M., Philipson, P., Poulin, B., Strauch, A., Tottrup, C., Truckenbrodt, J., Geijzendorffer, I.R., 2018. Mapping Mediterranean Wetlands With Remote Sensing: A Good-Looking Map Is Not Always a Good Map, in: Advances in Ecological Research. Elsevier, pp. 243–277. https://doi.org/10.1016/bs.aecr.2017.12.002

Perennou, C., Machado Beltrame, C., Guelmani, A., Vives, T., Caessteker, P.T., 2012. Existing areas and past changes of wetland extent in the Mediterranean region: an overview. Ecologia Mediterranea 38 (2).

Pétillon, J., Erfanzadeh, R., Garbutt, A., Maelfait, J.-P., Hoffmann, M., 2010. Inundation Frequency Determines the Post-Pioneer Successional Pathway in a Newly Created Salt Marsh. Wetlands 30, 1097–1105. https://doi.org/10.1007/s13157-010-0115-x

Pflugmacher, D., Rabe, A., Peters, M., Hostert, P., 2019. Mapping pan-European land cover using Landsat spectral-temporal metrics and the European LUCAS survey. Remote Sens. Environ. 221, 583–595. https://doi.org/10.1016/j.rse.2018.12.001

Prigent, C., Papa, F., Aires, F., Jimenez, C., Rossow, W.B., Matthews, E., 2012. Changes in land surface water dynamics since the 1990s and relation to population pressure: LAND

SURFACE WATER DYNAMICS. Geophys. Res. Lett. 39, n/a-n/a. https://doi.org/10.1029/2012GL051276

Ramsar, 2018. Global Wetland Outlook: State of the World's Wetlands and their Services to People. Ramsar Convention Secretariat, Gland, Switzerland.

Raymond, W.H., Rabin, R.M., Wade, G.S., 1994. Evidence of an Agricultural Heat Island in the Lower Mississippi River Floodplain. Bull. Am. Meteorol. Soc. 75, 1019–1025. https://doi.org/10.1175/1520-0477(1994)075<1019:EOAAHI>2.0.CO;2

Reschke, J., Hüttich, C., 2014. Continuous field mapping of Mediterranean wetlands using sub-pixel spectral signatures and multi-temporal Landsat data. Int. J. Appl. Earth Obs. Geoinformation 28, 220–229. https://doi.org/10.1016/j.jag.2013.12.014

Ritchie, H., Roser, M., 2017. Meat and Seafood Production & Consumption, from FAOSTAT [WWW Document]. Our World Data. URL https://ourworldindata.org/meat-and-seafood-production-consumption

Robinson, A.C., 2018. Elements of viral cartography. Cartogr. Geogr. Inf. Sci. 1–18. https://doi.org/10.1080/15230406.2018.1484304

Rosin, P.L., 2001. Unimodal thresholding. Pattern Recognit. 34, 2083–2096. https://doi.org/10.1016/S0031-3203(00)00136-9

Russi, D., ten Brink, P., Farmer, A., Badura, T., Coates, D., Förster, J., Kumar, R., Davidson, N., 2012. The economics of ecosystems and biodiversity for water and wetlands (Final consultation draft), A contribution to CBD COP2011. Ramsar.

Rybakov, G., Peuhkurinen, J., Latva-Käyrä, P., Villikka, M., Sirparanta, S., Kolesnikov, A., Junttila, V., Kauranne, T., 2018. Combining Camera Relascope-Measured Field Plots and Multi-Seasonal Landsat 8 Imagery for Enhancing the Forest Inventory of Boreal Forests in Central Russia. Remote Sens. 10, 1796. https://doi.org/10.3390/rs10111796

Schiermeier, Q., 2018. Europe is demolishing its dams to restore ecosystems. Nature 557, 290–291. https://doi.org/10.1038/d41586-018-05182-1

Schlaffer, S., Matgen, P., Hollaus, M., Wagner, W., 2015. Flood detection from multi-temporal SAR data using harmonic analysis and change detection. Int. J. Appl. Earth Obs. Geoinformation 38, 15–24. https://doi.org/10.1016/j.jag.2014.12.001

Scoones, I., 1992. Wetlands in Drylands: Key Resources for Agricultural and Pastoral Production in Africa. AMBIO 20, 366–371. https://www.researchgate.net/publication/279599897_Wetlands_in_Drylands_Key_Resources_for_Agricultural_and_Pastoral_Production_in_Africa

See, L., Laso Bayas, J., Schepaschenko, D., Perger, C., Dresel, C., Maus, V., Salk, C., Weichselbaum, J., Lesiv, M., McCallum, I., Moorthy, I., Fritz, S., 2017. LACO-Wiki: A New Online Land Cover Validation Tool Demonstrated Using GlobeLand30 for Kenya. Remote Sens. 9, 754. https://doi.org/10.3390/rs9070754

Sikorova, K., Gallop, P., 2015. Financing for hydropower in protected areas in Southeast Europe. CEE Nankwatch Network.

Skonieczny, C., Paillou, P., Bory, A., Bayon, G., Biscara, L., Crosta, X., Eynaud, F., Malaizé, B., Revel, M., Aleman, N., Barusseau, J.-P., Vernet, R., Lopez, S., Grousset, F., 2015. African humid periods triggered the reactivation of a large river system in Western Sahara. Nat. Commun. 6, 8751.

Stefanov, W.L., Ramsey, M.S., Christensen, P.R., 2001. Monitoring urban land cover change. Remote Sens. Environ. 77, 173–185. https://doi.org/10.1016/S0034-4257(01)00204-8

Stefanski, J., Kuemmerle, T., Chaskovskyy, O., Griffiths, P., Havryluk, V., Knorn, J., Korol, N., Sieber, A., Waske, B., 2014. Mapping Land Management Regimes in Western Ukraine Using Optical and SAR Data. Remote Sens. 6, 5279–5305. https://doi.org/10.3390/rs6065279

Sun, F., Sun, W., Chen, J., Gong, P., 2012. Comparison and improvement of methods for identifying waterbodies in remotely sensed imagery. Int. J. Remote Sens. 33, 6854–6875. https://doi.org/10.1080/01431161.2012.692829

Tian, F., Brandt, M., Liu, Y.Y., Verger, A., Tagesson, T., Diouf, A.A., Rasmussen, K., Mbow, C., Wang, Y., Fensholt, R., 2016. Remote sensing of vegetation dynamics in drylands: Evaluating vegetation optical depth (VOD) using AVHRR NDVI and in situ green biomass data over West African Sahel. Remote Sens. Environ. 177, 265–276. https://doi.org/10.1016/j.rse.2016.02.056

Tiner, R., 2015. Introduction to Wetland Mapping and Its Challenges, in: Tiner, R., Lang, M., Klemas, V. (Eds.), Remote Sensing of Wetlands. CRC Press, pp. 43–66.

TNBS, 2012. National Bureau of statistics, Tanzania census 2012. Tanzania.

Tucker, C.J., 1979. Red and photographic infrared linear combinations for monitoring vegetation. Remote Sens. Environ. 8, 127–150. https://doi.org/10.1016/0034-4257(79)90013-0

TWRI, 2013. Aerial census of large animals in the Selous–Mikumi Ecosystem. Tanzania Wildlife Research Institute, Tanzania.

Tyler, T., Bengtsson, F., Dahlberg, C.J., Lönnell, N., Hallingbäck, T., Reitalu, T., 2018. Determinants of bryophyte species composition and diversity on the Great Alvar of Öland, Sweden. J. Bryol. 40, 12–30. https://doi.org/10.1080/03736687.2017.1412387

UN, 2015. World Population Prospects: Key findings & advance tables. New York, USA.

UN stats Metadata repository [WWW Document], 2018. URL https://unstats.un.org/sdgs/metadata/

USGS, 2017. Landsat Collection 1 Level 1 product definition.

Valiela, I., Bowen, J.L., York, J.K., 2001. Mangrove Forests: One of the World's Threatened Major Tropical Environments. BioScience 51, 807. https://doi.org/10.1641/0006-3568(2001)051[0807:MFOOTW]2.0.CO;2

Valk, A.G. van der., 2005. Water-level fluctuations in North American prairie wetlands. Hydrobiologia 539, 171–188. https://doi.org/10.1007/s10750-004-4866-3

Van der Voorde, T., de Genst, W., Canters, F., 2007. Improving Pixel-based VHR Land-cover classifications of Urban areas with post-classification techniques. Photogramm. Eng. Remote Sens. 73, 017–1027.

Vejnovic, I., Gallop, P., 2018. Financing for hydropower in protected areas in Southeast Europe: 2018 update. CEE Nankwatch Network.

Verbesselt, J., Hyndman, R., Newnham, G., Culvenor, D., 2010. Detecting trend and seasonal changes in satellite image time series. Remote Sens. Environ. 114, 106–115. https://doi.org/10.1016/j.rse.2009.08.014

Verbesselt, J., Zeileis, A., Herold, M., 2012. Near real-time disturbance detection using satellite image time series. Remote Sens. Environ. 123, 98–108. https://doi.org/10.1016/j.rse.2012.02.022

Verhoeven, J.T.A., Setter, T.L., 2010. Agricultural use of wetlands: opportunities and limitations. Ann. Bot. 105, 155–163. https://doi.org/10.1093/aob/mcp172

Voormansik, K., Jagdhuber, T., Olesk, A., Hajnsek, I., Papathanassiou, K.P., 2013. Towards a detection of grassland cutting practices with dual polarimetric TerraSAR-X data. Int. J. Remote Sens. 34, 8081–8103. https://doi.org/10.1080/01431161.2013.829593

Wan, Z., 2014. New refinements and validation of the collection-6 MODIS land-surface temperature/emissivity product. Remote Sens. Environ. 140, 36–45. https://doi.org/10.1016/j.rse.2013.08.027

Wan, Z., 2008. New refinements and validation of the MODIS Land-Surface Temperature/Emissivity products. Remote Sens. Environ. 112, 59–74. https://doi.org/10.1016/j.rse.2006.06.026

Wan, Z., Zhang, Y., Zhang, Q., Li, Z.-L., 2004. Quality assessment and validation of the MODIS global land surface temperature. Int. J. Remote Sens. 25, 261–274. https://doi.org/10.1080/0143116031000116417

Waske, B., 2014. Synergies from SAR-Optical Data Fusion for LULC Mapping, in: Manakos, I., Braun, M. (Eds.), Land Use and Land Cover Mapping in Europe. Springer Netherlands, Dordrecht, pp. 179–191. https://doi.org/10.1007/978-94-007-7969-3_11

Waske, B., Benediktsson, J.A., 2007. Fusion of Support Vector Machines for Classification of Multisensor Data. IEEE Trans. Geosci. Remote Sens. 45, 3858–3866. https://doi.org/10.1109/TGRS.2007.898446

Waske, B., Braun, M., 2009. Classifier ensembles for land cover mapping using multitemporal SAR imagery. ISPRS J. Photogramm. Remote Sens. 64, 450–457. https://doi.org/10.1016/j.isprsjprs.2009.01.003

Watson, S.J., Luck, G.W., Spooner, P.G., Watson, D.M., 2014. Land-use change: incorporating the frequency, sequence, time span, and magnitude of changes into ecological research. Front. Ecol. Environ. 12, 241–249. https://doi.org/10.1890/130097

Wdowinski, S., Hong, S.-H., 2015. Wetland InSAR: A Review of the Technique and Applications, in: Tiner, R., Lang, M., Klemas, V. (Eds.), Remote Sensing of Wetlands. CRC Press, pp. 137–154.

Weiss, S., Apostolau, A., Dug, S., Marcic, Z., Musovic, M., Oikonomou, A., Shumka, S., Skrijelj, R., Simonovic, P., Vesnic, A., Zabric, D., 2018. Endangered Fish Species in Balkan Rivers: their distributions and threats from hydropower development. Riverwatch & EuroNatur.

Weng, Q., Fu, P., Gao, F., 2014. Generating daily land surface temperature at Landsat resolution by fusing Landsat and MODIS data. Remote Sens. Environ. 145, 55–67. https://doi.org/10.1016/j.rse.2014.02.003

White, L., Brisco, B., Dabboor, M., Schmitt, A., Pratt, A., 2015. A Collection of SAR Methodologies for Monitoring Wetlands. Remote Sens. 7, 7615–7645. https://doi.org/10.3390/rs70607615

White, L., Millard, K., Banks, S., Richardson, M., Pasher, J., Duffe, J., 2017. Moving to the RADARSAT Constellation Mission: Comparing Synthesized Compact Polarimetry and Dual Polarimetry Data with Fully Polarimetric RADARSAT-2 Data for Image Classification of Peatlands. Remote Sens. 9, 573. https://doi.org/10.3390/rs9060573

Willcock, S., Phillips, O.L., Platts, P.J., Swetnam, R.D., Balmford, A., Burgess, N.D., Ahrends, A., Bayliss, J., Doggart, N., Doody, K., Fanning, E., Green, J.M.H., Hall, J., Howell, K.L., Lovett, J.C., Marchant, R., Marshall, A.R., Mbilinyi, B., Munishi, P.K.T., Owen, N., Topp-Jorgensen, E.J., Lewis, S.L., 2016. Land cover change and carbon emissions over 100

years in an African biodiversity hotspot. Glob. Change Biol. 22, 2787–2800. https://doi.org/10.1111/gcb.13218

Wilson, E., McInnes, R., Mbaga, D.P., Ouedraogo, P., 2017. Ramsar Advisory Mission Report, Ramsar Site No. 1173, Kilombero Valley, United Republic of Tanzania (Ramsar Advisory Mission Report). Ramsar, Tanzania.

Wulder, M.A., Masek, J.G., Cohen, W.B., Loveland, T.R., Woodcock, C.E., 2012. Opening the archive: How free data has enabled the science and monitoring promise of Landsat. Remote Sens. Environ. 122, 2–10. https://doi.org/10.1016/j.rse.2012.01.010

WWF, 2017. The true cost of power. World Wildlife Fund, International, Gland, Switzerland.

Xie, Z., Chen, Y., Lu, D., Li, G., Chen, E., 2019. Classification of Land Cover, Forest, and Tree Species Classes with ZiYuan-3 Multispectral and Stereo Data. Remote Sens. 11, 164. https://doi.org/10.3390/rs11020164

Xiong, J., Thenkabail, P., Tilton, J., Gumma, M., Teluguntla, P., Oliphant, A., Congalton, R., Yadav, K., Gorelick, N., 2017. Nominal 30-m Cropland Extent Map of Continental Africa by Integrating Pixel-Based and Object-Based Algorithms Using Sentinel-2 and Landsat-8 Data on Google Earth Engine. Remote Sens. 9, 1065. https://doi.org/10.3390/rs9101065

Yang, G., Weng, Q., Pu, R., Gao, F., Sun, C., Li, H., Zhao, C., 2016. Evaluation of ASTER-Like Daily Land Surface Temperature by Fusing ASTER and MODIS Data during the HiWATER-MUSOEXE. Remote Sens. 8, 75. https://doi.org/10.3390/rs8010075

Yengoh, G.T., Dent, D., Olsson, L., Tengberg, A.E., Tucker III, C.J., 2015. Use of the Normalized Difference Vegetation Index (NDVI) to assess land degradation at multiple scales. Springer.

Zha, Y., Gao, J., Ni, S., 2003. Use of normalized difference built-up index in automatically mapping urban areas from TM imagery. Int. J. Remote Sens. 24, 583–594. https://doi.org/10.1080/01431160304987

Zhu, Z., Piao, S., Myneni, R.B., Huang, M., Zeng, Z., Canadell, J.G., Ciais, P., Sitch, S., Friedlingstein, P., Arneth, A., Cao, C., Cheng, L., Kato, E., Koven, C., Li, Y., Lian, X., Liu, Y., Liu, R., Mao, J., Pan, Y., Peng, S., Peñuelas, J., Poulter, B., Pugh, T.A.M., Stocker, B.D., Viovy, N., Wang, X., Wang, Y., Xiao, Z., Yang, H., Zaehle, S., Zeng, N., 2016. Greening of the Earth and its drivers. Nat. Clim. Change 6, 791.

Zhu, Z., Wang, S., Woodcock, C.E., 2015. Improvement and expansion of the Fmask algorithm: cloud, cloud shadow, and snow detection for Landsats 4–7, 8, and Sentinel 2 images. Remote Sens. Environ. 159, 269–277. https://doi.org/10.1016/j.rse.2014.12.014

Zhu, Z., Woodcock, C.E., 2014. Continuous change detection and classification of land cover using all available Landsat data. Remote Sens. Environ. 144, 152–171. https://doi.org/10.1016/j.rse.2014.01.011